Doctoral Dissertation

Less-invasive Cancer Therapy by the Combination of Drug Delivery System and Quantum Energy

Makoto SAKAI

October 2012

Graduate School of Engineering,
Osaka University

Doctoral Dissertation

Less-invasive Cancer Therapy by the Combination of Drug Delivery System and Quantum Energy

Makoto SAKAI

October 2012

Graduate School of Engineering,
Osaka University

Less-invasive Cancer Therapy by the Combination of Drug Delivery System and Quantum Energy
(量子エネルギーと薬物輸送システムを組み合わせた低侵襲がん治療技術の基礎的研究)

Contents

Chapter 1. Introduction

Cancer morbidity and mortality in Japan have been increasing. In addition, less-invasive and higher-QOL (quality of life) treatment for tumors has been in demand due to the aging of and diversification of values among the population.

There are 3 main methods of treating cancer: surgical, chemical, and radiation therapies. Surgery is the initial choice for almost all cancers in Japan, as it is an easy method of extirpating the tumor and allows malignancy grading. However, surgery necessarily imposes a strain on the patient and can be dangerous for elderly people. It is also difficult to surgically remove cancer from organs that require functional preservation, such as the brain or heart. In addition, some patients wish to avoid surgery for breast cancer or head and neck cancer.

The field of chemotherapy is making rapid progress. Various novel drugs have been announced and released. In the case of Acute Lymphocytic Leukemia, the outcome of chemotherapy is often favorable, with a probability of long-term survival of 30% to 50%[1-6]. On the other hand, chemotherapy is not preferred for definitive therapy of solid tumors. In Japan, it is often used as a supplementary pre- or post-treatment in combination with surgical or radiation therapy, especially as chemotherapy does not require knowledge of the exact position of the tumor. Chemotherapy can have a beneficial effect on residual or tiny metastatic cancers not detectable by CT or MRI. If a radical curative drug were to be developed, it would become the most widely used method. Further development of this field is anticipated.

Like surgery, radiotherapy requires identification of the position of the tumor. Unlike surgery, radiotherapy is not painful and can be administered as an outpatient treatment in a similar manner as chemotherapy. In radiotherapy, cancer is irradiated by an external source (or a small radiation source within the body). This outside energy has a lethal effect on cancer cells. Forms of external energy therapy other than radiotherapy include medical ultrasonic and radiofrequency ablation. In external energy therapy, the energy goes through the normal tissues in front of and behind the cancer tissue and injures the body parts surrounding the cancer. It is thus important to reduce the damage to normal cells; similar concerns apply to chemotherapy. Stereotactic irradiation[7-9] and heavy ion radiotherapy[10-12] were developed to treat deep-seated tumors by radiotherapy. In stereotactic irradiation, highly focused convergent beams are delivered so that only the desired target area receives the prescribed dose. A proton beam or carbon beam is used for heavy ion radiotherapy. Heavy ion beams can generate a Bragg peak, and this peak can readily be utilized to concentrate the radiation dose on the tumor volume. However, the damage produced by these therapies is not insignificant, as normal tissue can receive half of the dose delivered to the cancer tissue[13-15]. Furthermore, cancers near vital organs remain difficult to treat. These factors lead to cancer recurrence and poor outcomes[16].

To resolve this problem, a less invasive treatment was invented using chemotherapeutic methods. The process consists of injecting a specific drug which selectively accumulates at the lesion site; this is followed by local irradiation with an appropriate energy source. The drug is excited by the external energy to produce reactive oxygen species or radiation, leading to cytotoxicity. Therefore, only the cells that accumulate the drug are killed. Using appropriately selective drugs, cancers near vital organs can be treated because the distance is not important. Furthermore, infiltrative cancer cells near the main tumor mass are treated simultaneously.

Photodynamic therapy (PDT) and boron neutron capture therapy (BNCT) are 2 such therapies, both of which use a quantum beam to excite the drug. Visible light is used for exciting photosensitizers (light-sensitive substances) in PDT, while a neutron beam is used for exciting the ^{10}B isotope in BNCT. The directness of quantum beam is

higher than that of ultrasound waves or heat, thus enhancing the selectivity.

The selectivity of the drugs and efficient energy transportation are very important to maximize the benefit of these treatments. I investigated the potential for improving the efficacy of these therapies by using hemagglutinating virus of Japan envelope (HVJ-E), a novel drug delivery carrier. HVJ-E is a nonviral vector consisting of inactivated virus particles [17,18]. HVJ-E can deliver a variety of molecules into cells via its membrane fusion activity and can be more than 10–100 times more efficient than conventional delivery methods. HVJ-E is promising for the following reasons: 1) HVJ-E is in commercial mass production[19], 2) locally administered HVJ-E induces immuno-responses against tumors[20,21] and 3) additional selectivity can be obtained by adding transferrin, cationized gelatin, or monoclonal antibodies[22-24].

In this study, the accumulation of drugs delivered using HVJ-E was examined and the anti-tumor effect caused by such accumulation determined. After these initial experiments, I investigated the mechanism by which the reactive oxygen species or radiation produced by the excited drugs injure the cancer cells, as this knowledge is important for effective therapy. I found that the cytotoxicity is related to the protein expression and growth characteristics of cancer cells.

The second chapter deals with the application of HVJ-E to PDT. Various photosensitizers have been tested for selectivity with only limited success, especially as measured by their *in vivo* therapeutic effects[25-31]. HVJ-E was able to increase the intracellular drug concentration 20-fold, and the resulting cytotoxicity was also increased. These results demonstrate the benefits of HVJ-E. The effect of PDT depends not only on the intracellular drug concentration but also on protein expression. It is well known that the cells in tumor tissue are heterogeneous[32]. Herein, I isolated 5 types of cells from a single clone of KYSE70 cells. Some of these isolated cells were significantly more sensitive than others to PDT, irrespective of their intracellular concentrations of talaporfin sodium (the photosensitizer).

In the third chapter, the potential usefulness of HVJ-E for BNCT was determined based on the knowledge obtained for HVJ-PDT. An accelerator-based neutron source is necessary for accessible BNCT[33]. However, various engineering problems currently prevent the construction of such accelerators[34,35]. In particular, the neutron flux from existing accelerators is too low to be useful for BNCT. I therefore determined the possibility of using BNCT with low neutron flux when the boron concentration was increased by HVJ-E. The first section of this chapter describes the design calculations. When the boron concentration is increased 10-fold over that reached by the conventional method, more than 1×10^6 n/cm^2/s of thermal neutron flux is required to deliver the desired radiation dose. It is of course necessary to reduce the fast neutron contribution as much as possible while maintaining the thermal neutron flux intensity. The neutron transport was thus estimated using simulation calculations and the shape and size of the moderator and reflector determined. In the second section, the setup was built and the neutron flux measured. The strictness of the simulation calculation was ascertained by comparison with the experimental data. The BNCT effect was also tested using the setup. Cytotoxicity was confirmed at a dose of 10^6 n/cm^2/s, only a hundredth part of the amount required for conventional BNCT. Therefore, the increased boron concentration supported effective BNCT with low neutron flux and reduced the contributions of fast neutrons and gamma rays. This provides helpful information towards the development of accelerators for BNCT.

The fourth chapter is devoted to exploring the functional differences of different radiations using *Escherichia coli*. It is important to know the biological effects of radiation when evaluating the effects of radiation exposure or radiation treatment[36]. The levels of such effects vary depending on the LET or radiation type, most probably due to the differences in the radiation damage and subsequent repair processes. The

functional differences between radiations are also important for estimating the effect of BNCT, as various types of radiation are involved in the BNCT effect: the B (n,α) Li reaction produces alpha rays, Li rays, and gamma rays. DNA damage and repair mechanisms are poorly understood. The effect of LET was determined using various kinds of gene deletion mutants and examining the effects of different growth conditions. Then a qualitative difference in DNA damage was observed between alpha rays and gamma rays.

References

1. Kantarjian H, Thomas D, O'Brien S, Cortes J, Giles F, Jeha S, Bueso-Ramos CE, Pierce S, Shan J, Koller C, Beran M, Keating M, Freireich EJ. Long-term follow-up results of hyperfractionated cyclophosphamide, vincristine, doxorubicin, and dexamethasone (hyper-CVAD), a dose-intensive regimen, in adult acute lymphocytic leukemia. Cancer. 2004, 101: 2788-2801
2. Faderl S, Jeha S, Kantarjian HM. The biology and therapy of adult acute lymphoblastic leukemia. Cancer. 2003, 98: 1337-1354
3. Larson RA. Recent clinical trials in acute lymphocytic leukemia by the Cancer and Leukemia Group B. Hematol Oncol Clin North Am. 2000, 14: 1367-1379
4. Durrant IJ, Richards SM, Prentice HG, Goldstone AH. The Medical Research Council trials in adult acute lymphocytic leukemia. Hematol Oncol Clin North Am. 2000, 14: 1327-1352
5. Gökbuget N, Hoelzer D, Arnold R, Böhme A, Bartram CR, Freund M, Ganser A, Kneba M, Langer W, Lipp T, Ludwig WD, Maschmeyer G, Rieder H, Thiel E, Weiss A, Messerer D. Treatment of adult ALL according to protocols of the German Multicenter Study Group for Adult ALL (GMALL). Hematol Oncol Clin North Am. 2000, 14: 1307-1325
6. Thiebaut A, Vernant JP, Degos L, Huguet FR, Reiffers J, Sebban C, Lepage E, Thomas X, Fière D. Adult acute lymphocytic leukemia study testing chemotherapy and autologous and allogeneic transplantation. A follow-up report of the French protocol LALA 87. Hematol Oncol Clin North Am. 2000, 14: 1353-1366
7. Chi A, Liao Z, Nguyen NP, Xu J, Stea B, Komaki R. Systemic review of the patterns of failure following stereotactic body radiation therapy in early-stage non-small-cell lung cancer: Clinical implications, Radiotherapy and Oncology. 2010, 94(1): 1-11
8. Tipton K, Launders JH, Inamdar R, Miyamoto C, Schoelles K., Stereotactic Body Radiation Therapy: Scope of the Literature. Ann Intern Med. 2011, 154(11): 737-745
9. Chang BK, Timmerman RD. Stereotactic Body Radiation Therapy: A Comprehensive Review, American Journal of Clinical Oncology. 2007, 30(6): 637-644
10. Jäkel O, Schulz-Ertner D, Karger CP, Nikoghosyan A, Debus J. Heavy ion therapy: status and perspectives. Technol Cancer Res Treat. 2003, 2(5): 377-387
11. Lodge M, Pijls-Johannesma M, Stirk L, Munro AJ, De Ruysscher D, Jefferson T. A systematic literature review of the clinical and cost-effectiveness of hadron therapy in cancer. Radiotherapy and Oncology. 2007, 83(2): 110-122
12. Hamada N, Imaoka T, Masunaga S, Ogata T, Okayasu R, Takahashi A, Kato TA, Kobayashi Y, Ohnishi T, Ono K, Shimada Y, Teshima T. Recent Advances in the Biology of Heavy-Ion Cancer Therapy, Journal of Radiation Research. 2010, 51(4): 365-383
13. Nagata Y, Takayama K, Matsuo Y, Norihisa Y, Mizowaki T, Sakamoto T, Sakamoto M, Mitsumori M, Shibuya K, Araki N, Yano S, Hiraoka M. Clinical outcomes of a phase I/II study of 48 Gy of stereotactic body radiotherapy in 4 fractions for primary lung cancer using a stereotactic body frame. Int J Radiat Oncol Biol Phys. 2005, 63(5): 1427-1431
14. Jäkel O, Krämer M, Karger CP, Debus J. Treatment planning for heavy ion radiotherapy: clinical implementation and application. Phys Med Biol. 2001, 46(4): 1101-1116
15. Weyrather WK, Debus J. Particle Beams for Cancer Therapy. Clinical Oncology. 2003, 15(1): S23-S28
16. Hirohiko T, Tadashi K, Masayuki B, Hiroshi T, Hirotoshi K, Shingo K, Shigeru Y, Shigeo Y, Takeshi Y, Hiroyuki K, Ryusuke H, Naotaka Y, Junetsu M. Clinical advantages of carbon-ion radiotherapy Focus on Heavy Ions in Biophysics and

Medical Physics. New J. Phys. 2008, 10: 075009
17. Shimamura M, Morishita R, Endoh M, Oshima K, Aoki M, Waguri S, Uchiyama Y, Kaneda Y. HVJ-envelope vector for gene transfer into central nervous system. Biochem Biophys Res Commun. 2003, 300(2): 464-467
18. Nakamura H, Kimura T, Ikegami H, Ogita K, Koyama S, Shimoya K, Tsujie T, Koyama M, Kaneda Y, Murata Y. Highly efficient and minimally invasive in-vivo gene transfer to the mouse uterus using haemagglutinating virus of Japan (HVJ) envelope vector. Mol Hum Reprod. 2003, 9(10): 603-609
19. Kaneda Y, Yamamoto S, Nakajima T. Development of HVJ envelope vector and its application to gene therapy. Adv Genet. 2005, 53, 307-332
20. Kurooka M, Kaneda Y. Inactivated Sendai virus particles eradicate tumors by inducing immune responses through blocking regulatory T cells. Cancer Res. 2007, 67: 227–236
21. Fujihara A, Kurooka M, Miki T, Kaneda Y. Intratumoral injection of inactivated Sendai virus particles elicits strong antitumor activity by enhancing local CXCL10 expression and systemic NK cell activation. Cancer Immunol Immunother. 2008, 57: 73–84
22. Zhang Q, Li Y, Shi Y, Zhang Y. HVJ envelope vector, a versatile delivery system: its development, application, and perspectives. Biochem Biophys Res Commun. 2008, 373(3): 345-349
23. Mima H, Yamamoto S, Ito M, Tomoshige R, Tabata Y, Tamai K, Kaneda Y. Targeted chemotherapy against intraperitoneally disseminated colon carcinoma using a cationized gelatin-conjugated HVJ envelope vector. Mol. Cancer Ther. 2006, 5(4): 1021-1028
24. Shimbo T, Kawachi M, Saga K, Fujita H, Yamazaki T, Tamai K, Kaneda Y. Development of a transferrin receptor-targeting HVJ-E vector. Biochem. Biophys. Res. Commun. 2007, 364(3): 423-428
25. Mew D, Wat CK, Towers GH, Levy JG. Photoimmunotherapy: treatment of animal tumors with tumor-specific monoclonal antibody-hematoporphyrin conjugates," J. Immunol. 1983, 130: 1473–1477
26. Sobolev AS, Jans DA, Rosenkranz AA. Targeted intracellular delivery of photosensitizers. Prog. Biophys. Mol. Biol. 2000, 73: 51–90
27. Carcenac M, Dorvillius M, Garambois V, Glaussel F, Larroque C, Langlois R, Hynes NE, van Lier JE, Pèlegrin A. Internalisation enhances photo-induced cytotoxicity of monoclonal antibody-phthalocyanine conjugates. Br. J. Cancer. 2001, 85: 1787–1793
28. Vrouenraets MB, Visser GW, Stewart FA, Stigter M, Oppelaar H, Postmus PE, Snow GB, van Dongen GA. Development of meta-tetrahydroxyphenylchlorin-monoclonal antibody conjugates for photoimmunotherapy. Cancer Res. 1999, 59: 1505–1513
29. Vrouenraets MB, Visser GW, Stigter M, Oppelaar H, Snow GB, van Dongen GA. Targeting of aluminum (III) phthalocyanine tetrasulfonate by use of internalizing monoclonal antibodies: improved efficacy in photodynamic therapy. Cancer Res. 2001, 61: 1970–1975
30. Hamblin MR, Miller JL, Hasan T. Effect of charge on the interaction of sitespecific photoimmunoconjugates with human ovarian cancer cells. Cancer Res. 1996, 56: 5205–5210
31. Mew D, Lum V, Wat CK, Towers GH, Sun CH, Walter RJ, Wright W, Berns MW, Levy JG. Ability of specific monoclonal antibodies and conventional antisera conjugated to hematoporphyrin to label and kill selected cell lines subsequent to light activation. Cancer Res. 1985, 45: 4380–4386
32. Nowell PC. The clonal evolution of tumor cell populations. Science. 1976, 194: 23–

28
33. Suzuki M, Tanaka H, Sakurai Y, Kashino G, Yong L, Masunaga S, Kinashi Y, Mitsumoto T, Yajima S, Tsutsui H, Sato T, Maruhashi A, Ono K. Impact of accelerator-based boron neutron capture therapy (AB-BNCT) on the treatment of multiple liver tumors and malignant pleural mesothelioma. Radiother Oncol. 2009, 92(1): 89-95
34. Herrera MS, González SJ, Burlon AA, Minsky DM, Kreiner AJ, Treatment planning capability assessment of a beam shaping assembly for accelerator-based BNCT, Appl Radiat Isot. 2011, 69(12): 1870-1873
35. Ceballos C, Esposito J. The BSA modeling for the accelerator-based BNCT facility at INFN LNL for treating shallow skin melanoma. Appl Radiat Isot. 2009 , 67(7-8 Suppl): S274-S277
36. Friedberg EC, Walker GC, Siede W, Wood RD, Schulz RA, Ellenberger T. DNA repair and Mutagenesis, ASM press, 2006

Chapter 2. The Application of HVJ-E for PDT and Fundamental Study for Coverage Expansion

Photodynamic therapy (PDT) is a photochemical modality approved for the treatment of various cancers and other diseases with neovascularization[1,2]. PDT is based on the interaction of non-ionizing light with a photosensitizing dye. The benefit of light irradiation is that it is unlikely to be toxic except at thermal doses, limiting the damage to normal tissue caused by PDT. PDT has a 100-year history. O. Raab used acridine and halogen lamps to provide treatment for condyloma and female genital neoplasms[3]. Hematoporphyrin (HpD) was developed in 1961[4]. HpD accumulates in cancer tissue and initiates a photodynamic reaction, and Dougherty was able to use it to achieve a complete or partial remission in 111 of 113 patients[5]. In Japan in 1989–1992, Kato performed fundamental and clinical research on Photofrin and conducted a phase 2 trial for early-stage lung cancer[6]. Based on the results, Photofrin was authorized by the Ministry of Health and Welfare in 1994 and listed on the National Health Insurance price list in 1996.

The cancers initially targeted for PDT were superficial esophageal carcinoma, superficial early-stage stomach cancer, and early cervical cancer, and the outcomes were favorable. At first, the number of cases in which PDT was used was limited due to the side effects. Patients had to stay in dark rooms to avoid skin photosensitivity. Second-generation drugs (Laserphyrin for superficial early-stage lung cancer and Visudyne for age-related macular degeneration) have recently been authorized[7]. However, PDT is still only used for early cancers.

The PDT process consists of injecting a photosensitizer that selectively accumulates at the lesion site; this is followed by local illumination of the tumor with a laser of the wavelength appropriate to activate the specific drug (Figure. 2-1)[8]. Irradiation with light of the proper wavelength leads to the generation of singlet oxygen[9]. Activation of the photosensitizer transforms the drug from its ground state into an excited singlet state; from this state, the drug may decay directly back to the ground state by emitting fluorescence, a property that can be used clinically for photodetection. Alternatively, the photosensitizer can undergo electron spin conversion to its triplet state, the form in which it has a therapeutic photodynamic effect. In the presence of oxygen, this excited molecule can react directly with its substrate by proton or electron transfer to form radicals or radical ions that can further interact with oxygen to produce oxygenated products (a type I reaction). Alternatively, the energy of the excited photosensitizer can be transferred directly to oxygen to form singlet oxygen (a type II reaction), which is the most damaging species generated during PDT[10].

To improve the effect of PDT, the photosensitizer must be concentrated in order to maximize its effect on the cancer tissue and the reaction and the reaction in cancer tissue should be revealed clearly. The first section of this chapter describes my attempts to increase the photosensitizer concentration using HVJ-E. The concentration was in fact improved in *in vitro* experiments, and this change was accompanied by increased phototoxicity. The second section describes my examination of the relationship between cell characteristics and the effect of PDT. The cells in a tumor tissue are heterogeneous in terms of their morphologies and differentiation statuses, even if the tumor consists of the progeny of a single neoplastic cell. The effect of tumor cell heterogeneity on the sensitivity to PDT is not known. Here, I demonstrate that a single tumor cell has the potential to produce heterogeneous progeny. Understanding the effect of tumor cell heterogeneity on the clinical applications of PDT will aid in the design of new interventions and potentially improve the long-term survival of PDT-treated patients.

Figures

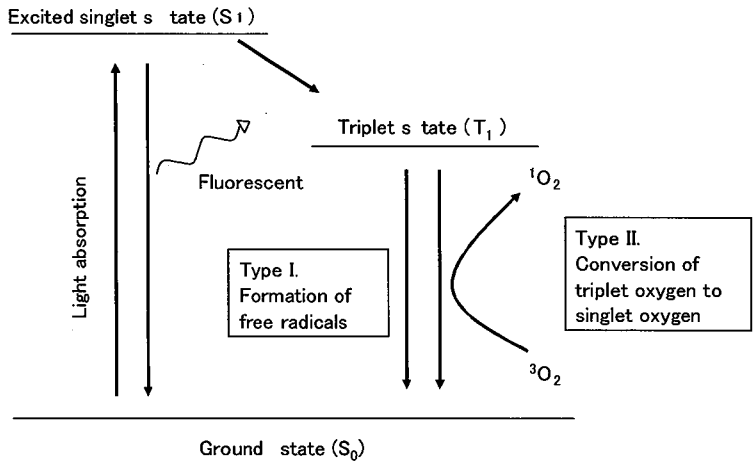

Figure 2-1. Diagram of photochemical reaction in PDT.

References

1. Schuitmaker JJ, Baas P, van Leengoed HL, van der Meulen FW, Star WM, van Zandwijk N. Photodynamic therapy: a promising new modality for the treatment of cancer. J Photochem Photobiol B. 1996, 34(1): 3-12
2. Lightdale CJ, Heier SK, Marcon NE, McCaughan JS Jr, Gerdes H, Overholt BF, Sivak MV Jr, Stiegmann GV, Nava HR. Photodynamic therapy with porfimer sodium versus thermal ablation therapy with Nd:YAG laser for palliation of esophageal cancer: a multicenter randomized trial. Gastrointest. Endosc. 1995, 42; 507–512
3. Raab O. Uber die wilkung flurescienden stoffe auf Infusorien. Z Biol. 1900, 39: 190-196
4. Lipson RL, Baldes EJ. The use of a dericative of heatoporphyrin in tumor detection, K Natl Cancer Inst. 1961, 62: 1-8
5. Dougherty TJ, Lawrence G, Kaufman JH, Boyle D, Weishaupt KR, Goldfarb A. Photodiation in the treatment of recurrent breast cancer. J Natl Cancer Inst. 1979, 62: 231-237
6. Kato H, Usuda J, Okunaka T. Furukawa K. The history of the study of photodynamic therapy and photodynamic diagnosis in the department of surgery. Tokyo Medical University, Photodiagnosis and Photodynamic Therapy. 2004, 1(2): 107-110
7. Kato H, Furukawa K, Sato M, Okunaka T, Kusunoki Y, Kawahara M, Fukuoka M, Miyazawa T, Yana T, Matsui K, Shiraishi T, Horinouchi H. Phase II clinical study of photodynamic therapy using mono-L-aspartyl chlorine e6 and diode laser for early suoerficial squamous cell carcinoma of the lung. Lung Cancer. 2003, 42: 103-111
8. Verma S, Watt GM, Mai Z, Hasan T. Strategies for enhanced photodynamic therapy effects. Photochem. Photobiol. 2007, 83: 996–1005
9. Buytaert E, Dewaele M, Agostinis P. Molecular effectors of multiple cell death pathways initiated by photodynamic therapy. Biochim. Biophys. Acta, 2007, 1776: 86–107
10. Foote CS. Definition of type I and type II photosensitized oxidation. Photochem. Photobiol. 1991, 54: 659

Section 1. In vitro investigation of efficient photodynamic therapy using a non-viral vector; hemagglutinating virus of Japan envelope

I. INTRODUCTION

Photodynamic therapy (PDT) is a photochemical modality approved for the treatment of various cancers, skin diseases, and diseases with neovascularization[1,2]. The PDT process comprises injection of a photosensitizer, which selectively accumulates at the lesion site, followed by local illumination of the site with a laser of appropriate wavelength to activate the photosensitizer. Irradiation of the photosensitized area with light at a specific wavelength leads to singlet oxygen generation[3].

The PDT treatment method is associated with minimal injury to patients because photosensitizers have low cytotoxicity and the excitation light is harmless in the visible light range. Therefore, PDT is expected to be a less invasive treatment method for early lung cancers and stomach carcinoma. Moreover, this treatment method also helps preserve organ function and limits pain compared to existing surgical treatments or anti-cancer drug therapies. PDT is an ideal treatment for elderly patients, and it may also improve the patient's quality of life.

Selective accumulation of the photosensitizer in the cancer cells is necessary to improve the therapeutic efficacy of PDT. However, a limitation of this therapy is the difficulty in photosensitizers reaching the diseased site, which reduces the efficiency of PDT therapy. To improve the effectiveness of PDT therapy, a new Drug Delivery System (DDS) needs to be developed for improving the selectivity of photosensitizers. The DDS is a technology designed to optimize drug therapy by controlling the drug disposition and selectively transporting drugs to a target site at a preferred density or time. The DDS should also effectively reduce side effects and improve the safety of a given drug.

For the accumulation of drugs in cancer cells, active targeting DDS using monoclonal antibodies were developed. However, conventional photosensitizers are mostly hydrophobic, and therefore, conjugation of photosensitizers to antibodies without compromising the immunoreactivity of the antibodies and thereby *in vivo* target accumulation is difficult. Various combinations of conventional photosensitizers and monoclonal antibodies have been tested to improve their selectivity, albeit with limited success, especially with regard to *in vivo* therapeutic efficacy[4-10].

Currently, liposomes are used clinically as drug carriers, and polymer micelles, silica nanoparticles, and carbon nanohorns are potential carriers that have also been extensively studied[11,12]. These carriers have also been investigated as photosensitizer carriers for PDT and have some advantages compared with the administration of the photosensitizer alone[13-16]. The carriers are composed of 2 defined layers: an outer envelope and an inner shell. The interaction between the living organism and the outer envelope of the carrier influences the characteristics of drug disposition, and the inner shell of the carrier contains the drug. These carriers can be used as active targeting systems by adding monoclonal antibodies to the outer envelope; the effect of adding monoclonal antibody was determined in *in vivo* experiments[17-18]. HVJ-E is a non-viral DDS carrier having the same bilayer structure and capability as the active targeting system with antibody[19-23]. In this study, the effectiveness of a new PDT DDS using a vector based on HVJ-E was examined.

HVJ-E not only encloses drugs and carries them to target sites but also has some advantages over other carriers. For example, HVJ-E is effective in fusing with other cells[24] and is therefore expected to improve accumulation of photosensitizers within the target tumor cells compared with other carriers. Tissue-specific HVJ envelope vectors have been constructed (Y. Kaneda, unpublished data, 2005) [25]; this is an additional advantage of this carrier over other carriers. HVJ-E alone has been shown to have an

antitumor effect[26-28]. In addition, a clinical grade HVJ envelope vector is currently being produced for use in clinical trials[29] Consequently, HVJ-E is a suitable drug carrier for PDT.

We constructed HVJ-PPIX by adding protoporphyrin IX (PPIX) to HVJ-E; PPIX is being widely used as a carrier in PDT for brain tumors[30,31]. PDT with PPIX is based on the endogenous accumulation of PPIX after topical or systemic administration of 5-aminolaevulinic acid (5-ALA) [32]. The cytotoxicity of PPIX and 5-ALA are low because they are normal products in healthy tissue. PPIX has absorption peaks at 405, 510, 545, 580, and 630 nm[33,34]. Very high absorption was observed at 405 nm, and high therapeutic effectiveness is expected at this wavelength. Further, the light at a wavelength of 630 nm is highly transmissible and appropriate for application to deep lesions[35]. PPIX is s synthesized inside mitochondria. The amount of PPIX in the cell depends on the amount of intracellular 5-ALA and the synthesis ability[36]. For this reason, there is a limit on the accumulation of PPIX induced 5-ALA. HVJ-E can transport PPIX directly and achieve the high concentration.

The membrane structure of HVJ-E is the same as that of biomembranes, and hence, small molecules leak out from HVJ-E. Synthetic compounds with their molecular weight more than 1,000 Da can be incorporated into HVJ-E[37]. Therefore, encapsulation of 5-ALA is difficult. 5-ALA must not be added any molecules for increasing the molecular size because it is required for the synthesis of PPIX for PDT. Therefore, we constructed HVJ-PPIX from PPIX-C17 (diheptadecanoyl-substituted protoporphyrin IX) using the PPIX-C17[38] solution technique.

We evaluated the amount of photosensitizer taken up by lung cancer and melanoma cells *in vitro* and the photocytotoxic effect of PDT on the cultured cells by using HVJ-E with added PPIX. The benefits of using HVJ-E as a DDS for PDT are an enhanced uptake efficiency of photosensitizer by tumor cells and a selective photocytotoxic effect because of the cytotoxicity of HVJ-E as well as the PDT.

II. MATERIALS AND METHODS

1. Photosensitizer and light source of PDT

5-ALA (A7793, Sigma-Aldrich Inc., USA) and PPIX (Sigma-Aldrich Inc.) were used as photosensitizers. HVJ-PPIX was generated from PPIX-C17. A continuous wave semiconductor laser generator was used for PDT at a wavelength of 405 nm, at which the photosensitizers showed a maximum peak of absorption. The cells were grown on a 96-well culture plate (Black with Clear Bottom 96-well Microtest™ Optilux™ Plate, BD Bioscience Inc., USA), and then irradiated by a laser via a fiber attached to the bottom of the culture plate. An optical instrument with an automated stage for positioning was purchased from Sigma Koki Co. Ltd., Japan.

2. Vector

The HVJ-E vector is a non-viral vector. The viral activities of the HVJ-E vector were abrogated by exposure to ultraviolet rays, but the vector still had cell fusion abilities. DNA, RNA, and proteins can be incorporated into HVJ-E and delivered efficiently both *in vitro* and *in vivo* based on its virus-to-cell fusion ability, which protects the contents of the HVJ-E vector from degradation by endosomes and lysosomes[28]. Virus replication was lost completely, but hemagglutinating activity was not affected[24].

3. Synthesis of HVJ-PPIX

An HVJ suspension of 10,000 HAU was inactivated by UV irradiation (99 J/cm^2). Phosphate buffered saline solution (300 μL) (PBS, pH 7.4, Sigma-Aldrich Inc.) and PPIX-C17 solution (87 μL at a concentration of 11.5 mg/mL) were added to the 10,000 HAU HVJ-E suspension. After centrifuge separation (15000 rpm, 4°C, 5 min), the

supernatant was removed and 200 μL of PBS was added. The PPIX-C17 was prepared according to the protocol of El-zaria[38]. The incorporation ratio of PPIX in HVJ-E was 2.5×10^{-18} mol per one HVJ-E vesicle (mean vesicle volume is about 0.11 mm^3).

4. Cell culture

The human lung cancer cell line A549 and the murine melanoma cell line B16 were used. The A549 cells were cultured in RPMI-1640 medium (Sigma-Aldrich Inc.) containing 10% fetal bovine serum (FBS, Biowest Inc., France), 100 units/mL penicillin, and 0.1 mg/mL streptomycin (Nacalai Tesque, Japan). The B16 cells were cultured in Dulbecco's Modified Eagle's Medium (DMEM) (Sigma-Aldrich Inc.) containing 10% FBS, 100 units/mL penicillin, and 0.1 mg/mL streptomycin. The cells were incubated at 37°C with 5% CO_2.

5. PPIX uptake by cells

For adherent cultures, 100 μL (2×10^4 cells/well) of the A549 cells were plated in a 96-well plate. Three hours later, when the cells had adhered to the plate, the medium was removed and replaced with FBS-free DMEM containing 100 μL of 5-ALA (800 μM), PPIX (100 μM), and HVJ-PPIX (100 μM) solution. Conjugation of eight ALA molecules yields PPIX in a mitochondria; ALA dehydratase synthesizes porphobilinogen (PBG) from two 5-ALA molecules. PBG deaminase converts four PBG molecules into hydroxymethylbilane. Linear hydroxymethylbilane is fused into a ring to make uroporphyrinogen III. Four carboxyl groups are removed to make coproporphyrinogen III. And a coproporphyrinogen oxidase converts coproporphyrinogen III to protoporphyrinogen IX[39]. After 2 hours, the supernatant was removed and the cells were washed once in PBS, lysed with 100 μL of 0.05% sodium dodecyl sulfate solution at 37°C for 30 min, and then the intracellular uptake of PPIX was quantified using a multi-mode microplate reader (SpectraMax M5®, Molecular Devices Co. Ltd., USA) with excitation and emission wavelengths of 405 and 635 nm, respectively.

6. Fluorescence imaging of intracellular PPIX

A549 cells were exposed to 5-ALA (800 μM), PPIX (100 μM), and HVJ-PPIX (100 μM) dissolved in FCS-free DMEM as described above. After the supernatant was removed and the cells were washed once in PBS, the distribution of PPIX in the cells was observed using fluorescent microscopy (BZ-9000, KEYENCE, Japan). The excitation wavelength was 405 nm, and fluorescence emission was detected at 650 nm. 4′,6-Diamidino-2-phenylindole hydrochloride (DAPI) (Nacalai Tesque, Japan) was used to locate the nucleus.

7. Evaluation of the difference of PPIX uptake between cell lines

The amount of drugs delivered using the HVJ-E vector varies depending on the cell line tested[40]. We used A549 cells and B16 cells to evaluate the delivery of PPIX via HVJ-E. The cells were plated into a 96-well plate (2×10^4 cells/well). Three hours later, the medium was removed and replaced with 100 μL of HVJ-PPIX suspension (0–200 μM; dissolved in FBS-free DMEM). After 2 hours, the supernatant was removed, the cells were washed and lysed, and the intracellular uptake of PPIX was quantified as described for the PPIX uptake assay.

8. Evaluation of the photocytotoxic activity of PDT

The B16 cells were inoculated into a 96-well Microtest™ Optilux™ plate (1.25×10^4 cells/well) and incubated for 48 hours. The medium was removed and replaced with 100 μL of 5-ALA solution (0–50 μM; dissolved in FBS-free DMEM) or HVJ-PPIX solution (0–6.25 μM; dissolved in FBS-free DMEM). After 2 hours, the cells were washed and

re-suspended in 100 μL of FBS-free DMEM. Cells were then subjected to laser irradiation (50 mW/cm^2) for 0, 30, 60, or 180 s. After laser irradiation, the culture medium was replaced with a complete growth medium. After 24 h, the Cell Counting Reagent SF kit (Nacalai Tesque, Japan), based on a water-soluble tetrazolium compound, was used to determine the effect of PDT on cell survival. The microplate reader was used to measure the absorbance at a wavelength of 450 nm. All experiments were performed in 3 repeats.

9. Statistical analyses

All data were expressed as the mean ± standard derivation. Statistical significance (defined as P values of <0.01) was evaluated using an unpaired Student's *t*-test (two-tailed).

III. RESULTS

1. Photosensitizer uptake by A549 cells

The relationship between the photosensitizer administered and the intracellular fluorescence intensity is presented in Figure 2-1-1. The amount of PPIX that was taken up by the cells reached a plateau at 2 h (data not shown). Fluorescence intensity with HVJ-PPIX was 3 times higher than that with the PPIX solution and 20 times higher than that with the 5-ALA solution. Thus, uptake of PPIX was significantly higher with the HVJ-PPIX solution than with the other solutions.

2. Fluorescence imaging of intracellular PPIX

Figure 2-2-2 shows the results of fluorescence microscopy. PPIX was located eccentrically in the cytoplasm when the cells were exposed to 5-ALA. However, PPIX was ubiquitously distributed in the cell when HVJ-PPIX was used.

3. Evaluation of the difference of PPIX uptake between cells

The relationship between the initial concentration of HVJ-PPIX in the culture medium and the fluorescence intensity from intracellular PPIX is shown in Figure 2-1-3. At HVJ-PPIX suspension concentrations of >50 μM, PPIX uptake was higher in the B16 cells than in the A549 cells.

4. Evaluation of the photocytotoxic activity of PDT

The cytotoxic effect of PDT was evaluated in A549 and B16 cells. The number of untreated cells was set at 100%, and the cell survival rate in the treatment groups was calculated relative to the untreated cells. Comparing Figures 2-1-4 and 2-1-6, or Figures 2-1-5 and 2-1-7, the HVJ-PPIX suspension showed a greater cytotoxicity after PDT than did the 5-ALA solution.

IV. DISCUSSION

PDT is one of the least invasive cancer therapies, but the accumulation of photosensitizers in tumor cells is inefficient. One way to overcome this limitation is to use a tumor-targeted DDS. In our study, we tested the novel DDS vector HVJ-E for the delivery of photoactive compounds used in PDT. HVJ-E is expected to be a novel DDS vector. Because HVJ-E is constructed from the inactivated Sendai virus, the components of HVJ-E are very similar to that of native HVJ. Two glycoproteins, fusion (F) protein and hemagglutinin-neuraminidase (HN) protein, are present on the viral envelope, and these proteins are important for membrane fusion[21,41]. It is likely that efficient uptake of PDT photosensitizing compounds occurs using this vector through the fusion of the vector membrane with the tumor cell membrane.

In the current PDT method, 5-ALA was used. PPIX is formed from 5-ALA in the mitochondria[42]. We developed a novel method for the direct transportation of PPIX in tumor cells using HVJ-E, and showed that HVJ-PPIX could be used to inject more photosensitizers into a cell than 5-ALA. It is unlikely that the improvement in the injection efficiency of HVJ-PPIX relative to PPIX was only due to differences in the compounds. HVJ-E increases the injection efficiency by supporting cell adhesion and membrane fusion using surface proteins. The amount of PPIX induced by HVJ-PPIX was 20 times higher than that induced by 5-ALA solution (Fig. 2-1-1), which yields about 2 to 5 times better results compared with other vectors in earlier studies[43-46].

The distribution of PPIX in the cell was observed using fluorescence microscopy (Fig. 2-1-2). PPIX was located eccentrically in the cytoplasm when the cells were exposed to 5-ALA. 5-ALA is metabolized along a pathway in the mitochondria into PPIX. Thus ALA-PPIX is localized in mitochondria[47]. On the other hand, PPIX was ubiquitously distributed in the cell by applying HVJ-PPIX. The PDT ability was maintained. HVJ-E transfers drugs into cells by cell fusion. The membrane fusion pathway can spare the endosomal and lysosomal degradation[25]. In our study, It was considered that PPIX also would take up using the membrane fusion pathway.

In addition, PPIX-induced HVJ-PPIX was observed in the nucleus. Because HVJ-E is often used in gene transfer[48-50], it is very likely that HVJ-E allows PPIX to move into the nucleus by a similar mechanism. PDT results in reactive oxygen species (ROS) and damage to cellular DNA. Thus, the use of HVJ-PPIX has an advantage over PPIX induced by 5-ALA[28].

The amount of PPIX taken up by the B16 and A549 cells was measured (Fig. 3), and we determined that B16 cells took up significantly about 20-40 percent more PPIX than A549 cells. Of course, the growth rate was different between these cells. Although the uptake of PPIX can affect cell growth, our experiments lasted for only 2 h in serum-free medium, which eliminated the effect of changes on the cell growth rate[51].

HVJ-E binding to the cell surface is mediated by an acetyl-type sialic acid recognized by the HN protein on the vector[52]. HN-depleted HVJ has low hemagglutinating activity and the infection activity was suppressed[53]. On the other hand, the transportation by HVJ-E is not affected by inhibitors of endocytosis[21,22,54]. HVJ-E vector–mediated membrane fusion was also observed by electron microscopy[21,55],. These results indicate that the PPIX can be directly delivered to the cytoplasm. Because membrane fusion is needed to the derivation, the receptor of A549 and B16 would take an interest in the amount of intracellular PPIX. The membrane fusion pathway has a higher potential to increase uptake efficiency than does endocytosis because the endosome aggregates PPIX and decreases the efficiency of absorption of light[56,57] Furthermore the retention time is shortened because PPIX in coated vesicles is dissolved by the lysosomes[58].

The photocytotoxicity of HVJ-PPIX (Figs. 2-1-6 and 2-1-7) was evaluated in comparison with that induced by 5-ALA (Figs. 2-1-4 and 2-1-5). High cytotoxicity was observed both in A549 and B16 cell lines. The cytotoxicity for B16 cells (Fig. 2-1-7) was twice as large as that for A549 cells (Fig. 2-1-6), which corresponded to the measured uptake results. The photocytotoxicity of B16 cells was higher than that of A549 cells compared in the same intracellular PPIX concentration. Thus, we demonstrated that the use of HVJ-PPIX resulted in efficient photocytotoxicity considering the amount of PPIX uptake.

HVJ-E alone has demonstrated antitumor efficacy without the addition of any therapeutic agents[28,59]. When the concentration of the HVJ-PPIX suspension was greater than 6.25 μM, little cytotoxicity was observed without laser irradiation (Figs. 2-1-6 and 2-1-7). This suggests that HVJ-PPIX retains its antitumor effect. Evaluation of the photocytotoxic effects of HVJ-PPIX in the tumor-bearing mouse models should

also be evaluated, along with the *in vivo* cytotoxicity of the carrier alone. These findings may be useful for the clinical application of phototherapy in cancer patients.

The *in vitro* experiments reported in this study did not allow us to evaluate the tumor selectivity of the HVJ-PPIX, but the *in vivo* selectivity has been demonstrated in previous research[19-23]. The accumulation of photosensitizing compounds *in vivo* is critical in the medical application of PDT.

V. SUMMARY

In this study, HVJ-E was applied to PDT as a novel DDS carrier, and the efficacy of PDT using HVJ-PPIX was evaluated *in vitro*. As a result, the uptake quantities of the photosensitizers increased to a greater extent with HVJ-PPIX with previously reported compounds. Future studies should evaluate the drug kinetics, the amount of accumulation in the tumor, and the photocytotoxic effect of PDT with HVJ-PPIX using *in vivo* tumor-bearing animal models..

Figures

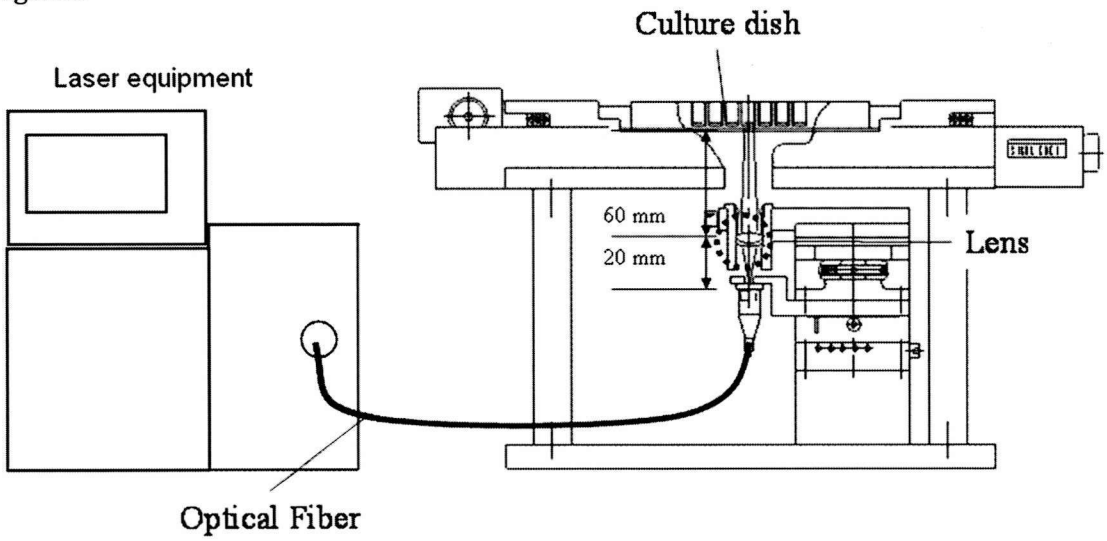

Fig. 2-1-1. Experimental setup for laser irradiation of cultured cells on the automated positioning stage. Cells were irradiated with a laser via a fiber attached to the bottom of the culture plate.

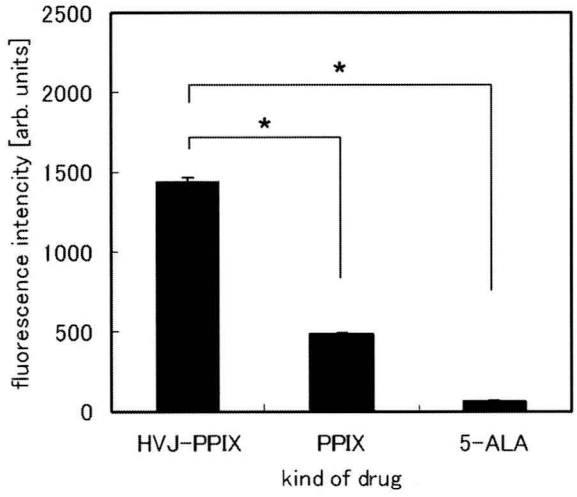

Figure 2-1-2. The intracellular uptake of photosensitiazer by each cell lines. Graphs show the fluorescence intensity of intracellular PPIX that was taken up by each cell lines after 2 h of culture in serum free culture medium.(*P < 0.01)

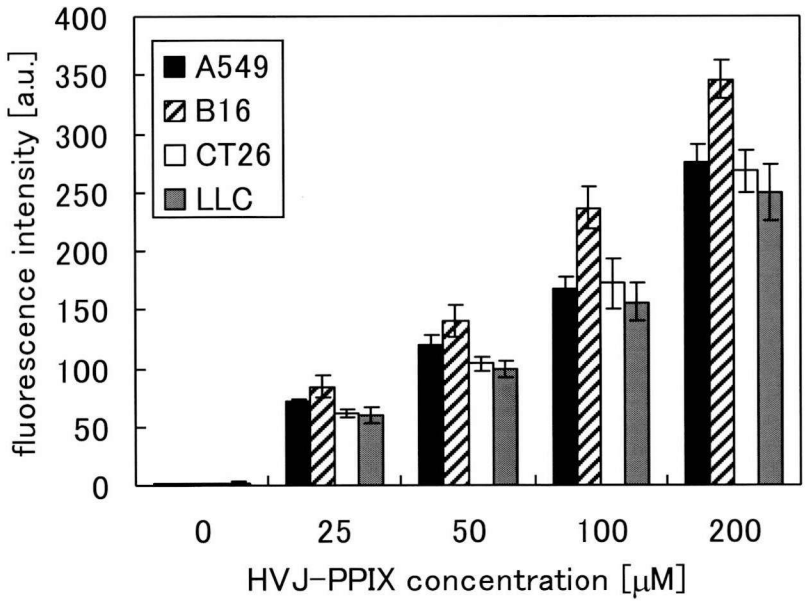

Figure 2-1-3. Intracellular uptake amount of talaporfin sodium A549, B16, CT26 and LLC cell lines. Fluorescence intensity was expressed against the initial concentration of HVJ-PPIX. The bars indicate cell lines (black bar; A549,slashed bar; #2, white bar; CT26 and gray bar; LLC). Significant differences ($P < 0.05$) were shown below; 26 μM:A549 against CT26. 50 μM : A549 against all other groups B16 against all other groups. 100 μM : B16 against all other groups. and 200μM :, A549 against B16 and LLC, B16 against all other groups.

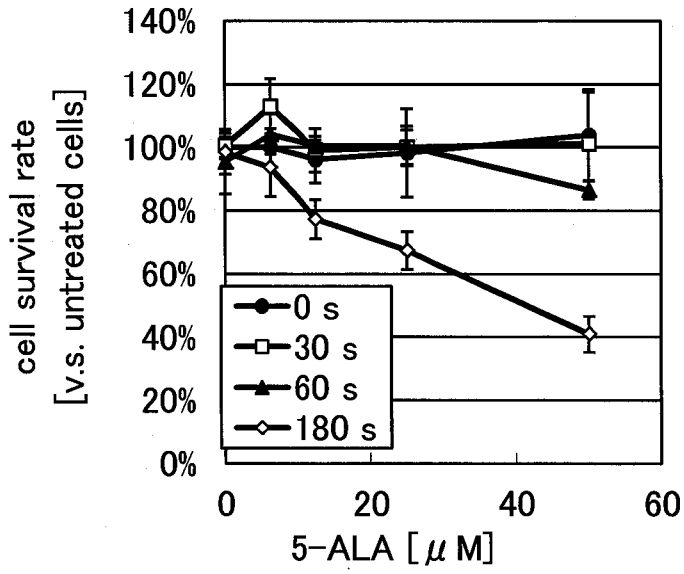

Figure 2-1-4. Antitumor effect of PDT for the A549 cells using 5-ALA. The cell survival rate (%) is expressed against laser irradiation time. The irradiation time is indicated as ●;0 s, □; 30 s, ▲; 60 s, ◇; 180 s.

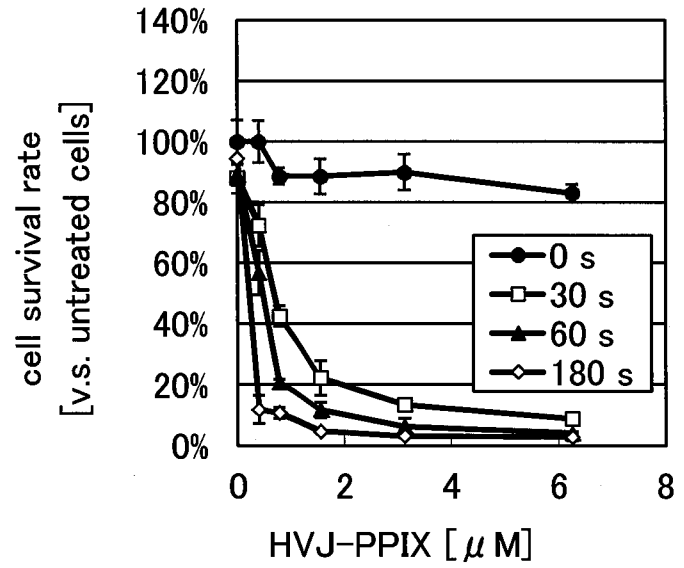

Figure 2-1-5. Antitumor effect of PDT for the A549 cells using HVJ-PPIX. The cell survival rate (%) is expressed against laser irradiation time. The initial dose concentration is indicated as ●;0 s, □; 30 s, ▲; 60 s, ◇; 180 s.

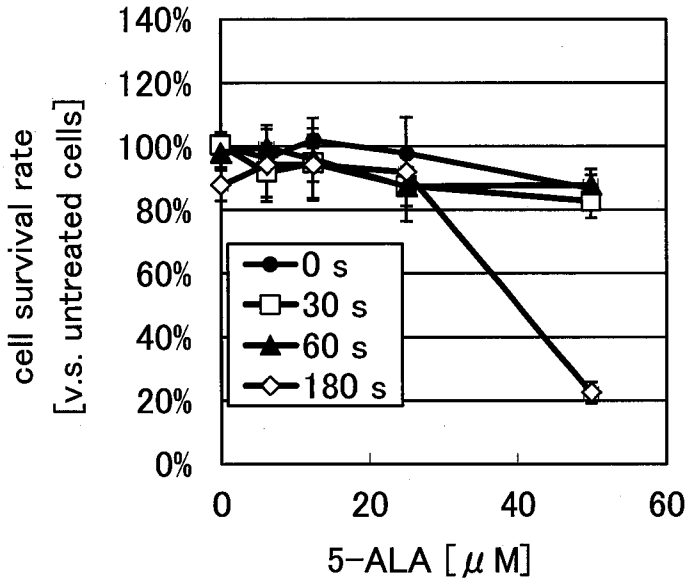

Figure 2-1-6. Antitumor effect of PDT for the B16 cells using 5-ALA. The cell survival rate (%) is expressed against laser irradiation time. The initial dose concentration is indicated as ●;0 s, □; 30 s, ▲; 60 s, ◇; 180 s.

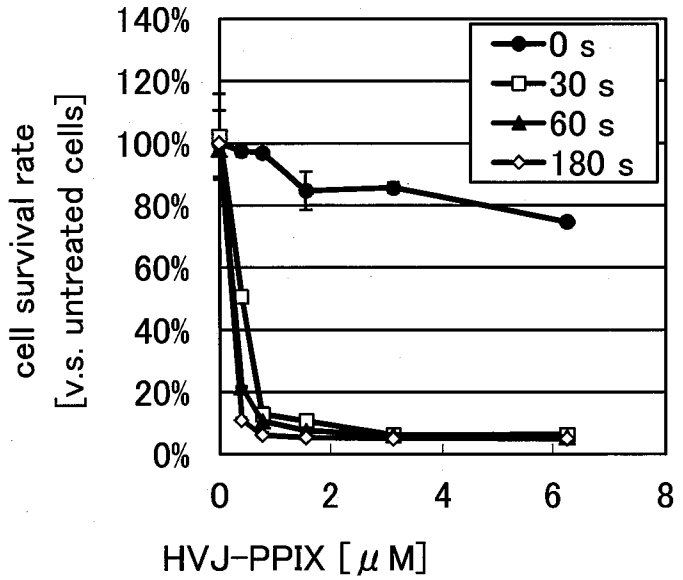

Figure 2-1-7. Antitumor effect of PDT for the B16 cells using HVJ-PPIX. The cell survival rate (%) is expressed against laser irradiation time. The initial dose concentration is indicated as ●;0 s, □; 30 s, ▲; 60 s, ◇; 180 s.

References

1. Macdonald IJ. Dougherty TJ. Basic principles of photodynamic therapy. J. Porhyrins Phthalocyanines. 2001, 5(2): 105-129
2. Lightdale CJ, Heier SK, Marcon NE, McCaughan JS Jr, Gerdes H, Overholt BF, Sivak MV Jr, Stiegmann GV, Nava HR. Photodynamic therapy with porfimer sodium versus thermal ablation therapy with Nd:YAG laser for palliation of esophageal cancer: a multicenter randomized trial. Gastrointest Endosc. 1995, 42(6): 507-512
3. Buytaert E, Dewaele M, Agostinis P. Molecular effectors of multiple cell death pathways initiated by photodynamic therapy. Biochim Biophys Acta. 2007, 1776(1): 86-107
4. Mew D, Wat CK, Towers GH, Levy JG. Photoimmunotherapy: treatment of animal tumors with tumor-specific monoclonal antibody-hematoporphyrin conjugates. J Immunol. 1983, 130(3): 1473-1477
5. Sobolev AS, Jans DA, Rosenkranz AA. Targeted intracellular delivery of photosensitizers. Prog Biophys Mol Biol. 2000, 73(1): 51-90
6. Carcenac M, Dorvillius M, Garambois V, Glaussel F, Larroque C, Langlois R, Hynes NE, van Lier JE, Pelegrin A. Internalisation enhances photo-induced cytotoxicity of monoclonal antibody-phthalocyanine conjugates. Br J Cancer. 2001, 85(11): 1787-1793
7. Vrouenraets MB, Visser GW, Stewart FA, Stigter M, Oppelaar H, Postmus PE, Snow GB, van Dongen GA. Development of meta-tetrahydroxyphenylchlorin-monoclonal antibody conjugates for photoimmunotherapy. Cancer Res. 1999, 59(7): 1505-1513
8. Vrouenraets MB, Visser GW, Stigter M, Oppelaar H, Snow GB, van Dongen GA. Targeting of aluminum (III) phthalocyanine tetrasulfonate by use of internalizing monoclonal antibodies: improved efficacy in photodynamic therapy. Cancer Res. 2001, ;61(5): 1970-1975
9. Hamblin MR, Miller JL, Hasan T. Effect of charge on the interaction of site-specific photoimmunoconjugates with human ovarian cancer cells. Cancer Res. 1996, 56(22): 5205-5210
10. Mew D, Lum V, Wat CK, Towers GH, Sun CH, Walter RJ, Wright W, Berns MW, Levy JG. Ability of specific monoclonal antibodies and conventional antisera conjugated to hematoporphyrin to label and kill selected cell lines subsequent to light activation. Cancer Res. 1985, 45(9): 4380-4386
11. V.V. Ranade and M.A. Hollinger. "Drug Delivery Systems, Second Edition," CRC Press 2003
12. Zhang M, Murakami T, Ajima K, Tsuchida K, Sandanayaka AS, Ito O, Iijima S, Yudasaka M. Fabrication of ZnPc/protein nanohorns for double photodynamic and hyperthermic cancer phototherapy. Proc Natl Acad Sci U S A. 2008, 105(39): 14773-14778
13. Derycke AS, de Witte PA. Liposomes for photodynamic therapy. Adv Drug Deliv Rev. 2004, 56(1): 17-30
14. Chen B, Pogue BW, Hasan T. Liposomal delivery of photosensitising agents. Expert Opin Drug Deliv. 2005, 2(3): 477-487
15. McCarthy JR, Perez JM, Brückner C, Weissleder R. Polymeric nanoparticle preparation that eradicates tumors. Nano Lett. 2005, 5(12): 2552-2556
16. Roy I, Ohulchanskyy TY, Pudavar HE, Bergey EJ, Oseroff AR, Morgan J, Dougherty TJ, Prasad PN. Ceramic-based nanoparticles entrapping water-insoluble photosensitizing anticancer drugs: a novel drug-carrier system for photodynamic therapy. J Am Chem Soc. 2003, 125(26): 7860-7865
17. Maruyama K. PEG-liposome in DDS and clinical studies Nihon Rinsho. 1998, 56(3):

632-637 [Article in Japanese]
18. Beilvert A, Cormode DP, Chaubet F, Briley-Saebo KC, Mani V, Mulder WJ, Vucic E, Toussaint JF, Letourneur D, Fayad ZA. Tyrosine polyethylene glycol (PEG)-micelle magnetic resonance contrast agent for the detection of lipid rich areas in atherosclerotic plaque. Magn Reson Med. 2009, 62(5): 1195-1201
19. Zhang Q, Li Y, Shi Y, Zhang Y. HVJ envelope vector, a versatile delivery system: its development, application, and perspectives. Biochem Biophys Res Commun. 2008, 373(3): 345-349
20. Maeda H. The enhanced permeability and retention (EPR) effect in tumor vasculature: the key role of tumor-selective macromolecular drug targeting. Adv Enzyme Regul. 2001, 41: 189-207
21. Mima H, Yamamoto S, Ito M, Tomoshige R, Tabata Y, Tamai K, Kaneda Y. Targeted chemotherapy against intraperitoneally disseminated colon carcinoma using a cationized gelatin-conjugated HVJ envelope vector. Mol Cancer Ther. 2006, 1021-1028
22. Mima H, Tomoshige R, Kanamori T, Tabata Y, Yamamoto S, Ito S, Tamai K, Kaneda Y. Biocompatible polymer enhances the in vitro and in vivo transfection efficiency of HVJ envelope vector. J Gene Med. 2005, 7(7): 888-897
23. Shimbo T, Kawachi M, Saga K, Fujita H, Yamazaki T, Tamai K, Kaneda Y. Development of a transferrin receptor-targeting HVJ-E vector. Biochem Biophys Res Commun. 2007, 364(3): 423-428.
24. Kaneda Y, Nakajima T, Nishikawa T, Yamamoto S, Ikegami H, Suzuki N, Nakamura H, Morishita R, Kotani H. Hemagglutinating virus of Japan (HVJ) envelope vector as a versatile gene delivery system. Mol Ther. 2002, 6(2): 219-226
25. Kaneda Y, Tabata Y. Non-viral vectors for cancer therapy. Cancer Sci. 2006, 97(5): 348-354
26. Kondo Y, Fushikida K, Fujieda T, Sakai K, Miyata K, Kato F, Kato M. Efficient delivery of antibody into living cells using a novel HVJ envelope vector system. J Immunol Methods. 2008, 332(1-2): 10-17
27. Suzuki H, Kurooka M, Hiroaki Y, Fujiyoshi Y, Kaneda Y. Sendai virus F glycoprotein induces IL-6 production in dendritic cells in a fusion-independent manner. FEBS Lett. 2008, 582(9): 1325-1329
28. Kurooka M, Kaneda Y. Inactivated Sendai virus particles eradicate tumors by inducing immune responses through blocking regulatory T cells. Cancer Res. 2007, 67(1): 227-236
29. Tanaka M, Shimbo T, Kikuchi Y, Matsuda M, Kaneda Y. Sterile alpha motif containing domain 9 is involved in death signaling of malignant glioma treated with inactivated Sendai virus particle (HVJ-E) or type I interferon. Int J Cancer. 2010, 126(8): 1982-1991
30. Friesen SA, Hjortland GO, Madsen SJ, Hirschberg H, Engebraten O, Nesland JM, Peng Q. 5-Aminolevulinic acid-based photodynamic detection and therapy of brain tumors (review). Int J Oncol. 2002, 21(3): 577-582
31. Kloek J, Akkermans W, Beijersbergen van Henegouwen GM. Derivatives of 5-aminolevulinic acid for photodynamic therapy: enzymatic conversion into protoporphyrin. Photochem Photobiol. 1998, 67(1): 150-154
32. Kennedy JC, Pottier RH. Endogenous protoporphyrin IX, a clinically useful photosensitizer for photodynamic therapy. J Photochem Photobiol B. 1992, 14(4): 275-292
33. Pottier RH, Chow YF, LaPlante JP, Truscott TG, Kennedy JC, Beiner LA. Non-invasive technique for obtaining fluorescence excitation and emission spectra in vivo. Photochem Photobiol. 1986, 44(5): 679-687
34. Peng Q, Warloe T, Berg K, Moan J, Kongshaug M, Giercksky KE, Nesland JM.

5-Aminolevulinic acid-based photodynamic therapy. Clinical research and future challenges. Cancer. 1997, 79(12): 2282-2308
35. Koenig K. Kienle A. Boehncke WH. Kaufmann R. Rueck AC. Meier T.H. Steiner RW. Photodynamic tumor therapy and on-line fluorescence spectroscopy after ALA administration using 633-nm light as therapeutic and fluorescence excitation radiation. Opt. Eng. 1994, 33(09): 2945-2952
36. Perotti C, Fukuda H, DiVenosa G, MacRobert AJ, Batlle A, Casas A. Porphyrin synthesis from ALA derivatives for photodynamic therapy. In vitro and in vivo studies. Br J Cancer. 2004, 90(8): 1660-1665
37. ISHIHARA SANGYO KAISHA, LTD. "FAQ for GenomONE-Neo EX"
38. El-Zaria ME, Ban HS, Nakamura H. Boron-containing protoporphyrin IX derivatives and their modification for boron neutron capture therapy: synthesis, characterization, and comparative in vitro toxicity evaluation. Chemistry. 2010, 16(5): 1543-1552
39. Anzaldi LL, Skaar EP. Overcoming the heme paradox: heme toxicity and tolerance in bacterial pathogens. Infect Immun. 2010 Dec;78(12):4977-4989
40. Ito M, Yamamoto S, Nimura K, Hiraoka K, Tamai K, Kaneda Y. Rad51 siRNA delivered by HVJ envelope vector enhances the anti-cancer effect of cisplatin. J Gene Med. 2005, 7(8): 1044-1052
41. Okada Y. Sendai virus-induced cell fusion. Methods Enzymol. 1993;221: 18-41
42. Ohgari Y, Nakayasu Y, Kitajima S, Sawamoto M, Mori H, Shimokawa O, Matsui H, Taketani S. Mechanisms involved in delta-aminolevulinic acid (ALA)-induced photosensitivity of tumor cells: relation of ferrochelatase and uptake of ALA to the accumulation of protoporphyrin. Biochem Pharmacol. 2005, 71(1-2): 42-49
43. Nishiyama N, Nakagishi Y, Morimoto Y, Lai PS, Miyazaki K, Urano K, Horie S, Kumagai M, Fukushima S, Cheng Y, Jang WD, Kikuchi M, Enhanced photodynamic cancer treatment by supramolecular nanocarriers charged with dendrimer phthalocyanine. J Control Release. 2009, 133(3): 245-251
44. Herlambang S, Kumagai M, Nomoto T, Horie S, Fukushima S, Oba M, Miyazaki K, Morimoto Y, Nishiyama N, Kataoka K. Disulfide crosslinked polyion complex micelles encapsulating dendrimer phthalocyanine directed to improved efficiency of photodynamic therapy. J Control Release. 2011, 155(3): 449-445
45. De Rosa FS, Marchetti JM, Thomazini JA, Tedesco AC, Bentley MV. A vehicle for photodynamic therapy of skin cancer: influence of dimethylsulphoxide on 5-aminolevulinic acid in vitro cutaneous permeation and in vivo protoporphyrin IX accumulation determined by confocal microscopy. J Control Release. 2000, 65(3): 359-366
46. De Rosa FS, Lopez RF, Thomazine JA, Tedesco AC, Lange N, Bentley MV. In vitro metabolism of 5-ALA esters derivatives in hairless mice skin homogenate and in vivo PpIX accumulation studies. Pharm Res. 2004, 21(12): 2247-2252
47. Furre IE, Shahzidi S, Luksiene Z, Møller MT, Borgen E, Morgan J, Tkacz-Stachowska K, Nesland JM, Peng Q. Targeting PBR by hexaminolevulinate-mediated photodynamic therapy induces apoptosis through translocation of apoptosis-inducing factor in human leukemia cells. Cancer Res. 2005, 65(23): 11051-11060
48. Nakamura H, Kimura T, Ikegami H, Ogita K, Koyama S, Shimoya K, Tsujie T, Koyama M, Kaneda Y, Murata Y. Highly efficient and minimally invasive in-vivo gene transfer to the mouse uterus using haemagglutinating virus of Japan (HVJ) envelope vector. Mol Hum Reprod. 2003, 9(10): 603-609
49. Nishikawa M, Huang L. Nonviral vectors in the new millennium: delivery barriers in gene transfer. Hum Gene Ther. 2001, 12(8):861-870
50. Morishita N, Nakagami H, Morishita R, Takeda S, Mishima F, Terazono B,

Nishijima S, Kaneda Y, Tanaka N. Magnetic nanoparticles with surface modification enhanced gene delivery of HVJ-E vector. Biochem Biophys Res Commun. 2005, 334(4): 1121-1126
51. Kushibiki T, Sakai M, Awazu K. Differential effects of photodynamic therapy on morphologically distinct tumor cells derived from a single precursor cell. Cancer Lett. 2008, 268(2): 244-251
52. Kaneda Y, Saeki Y, Morishita R. Gene therapy using HVJ-liposomes: the best of both worlds? Mol Med Today. 1999, 5(7): 298-303
53. Saga K, Tamai K, Kawachi M, Shimbo T, Fujita H, Yamazaki T, Kaneda Y. Functional modification of Sendai virus by siRNA. J Biotechnol. 2008, 133(3): 386-394
54. Kaneda Y, Tabata Y. Non-viral vectors for cancer therapy. Cancer Sci. 2006, 97(5): 348-354
55. Kaneda Y, Yamamoto S, Nakajima T. Development of HVJ Envelope Vector and Its Application to Gene Therapy. Adv Genet. 2005, 53PA: 307-332
56. Geze M, Morliere P, Maziere JC, Smith KM, Santus R. Lysosomes, a key target of hydrophobic photosensitizers proposed for photochemotherapeutic applications. J Photochem Photobiol B. 1993, 20(1): 23-35
57. Berg K, Moan J. Lysosomes and microtubules as targets for photochemotherapy of cancer. Photochem Photobiol. 1997, 65(3): 403-409
58. MacDonald IJ, Morgan J, Bellnier DA, Paszkiewicz GM, Whitaker JE, Litchfield DJ, Dougherty TJ. Subcellular localization patterns and their relationship to photodynamic activity of pyropheophorbide-a derivatives. Photochem Photobiol. 1999, 70(5): 789-797
59. Kawaguchi Y, Miyamoto Y, Inoue T, Kaneda Y. Efficient eradication of hormone-resistant human prostate cancers by inactivated Sendai virus particle. Int J Cancer. 2009, 24(10): 2478-2487

Section 2. Differential effects of photodynamic therapy on morphologically distinct tumor cells derived from a single precursor cell

I. Introduction

Currently, PDT has been approved for localized diseases and precancerous lesions, such as bladder cancers, pituitary tumors, and glioblastomas[1,2]. Furthermore, numerous ongoing clinical studies have been designed to optimize the conditions of PDT, and thereafter PDT has been approved in several countries. However, one inherent consequence of PDT is local hypoxia, which can arise directly from oxygen consumption during treatment[3-5] or indirectly from the destruction of the tumor vasculature as a result of effective treatment[6,7]. Hypoxia is a major stimulus for angiogenesis, through its stabilization of the hypoxia-inducible factor-1α (HIF-1α) transcription factor[8], which results in an increase in the production and secretion of vascular endothelial growth factor (VEGF)[9]. Following PDT, an increase in VEGF secretion[10,11] and angiogenic responses have been documented *in vivo*[12,13]. VEGF induction could contribute to tumor survival and regrowth, and therefore could be one of the factors impairing PDT from achieving its full tumoricidal potential. Therefore, a better understanding of responses by tumor cells following PDT will help design new interventions and potentially improve the long-term survival of PDT treated patients.

It is well known that the cells in a tumor tissue are heterogeneous in terms of their morphologies and differentiation statuses, even if the tumor tissue consists of a progeny that is derived from a single neoplastic cell[14]. Although cultured tumor cells have also been characterized by their morphological heterogeneity, the extent of cellular morphological heterogeneity cannot be easily evaluated. When Shimada et al. assessed the survival of 31 cultured human esophageal tumor cells using a colony-forming assay[15], they found that one cell group (KYSE 70) formed multiple morphologically distinct colonies in a single dish. Classification of the colonies made it possible to evaluate the extent of the morphological heterogeneity. Here, I isolated five types of cells from a single clone of KYSE70 cells. The sensitivity of some of these isolated cells to PDT was significantly higher than that of others, irrespective of their intracellular concentration of talaporfin sodium (the photosensitizer). In addition, the VEGF production by each cell type was different after PDT. Based on these results, I propose that a small fraction of tolerant cells may actively grow and predominate after PDT, even though most of the non-tolerant cells in the original tumor tissue were selectively killed by the repeated treatment in clinical therapy.

II. Materials and methods

1. Materials

Talaporfin sodium (Mono-l-aspartyl chlorin e6, Laserphyrin®, kindly provided by Meiji Seika Co. Ltd., Japan), composed of aspartic acid conjugated by means of an amide bond to the D ring of the chlorin structure, with an absorption peak at 664 nm, was used as the photosensitizer. A continuous wave semiconductor laser generator was used, wavelength; 664 ± 1 nm (JENOPTIK unique-mode GmbH, Germany). The cells on a culture plate were irradiated by the laser via a fiber attached to the bottom of the culture plate. An optical instrument with an automated stage for positioning was purchased from Sigma Koki Co. Ltd., Japan.

2. Cell culture and isolation

The KYSE70 cells were cultured at 37 °C and 5% CO2 in Dulbecco's Modified Eagle's Medium (DMEM) (Sigma-Aldrich Inc., MO) containing 10% fetal calf serum (FCS, BioWest Inc., France), 100 units/mL penicillin, and 0.1 mg/mL streptomycin (Nacalai Tesque, Japan). Shimoda et al. previously described the origins and other details of this

cell type and established the KYSE70 cells from a poorly differentiated human squamous cell carcinoma (from an esophageal cancer that had developed in a 77-year-old Japanese male)[15,16]. A KYSE70 cell suspension (10 cells/mL) was inoculated into each well of a 96-well plate (100 μL/well, Corning Inc., NY), and the cells were incubated for 3 days. Under microscopic observation, only a single morphological formation of cells in each well was selected and cultured continuously. The cell number of each cell type was sequentially counted to calculate the cell growth rate.

3. Growth speed

For stationary culture, 100 μL of each selected morphological cell subclone was inoculated into 96-well (625 cells/well). 24, 48, 72, 96, 120 hours later, the cells were counted by MTT assay. The Cell Counting Reagent SF kit (Nacalai Tesque), based on a water-soluble tetrazolium compound, was used for the counting assay.

4. Setermination of the cell size

The suspending solution (1×10^6 cells/mL) was made and cell diameter was measured by Coulter counter method using flow cytometer (Cell Lab Quanta SC MPL, Beckman Coulter Inc.).

5. Anticancer drug resistance

For stationary culture, 100 μL of each selected morphological cell subclone was inoculated into 96-well (5×10^3 cells/well). Twenty-four hours later, when the cells had adhered to the plate, the medium was removed and the cultures were washed three times in a phosphate buffered saline solution (PBS, pH 7.4, Sigma). Then, 100 μL of 5-Fluorouracil (5-FU, Sigma-Aldrich Inc. was added to each well (62.5, 125, 250, 500 or 1000 μg/mL) dissolved in FCS free DMEM). After 48 h, the cells were counted by MTT assay.

6. Talaporfin sodium uptake by cells

For stationary culture, 100 μL of each selected morphological cell subclone was inoculated into a Black with Clear Bottom 96-well Microtest™ Optilux™ Plate (BD Bioscience Inc., CA) (1×10^4 cells/well). Twenty-four hours later, when the cells had adhered to the plate, the medium was removed and the cultures were washed three times in a phosphate buffered saline solution (PBS, pH 7.4, Sigma). Then, 100 μL of talaporfin sodium was added to each well (10, 30, or 50 μg/mL; dissolved in FCS free DMEM). After 2 h, the supernatant was removed and the cells were washed three times thoroughly with PBS, lysed with 100 μL of 0.05% sodium dodecyl sulfate solution at 37 °C for 20 min, and the intracellular uptake of talaporfin sodium was quantified using a multi-mode microplate reader (SpectraMax M5®, Molecular Devises Co. Ltd., CA) with excitation and emission wavelength of 405 and 672 nm, respectively. Then the cells were counted by fluorometric quantitation of cell DNA with Hoechst 33342 solution (Nacalai Tesque, Japan) according to the assay protocol[17]. The fluorescence interference between the intercalated Hoechst 33342 and the talaporfin sodium was separated using an optical filter instrument. A calibration curve between the concentration of DNA and the number of cells was made using cell suspensions with different known cell concentrations. All experiments were performed seven independent times.

7. Amount of generated ROS

The way of talaporfin sodium uptake was described above. The medium was replaced to FCS free DMEM added Fluorescent detector of highly ROS (Aminophenyl fluorescein, APF). Cells were then subjected to laser irradiation (30 mW/cm^2) for 0, 30, 60, or 180 s.

After PDT, the fluorescence of APF (405 nm) was measured.

8. Evaluation of the antitumor activity of PDT using talaporfin sodium and a semiconductor laser

Each selected morphological cell subclone was inoculated and exposed to talaporfin sodium dissolved in FCS free DMEM (10, 30, or 50 μg/mL) as described for the talaporfin sodium uptake assay. Cells in FCS free DMEM were then subjected to laser irradiation (30 mW/cm^2) for 0, 5, 10, 30, 60, or 180 s. After laser irradiation, the culture medium was replaced with complete growth medium. After 24 h, the number of cells was counted to evaluate their sensitivity to PDT using MTT assay. The SpectraMax M5 was used to measure the absorbance at a wavelength of 450 nm. All experiments were done three independent times. The results of these counts were independently verified using a DNA based counting method.

Colony assay was also used to counting cell number. The cells after PDT were retrieved and inoculated into a 6-well plate (costar(R) 3595, Corning Inc.) (100 cells/well or 1000 cells/well). They were cultured for 7days using DMEM containing 1.2% methylcellulose (R&D Systems, Inc.) and the number of colony was counted.

Chronological change of cell survival rate was also measured. Cells were counted 3, 6, 12 or 24 h after PDT using MTT assay.

To determine the rate of talaporfin sodium photobleaching, a photobleaching test was performed using a talaporfin sodium solution. The talaporfin sodium was photobleached based on the formula: $C = C_0 \exp(-kt)$, where C is the concentration at time (t), C0 is the initial concentration of talaporfin sodium, and k is the coefficient of photobleaching. The value of k was determined experimentally to be 0.0024, when the initial concentration of talaporfin sodium was 10, 30, or 50 μg/mL. From this result, we estimated that 90% of talaporfin sodium remained in the cells after a 60 s laser irradiation.

9. Area under the curve (AUC) calculations

To clarify the relationships between phototoxicity (PDT effects), laser irradiation time, and the intracellular uptake of talaporfin sodium, the area under the phototoxicity–laser irradiation time curve (AUC) was calculated using the linear trapezoidal method and the correlation between the AUC and the intracellular concentration of talaporfin sodium was evaluated.

10. ELISAs

Each selected morphological cell subclone was inoculated, exposed talaporfin sodium dissolved in FCS free DMEM (10, 30, or 50 μg/mL), and laser irradiated as described above. Twenty-four hours later, the VEGF level in the cell culture medium was quantified from each sample using a Quantikine human VEGF ELISA kit (R&D Systems, Minneapolis, MN).

11. Statistical analyses

All data were expressed as means ± the standard derivation. Statistical significance (defined as P values <0.01) was evaluated using an unpaired Student's t-test (two-tailed).

III. Results

1. Appearance of morphologically variable cells

Cells with varying morphologies were observed in a well, in which a single KYSE70 cell had been inoculated (Figure 2-2-1). These cells were classified into five types (subclones

#1–5): Subclones #1, #3, and #4 were flat and diffusive cells, and subclones #2 and #5 consisted of cell mounds.

The cell growth rate was different for each subclone, but there were no correlations between cell morphology and growth rate (Figure 2-2-2). The cell diameter was measured by Coulter counter method (Table 2-2-1.). Each subclone is significant difference from all other subclones. The biggest is #4 and the smallest is #5. And the sensitivity to anti-cancer drug was shown in Figure 2-2-3. Subclone #3, #4 had have great sensitivity.

2. Photosensitizer uptake by cells

The relationship between the initial concentration of talaporfin sodium in the culture medium and its intracellular uptake is shown in Figure 2-2-4. The amount of talaporfin sodium that was taken up by the cells reached a plateau at 2 h (data not shown). Irrespective of the concentration of talaporfin sodium in the medium, the cells from subclone #3 took up much talaporfin sodium. However, there was no correlation between the amount of intracellular talaporfin sodium uptake and cell morphology. When observed under fluorescence microscopy, the cytoplasm was the major site for talaporfin sodium uptake, with little talaporfin sodium in the nuclei of any of the cell subclones (data not shown).

To ensure that the lack of serum did not affect the uptake of talaporfin sodium, I measured the intracellular uptake by each cell subclone in culture medium containing 10% serum. Under these conditions, the uptake of talaporfin sodium was slightly lower compared with the uptake in serum free culture medium. However, these differences were not significant.

3. Amount of generated ROS

The amount of ROS generated by PDT was measured using APF fluorescence. The fluorescence intensity was expressed against the laser irradiation time in Figure 2-2-5. Subclone #1, #2 and #4 generate more ROS than #3 and #5 regardless of talaporfin sodium

4. Evaluation of the antitumor activity and VEGF secretion after PDT using talaporfin sodium and a semiconductor laser

The cytocidal effects of PDT were evaluated for each cell subclone. When the concentration of talaporfin sodium was 30 or 50 μg/mL, the phototoxicity of PDT was proportional to the length of laser irradiation (Figure 2-2-6). However, irrespective of talaporfin sodium concentration, the phototoxicity in subclones #2 and #5 was markedly lower than in the other clones 3 h after PDT. Additionally, when the concentration of talaporfin sodium was 10 μg/mL, there was no obvious effect of PDT on any of the subclones. Figure 2-2-7 is a result of antitumor activity measured by colony assay. The antitumor effect was measured larger compared with MTT assay.

The correlations between the areas under the phototoxicity–laser irradiation time curves (AUC, calculated from Fig. 2-2-5) and the amounts of intracellular talaporfin sodium uptake (Fig. 2-2-4) are shown in Figure 2-2-8. These data revealed that under these conditions, subclones #3 and #4 were more resistant to PDT than subclones #1, #2 and #5, irrespective of the amount of intracellular talaporfin sodium or the laser irradiation time.

The amount of VEGF released into the cell culture medium was quantified 24 h after PDT for each subclone (Figure 2-2-9). Since PDT decreased the number of cells for subclones #1 and #2, the concentrations of VEGF in the culture media was also decreased when 30 or 50 μg/mL of talaporfin sodium was added. However, their VEGF concentrations were increased after PDT when the talaporfin sodium concentration was

10 μg/mL. In contrast, VEGF production was not detected in culture media of subclones #3–5 before or after PDT.

IV. Discussion

Morphological heterogeneity is frequently observed in cells cultured in vitro[15-18]. In general, these alterations are induced by intracellular and/or microenvironmental alterations and are considered to be reversible. Shimoda et al. found that a single cultured human tumor cell (KYSE70) formed multiple types of colonies in a culture dish[15]. I classified these cells into 5 groups according to their morphologies (Fig. 2-2-1), which did not change over the course of our experiments.

I compared the growth speeds (Fig. 2-2-2), cell diameters (Table 2-2-1), and resistances to anti-tumor drugs (Fig. 2-2-3) among the 5 groups and found that subclone #3 grew the most rapidly but was less sensitive to drugs than was subclone #4 and more sensitive than were subclones #1, #2, and #5. Although highly proliferative cells are generally more drug-sensitive, subclone #5 was the most drug-sensitive despite a growth rate similar to those of subclones #1, #2, and #4. These results show that the proliferation potential of the 5 subclones was not related to the 5-FU sensitivity. There have been some reports of a drug-efflux pump effective against 5-FU, and some of the subclones may express this pump[19].

From the morphologically variable appearances of the cells, it might be expected that differences in cell surface area would influence the intracellular concentrations of talaporfin sodium, as the cell surface area can contribute to the uptake of this drug,. However, there was no correlation between the apparent cell surface areas and the intracellular talaporfin sodium levels, suggesting that the cell populations, although derived from a single cell, have markedly heterogeneous intrinsic talaporfin sodium uptake properties. While the growth rates differed among these cell subclones and may have affected the uptake of talaporfin sodium, my experiments only lasted 2 h in serum-free medium, allowing us to ignore any growth-related changes in uptake.

In PDT, the presence of a drug-efflux pump would reduce the drug amount. In my experiments, therefore, the presence of a drug-efflux pump should be related to the PDT effect. The survival rates for the subclones after PDT were measured by the MTT assay and the values found to differ (Fig. 2-2-7). The cell proliferation and the times between cell damage and death after PDT were also different. The cytotoxicity estimated by colony assay was higher than indicated by the MTT assay, possibly because cells may not die until a few days after the damage occurs[27,28]. In my experiments, the cells continued to die over 24 h after PDT.

To clarify the correlation between the effects of PDT (phototoxicity vs. laser irradiation time) and the intracellular talaporfin sodium concentrations, I analyzed the relationship between AUC (calculated from a graph plotting phototoxicity against laser irradiation time) and the intracellular concentration of talaporfin sodium (Fig. 2-2-4). The results indicated that cell subclones #1, #2 and #5 were more sensitive to PDT than were cell subclones #3 and #4, despite having lower levels of intracellular talaporfin sodium. Therefore, although cell subclones #3 and #4 took up larger amounts of talaporfin sodium, this uptake did not boost the effects of PDT. A number of studies have examined the effectiveness of photosensitizers on multidrug resistant cellswith a focus on the effects of the P-glycoprotein (P-gp) or the ATP binding cassette (ABC) transporter on the efficacy of PDT[20-26]. Some multidrug-resistant ABC transporters might be expressed in KYSE70 cells; the possibilities include MDR1/P-gp/ABCB1 (multidrug resistance gene 1/P-glycoprotein/ATP-binding cassette family B1), MRP1/ABCC1 (multidrug resistance-associated protein/ATP-binding cassette family C1), and BCRP/ABCG2 (breast cancer resistance protein/ATP-binding cassette family G2). Therefore, due to the potential influence of drug efflux pumps on intracellular

talaporfin sodium levels and consequently on PDT, in this study I measured the amounts of intracellular talaporfin sodium just before laser irradiation.

Numerous studies have reported biological changes in cells in response to PDT, such as decreased cell adhesion[29,30] and increased production of cytokines[31] and levels of heat shock proteins[32]. Those studies also described the effects of subcurative PDT and reported increased VEGF production both *in vitro* and *in vivo*. In this study, only 2 of the 5 subclones expressed VEGF (Fig. 2-2-9), and VEGF expression was decreased after PDT (in proportion to the decrease in cell number) in those subclones. However, VEGF production was increased when the PDT effect was not sufficient to decrease the number of cells (10 μg/mL talaporfin sodium). The details of the clinical relevance of the induction of VEGF by PDT are currently under investigation, but VEGF could contribute to tumor survival and regrowth and could therefore be one of the factors preventing PDT from achieving its full tumoricidal potential. A better understanding of the responses to PDT and VEGF secretion capacities of morphologically heterogeneous tumor cells could significantly improve therapeutic outcomes.

Morphologically heterogeneous cells have been observed frequently not only in primary tumors[14] but also in metastatic[33] and recurrent tumors[34] after tumor therapy, although it remains unknown whether such morphological alterations are reversible. Tumor recurrence is a serious problem for patients because recurrent tumors are frequently more malignant than primary tumors[35]. Furthermore, it is well known that recurrent tumors are usually more resistant to further chemo- or radiotherapy. Two hypotheses might explain this resistance. First, treated cells become committed to de-differentiation and thus acquire tolerance. Second, a large fraction of the non-tolerant cells in the original tumor tissue are selectively killed by repeated treatments, leaving only a small number of more tolerant cells to grow actively and become predominant. My data show that cell subclones #1, #2, and #5 were more PDT-sensitive than were subclones #3 and #4. If the subclone #3 and #4 cells more actively migrate to other tissues, it could explain why PDT has been slow to gain acceptance as an alternative to conventional tumor therapies. Therefore, a better understanding of the influence of tumor cell heterogeneity on the clinical applications of PDT will aid in the design of new interventions and potentially improve the long-term survival of PDT-treated patients. Further improvements in the clinical applications of PDT for heterogeneous tumor cells can be expected, and improved PDT may ultimately be useful as a clinical antitumor therapy.

Figures

Table 2-2-1 The cell diameter in each subclones. Each subclone is significant difference from all other subclones.

cell subclone	Cell diameter (± SD) [μm]
#1	13.8 (± 3.8)
#2	13.2 (± 3.4)
#3	15.4 (± 4.3)
#4	17.2 (± 4.7)
#5	12.5 (± 3.5)

Table 2-2-2. Differential reactions on morphologically distinct tumor cells derived from a single precursor cell for talaporfin sodium Phortodynamic Therapy. Typical results are expressed. The bold face numbers indicate higher impacts or quantity than the other subclones.

	#1	#2	#3	#4	#5
Growth rate in five days	14	19	**45**	14	17
Intracellular concentration of talaporfin sodium [mg/cell] (dose concentration = 50 mg/mL)	1.10	1.30	**1.90**	**1.70**	0.81
Emergence amounts of ROS measured by APF intensity [a.u] (dose concentration = 50 mg/mL, Irradiatioin time = 180 s)	386	409	**806**	346	**666**
Survival rate of control after PDT (dose concentration = 50 mg/mL, Irradiatioin time = 180 s)	**0.06**	**0.08**	0.30	0.15	0.21
Amount of VEGF after PDT (dose concentration = 10 mg/mL, Irradiatioin time = 180 s)	**257**	**84**	0	2.6	9.7

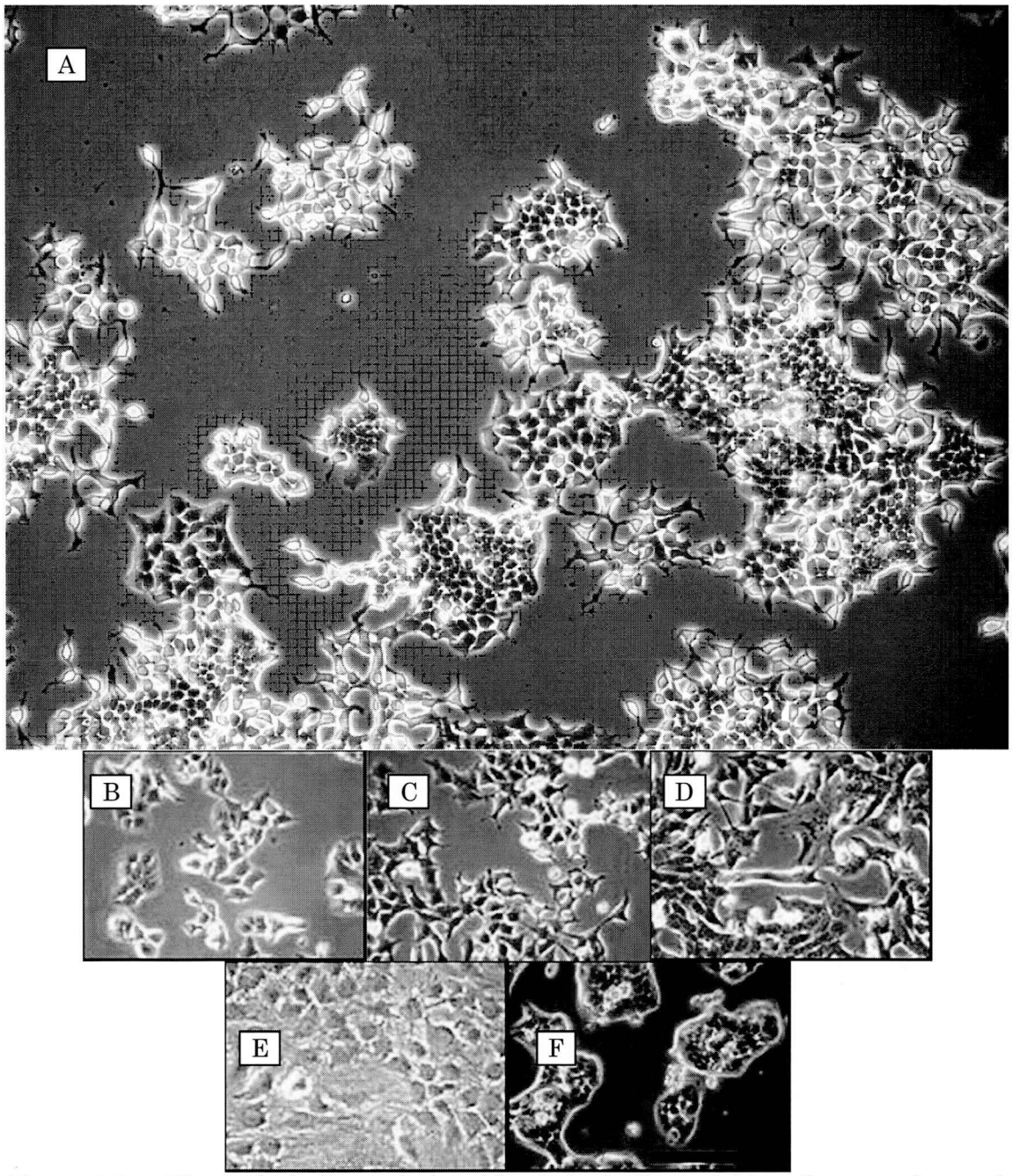

Figure 2-2-1. Morphologically variation. Morphologically variable cells were observed. (A) Only a single morphological formation of cells in one well were selected and cultured continuously. (B-F) Five subclones were separated from a single clone of KYSE70 cells. Bar = 200 μm.

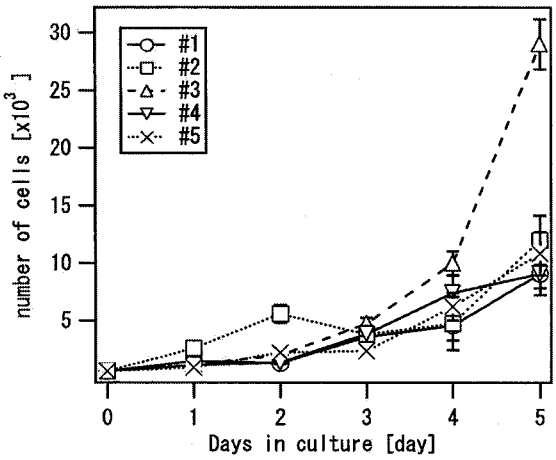

Figure 2-2-2. The cell growth rates of subclones #1–5. The cell growth rate was different for each subclone and there was no correlation between the morphology of a cell and its growth rate. The symbols indicate cell subclones (○; #1,□; #2, △; #3, ▽; #4. ×; #5).

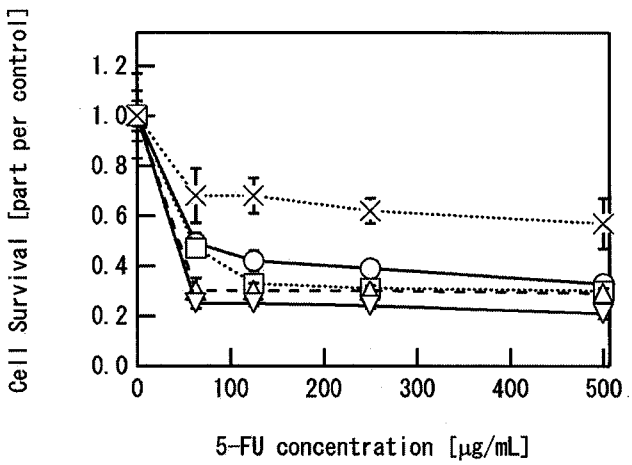

Figure 2-2-3. Antitumor effect of 5-FU in each subclone. The cell survival rate was expressed against the concentration of 5-FU. Cell subclone # is indicated as ○; #1,□; #2, △; #3, ▽; #4. ×; #5. *Significant differences were shown below; 62.5 μg/mL: subclone #1 against #3, 4, subclone #2 against #3, 4, 5, subclone #3 against #1, 2, 5, subclone #4 against #1, 2, 5, subclone #5 against #2, 3, 4. 125 μg/mL : subclone #1 against #3, 4, 5, subclone #2 against #4, 5, subclone #3 against #1, 4, 5, subclone #4 against all other groups, subclone #5 against all other groups. 250 μg/mL : subclone #1 against all other groups, subclone #2 against #1, 4, 5, subclone #3 against #1, 4, 5, subclone #4 against all other groups, subclone #5 against all other groups, 500 μg/mL : subclone #1 against #4, 5, subclone #2 against #4, 5, subclone #3 against #4, 5, subclone #4 against all other groups, subclone #5 against all other groups.

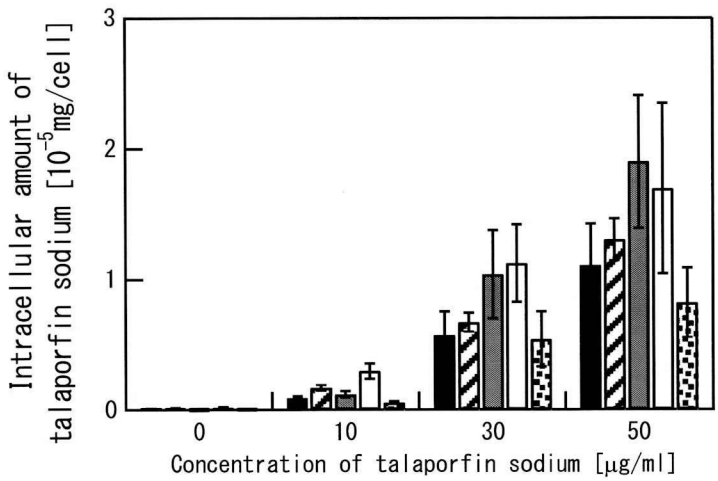

Figure 2-2-4. Intracellular uptake amount of talaporfin sodium into each cell subclone. Intracellular amount of talaporfin sodium was expressed against the initial concentration of talaporfin sodium in the culture medium. The bars indicate cell subclones (black bar; #1,slashed bar; #2, gray bar; #3, white bar; #4. dotted bar; #5).*Significant differences were shown below; 10 μg/mL: subclone #1 against #2, 4, 5, subclone #2 against #1, 4, 5, subclone #3 against #5, subclone #4 against #1, 2, 5, subclone #5 against all other groups. 30 μg/mL : subclone #1 against #4, subclone #2 against #4, subclone #4 against #1, 2, 5, subclone #5 against #4. 50 μg/mL : subclone #2 against #5, subclone #3 against #5, subclone #4 against #5, subclone #5 against #2, 3, 4.

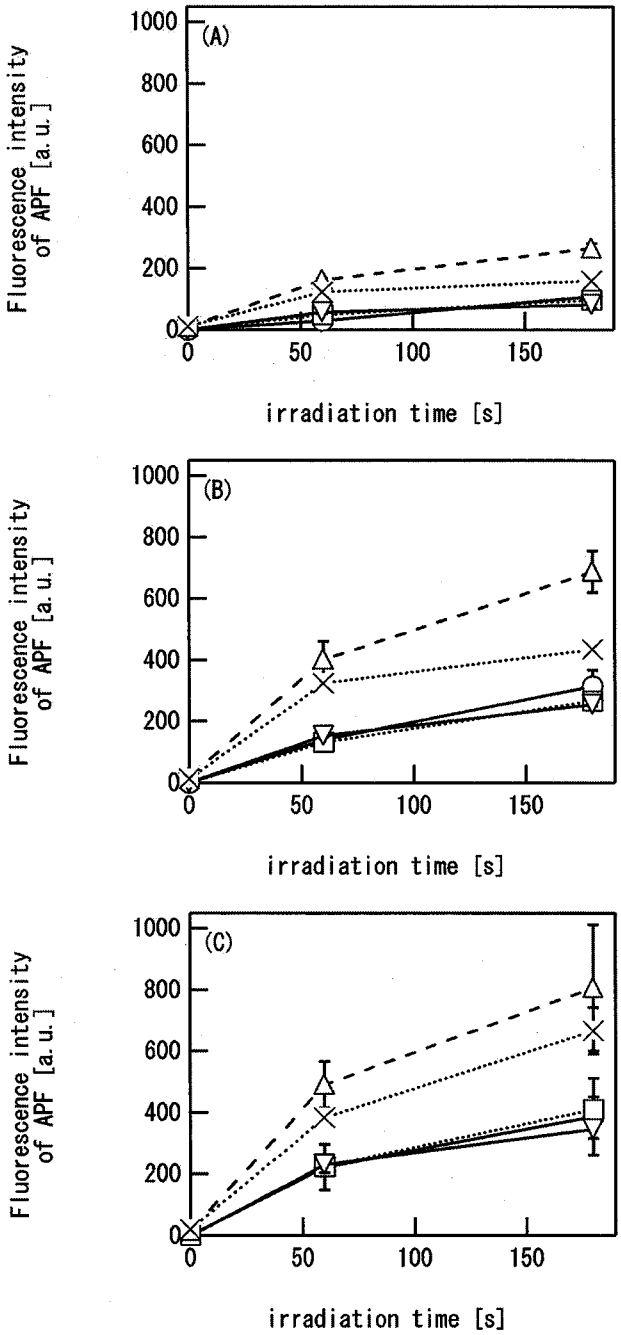

Figure 2-2-5. Fluorescence intensity of APF was expressed against the laser irradiation time when the initial concentration of talaporfin sodium in the culture medium was (A)10, (B)30, and (C)50 μg/mL. Cell subclone is indicated as ○; #1,□; #2, △; #3, ▽; #4. ×; #5.

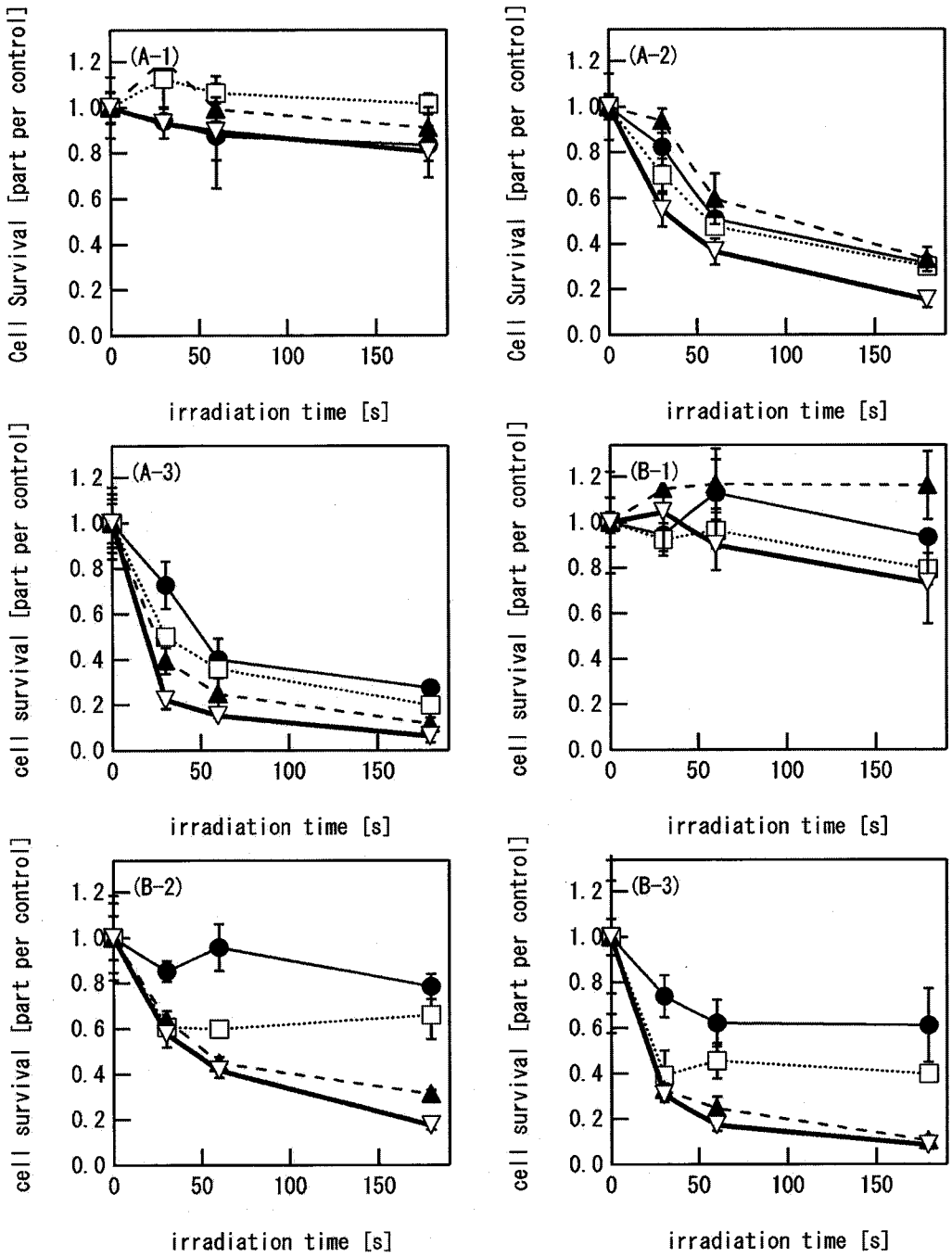

Figure 2-2-6. Chronological change of cell survival rate. The cell survival rate was expressed against the laser irradiation time when cell subclone is (A)subclone #1 and (B)#2, and subscript expressed the initial concentration of talaporfin sodium in the culture medium as (1)10, (2)30, and, (3)50 μg/mL.. Elapsed time is indicated as ●; 3 h, □; 6 h, ▲;12 h, ▽; 24 h. The initial concentration of talaporfin sodium in the culture medium was 50 μg/mL. (continued)

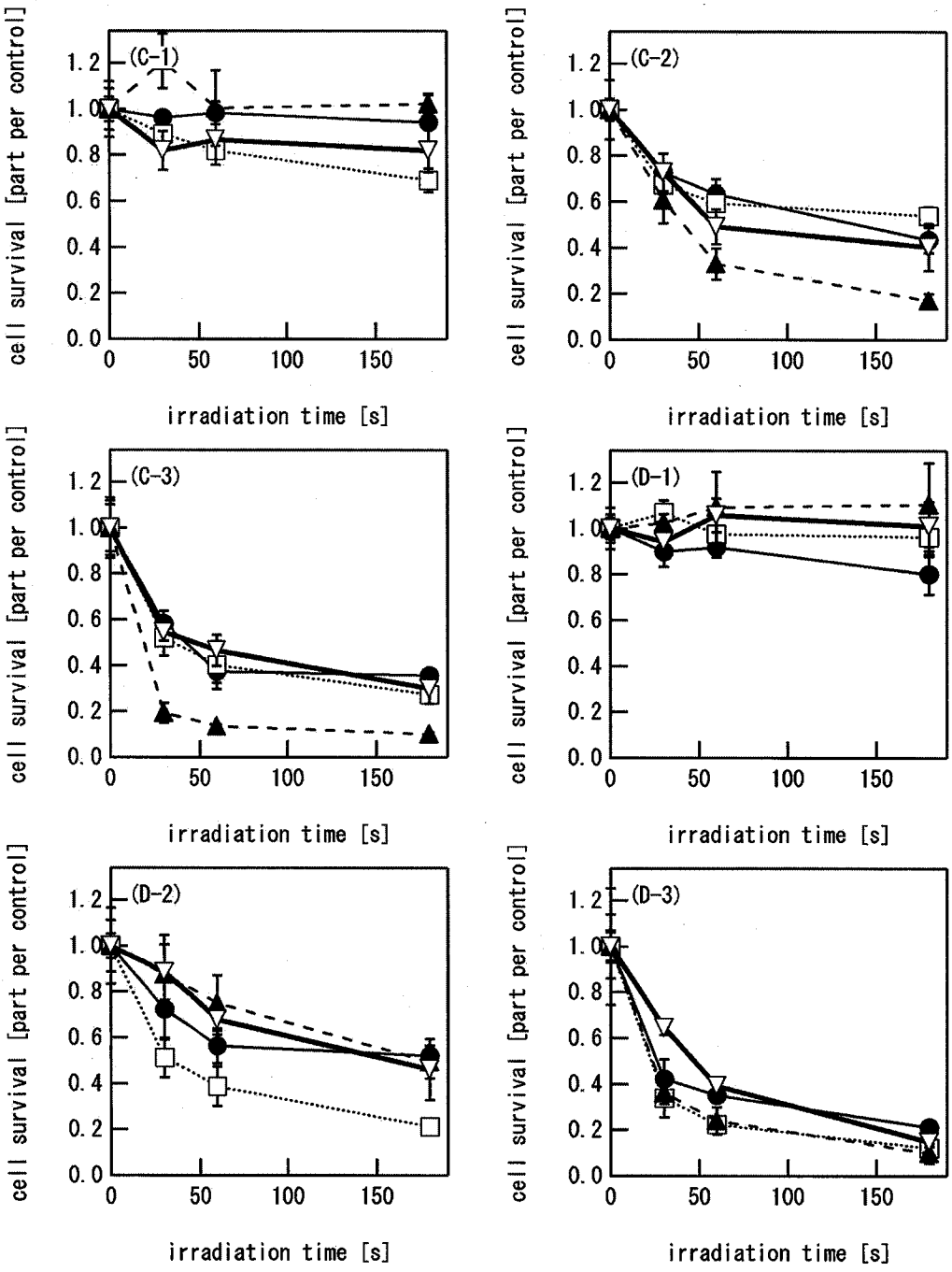

Figure 2-2-6. Chronological change of cell survival rate. The cell survival rate was expressed against the laser irradiation time when cell subclone is (C)subclone #3 and (D)#4 and subscript expressed the initial concentration of talaporfin sodium in the culture medium as (1)10, (2)30, and, (3)50 μg/mL.. Elapsed time is indicated as ●; 3 h, □; 6 h, ▲;12 h, ▽; 24 h. The initial concentration of talaporfin sodium in the culture medium was 50 μg/mL. (continued)

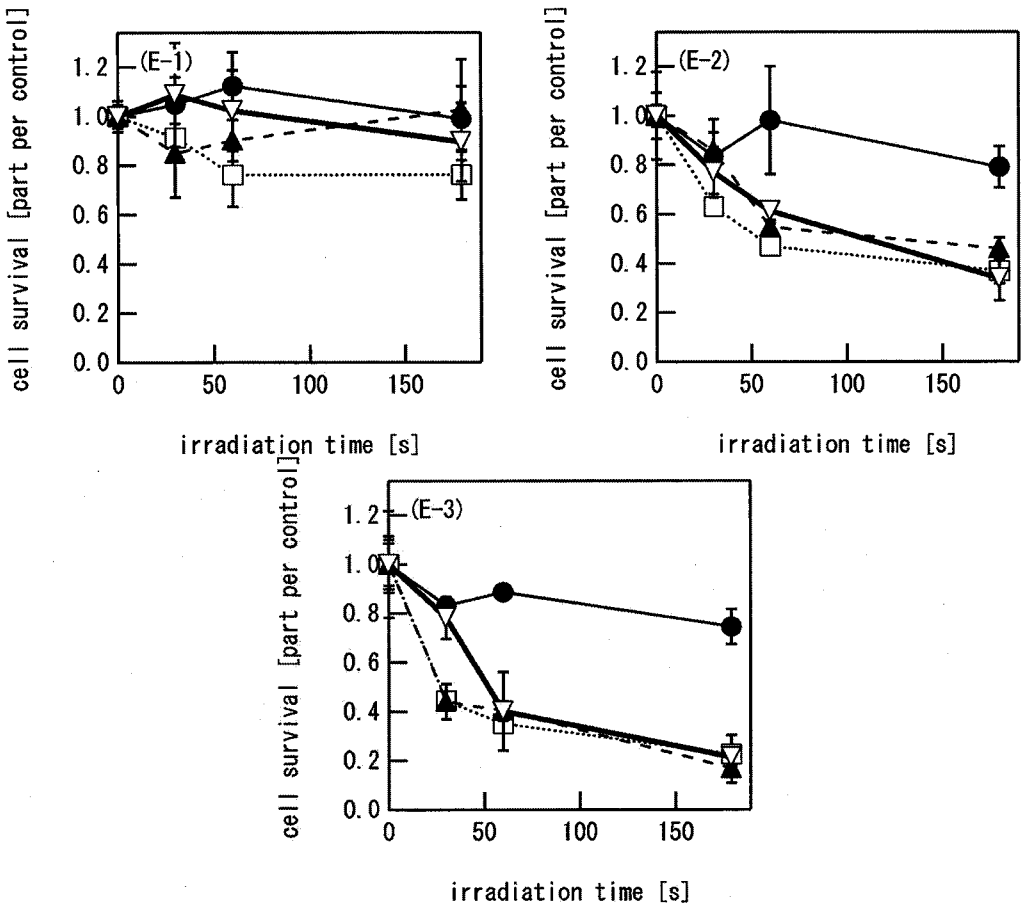

Figure 2-2-6. Chronological change of cell survival rate. The cell survival rate was expressed against the laser irradiation time when cell subclone is (A)subclone #1, (B)#2, (C)#3, (D)#4 and (E)#5 and subscript expressed the initial concentration of talaporfin sodium in the culture medium as (1)10, (2)30, and, (3)50 μg/mL.. Elapsed time is indicated as ●; 3 h, □; 6 h, ▲;12 h, ▽; 24 h. The initial concentration of talaporfin sodium in the culture medium was 50 μg/mL.

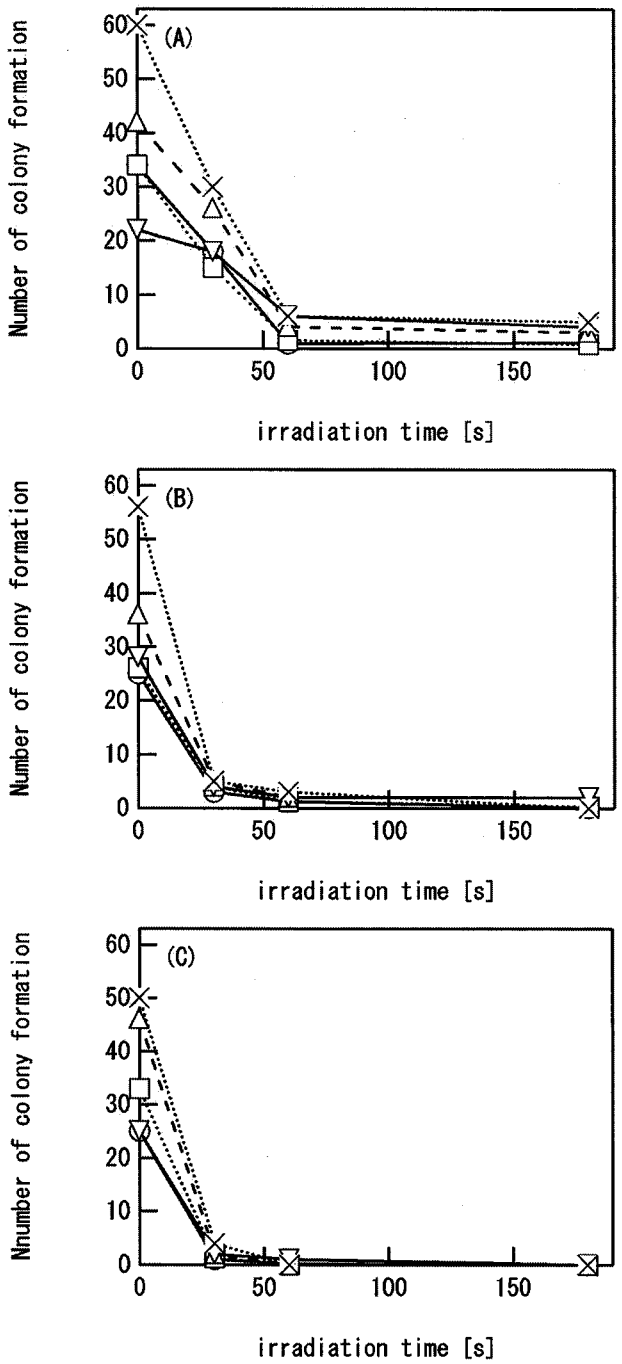

Figure 2-2-7. Antitumor effect of PDT using talaporfin sodium measured by colony forming assay. The number of colony formation was expressed against the laser irradiation time when the initial concentration of talaporfin sodium in the culture medium was (A)10, (B)30, and, (C)50 μg/mL. Cell subclone is indicated as ○; #1,□; #2, △; #3, ▽; #4. ×; #5.

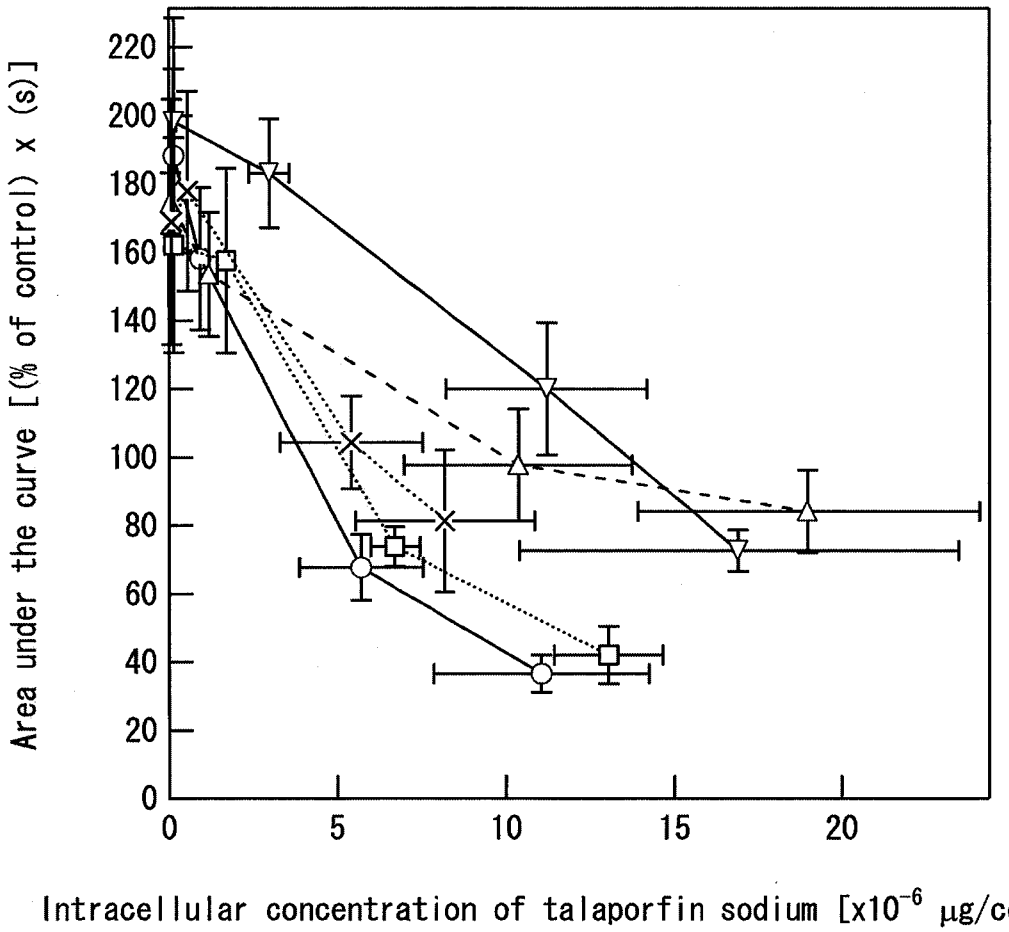

Figure 2-2-8. Relationship between AUC (calculated from cell survival rate-laser irradiation time; Fig. 2-2-4) and intracellular concentration of talaporfin sodium. Cell subclone was indicated as ○; #1,□; #2, △; #3, ▽; #4. ×; #5.

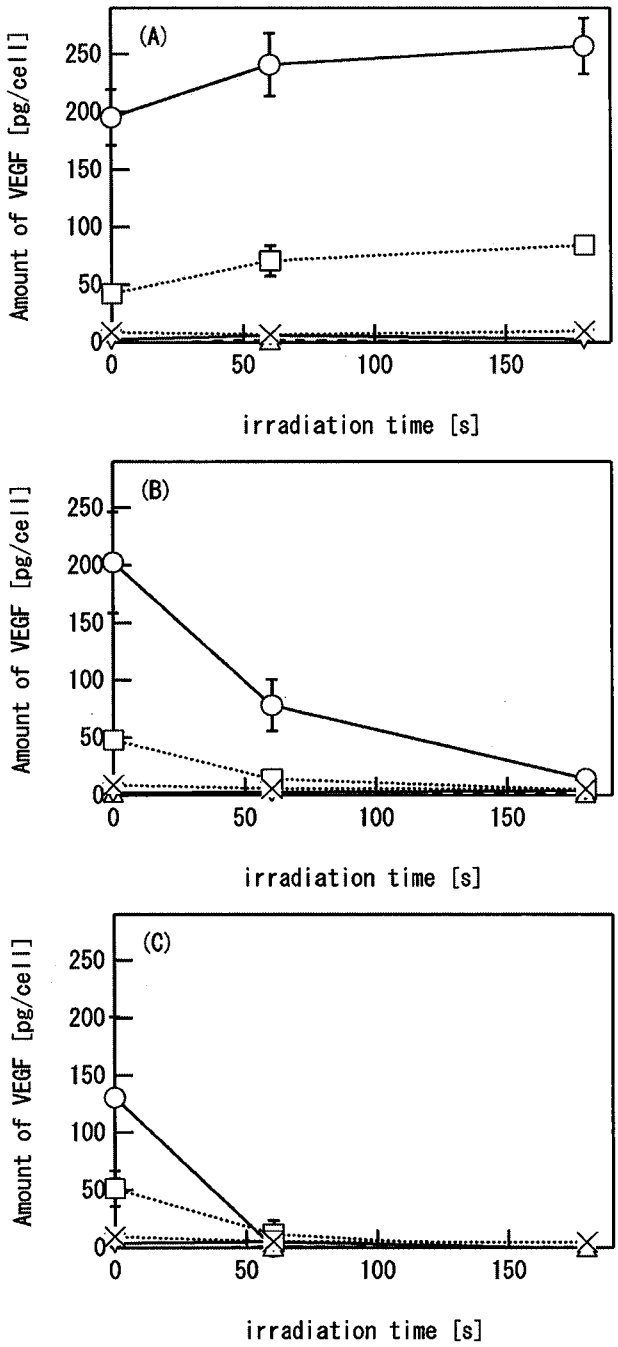

Figure 2-2-9. Amount of VEGF after PDT using talaporfin sodium. Amount of VEGF was expressed against the irradiation time when the initial dose concentration of talaporfin sodium in the culture medium was; 10(A), 30(B), and 50(C) μg/mL. Cell subclone is indicated as ○; #1,□; #2, △; #3, ▽; #4. ×; #5.

References

1. SB, Brown EA, Walker I. The present and future role of photodynamic therapy in cancer treatment. Lancet Oncol. 2004, 5(8):497-508
2. Dougherty TJ. An update on photodynamic therapy applications. J Clin Laser Med Surg. 2002, 20(1):3-7
3. Sitnik TM, Hampton JA, Henderson BW. Reduction of tumour oxygenation during and after photodynamic therapy in vivo: effects of fluence rate. Br J Cancer. 1998, 77(9):1386-1394
4. Henderson BW, Busch TM, Vaughan LA, Frawley NP, Babich D, Sosa TA, Zollo JD, Dee AS, Cooper MT, Bellnier DA, Greco WR, Oseroff AR. Photofrin photodynamic therapy can significantly deplete or preserve oxygenation in human basal cell carcinomas during treatment, depending on fluence rate. Cancer Res. 2000, 60(3):525-529
5. Chen Q, Huang Z, Chen H, Shapiro H, Beckers J, Hetzel FW. Improvement of tumor response by manipulation of tumor oxygenation during photodynamic therapy. Photochem Photobiol. 2002, 76(2):197-203
6. Engbrecht BW, Menon C, Kachur AV, Hahn SM, Fraker DL. Photofrin-mediated photodynamic therapy induces vascular occlusion and apoptosis in a human sarcoma xenograft model. Cancer Res. 1999, 59(17):4334-4342
7. Fingar VH, Kik PK, Haydon PS, Cerrito PB, Tseng M, Abang E, Wieman TJ. Analysis of acute vascular damage after photodynamic therapy using benzoporphyrin derivative (BPD). Br J Cancer. 1999, 79(11-12):1702-178
8. Semenza GL. HIF-1 and mechanisms of hypoxia sensing. Curr Opin Cell Biol. 2001, 13(2):167-171
9. Forsythe JA, Jiang BH, Iyer NV, Agani F, Leung SW, Koos RD, Semenza GL. Activation of vascular endothelial growth factor gene transcription by hypoxia-inducible factor 1. Mol Cell Biol. 1996, 6(9):4604-4613
10. Deininger MH, Weinschenk T, Morgalla MH, Meyermann R, Schluesener HJ. Release of regulators of angiogenesis following Hypocrellin-A and -B photodynamic therapy of human brain tumor cells. Biochem Biophys Res Commun. 2002, 298(4):520-530
11. Ferrario A, von Tiehl KF, Rucker N, Schwarz MA, Gill PS, Gomer CJ. Antiangiogenic treatment enhances photodynamic therapy responsiveness in a mouse mammary carcinoma. Cancer Res. 2000, 60(15):4066-4069
12. Jiang F, Zhang ZG, Katakowski M, Robin AM, Faber M, Zhang F, Chopp M. Angiogenesis induced by photodynamic therapy in normal rat brains. Photochem Photobiol. 2004, 79(6):494-498
13. Schmidt-Erfurth U, Schlotzer-Schrehard U, Cursiefen C, Michels S, Beckendorf A, Naumann GO. Influence of photodynamic therapy on expression of vascular endothelial growth factor (VEGF), VEGF receptor 3, and pigment epithelium-derived factor. Invest Ophthalmol Vis Sci. 2003, 44(10):4473-4480
14. Nowell PC. The clonal evolution of tumor cell populations. Science. 1976, 194(4260):23-28
15. Shimada Y, Imamura M, Wagata T, Yamaguchi N, Tobe T. Characterization of 21 newly established esophageal cancer cell lines. Cancer. 1992 Jan 15;69(2):277-284
16. Shimada Y, Maeda M, Watanabe G, Yamasaki S, Komoto I, Kaganoi J, Kan T, Hashimoto Y, Imoto I, Inazawa J, Imamura M. Cell culture in esophageal squamous cell carcinoma and the association with molecular markers. Clin Cancer Res. 2003, 9(1):243-249
17. Rao J, Otto WR. Fluorimetric DNA assay for cell growth estimation. Anal Biochem. 1992, 207(1):186-192
18. Bai J, Nakamura H, Ueda S, Kwon YW, Tanaka T, Ban S, Yodoi J.

Proteasome-dependent degradation of cyclin D1 in 1-methyl-4-phenylpyridinium ion (MPP+)-induced cell cycle arrest. J Biol Chem. 2004, 279(37):38710-38714
19. Yuan J, Lv H, Peng B, Wang C, Yu Y, He Z. Role of BCRP as a biomarker for predicting resistance to 5-fluorouracil in breast cancer. Cancer Chemother Pharmacol. 2009, 63(6):1103-1110
20. Capella MA, Capella LS. A light in multidrug resistance: photodynamic treatment of multidrug-resistant tumors. J Biomed Sci. 2003, 10(4):361-366
21. Merlin JL, Gautier H, Barberi-Heyob M, Teiten MH, Guillemin F. The multidrug resistance modulator SDZ-PSC 833 potentiates the photodynamic activity of chlorin e6 independently of P-glycoprotein in multidrug resistant human breast adenocarcinoma cells. Int J Oncol. 2003, 22(4):733-739
22. Li W, Zhang WJ, Ohnishi K, Yamada I, Ohno R, Hashimoto K. 5-Aminolaevulinic acid-mediated photodynamic therapy in multidrug resistant leukemia cells. J Photochem Photobiol B. 2001, 60(2-3):79-86
23. Teiten MH, Bezdetnaya L, Merlin JL, Bour-Dill C, Pauly ME, Dicato M, Guillemin F. Effect of meta-tetra(hydroxyphenyl)chlorin (mTHPC)-mediated photodynamic therapy on sensitive and multidrug-resistant human breast cancer cells. J Photochem Photobiol B. 2001, 62(3):146-152
24. Zhou S, Zong Y, Ney PA, Nair G, Stewart CF, Sorrentino BP. Increased expression of the Abcg2 transporter during erythroid maturation plays a role in decreasing cellular protoporphyrin IX levels. Blood. 2005, 105(6):2571-2576
25. Robey RW, Steadman K, Polgar O, Bates SE. ABCG2-mediated transport of photosensitizers: potential impact on photodynamic therapy. Cancer Biol Ther. 2005, 4(2):187-194
26. Limoli CL, Hartmann A, Shephard L, Yang CR, Boothman DA, Bartholomew J, Morgan WF. Apoptosis, reproductive failure, and oxidative stress in Chinese hamster ovary cells with compromised genomic integrity. Cancer Res. 1998, 58(16):3712-3718
27. Lock RB, Stribinskiene L. Dual modes of death induced by etoposide in human epithelial tumor cells allow Bcl-2 to inhibit apoptosis without affecting clonogenic survival. Cancer Res. 1996, 56(17):4006-4012
28. Runnels JM, Chen N, Ortel B, Kato D, Hasan T. BPD-MA-mediated photosensitization in vitro and in vivo: cellular adhesion and beta1 integrin expression in ovarian cancer cells. Br J Cancer. 1999, 80(7):946-953
29. Rousset N, Vonarx V, Eleouet S, Carre J, Kerninon E, Lajat Y, Patrice T. Effects of photodynamic therapy on adhesion molecules and metastasis. J Photochem Photobiol B. 1999, 52(1-3):65-73
30. Dougherty TJ, Marcus SL. Photodynamic therapy. Eur J Cancer. 1992, 28A(10):1734-1742
31. Luna MC, Ferrario A, Wong S, Fisher AM, Gomer CJ. Photodynamic therapy-mediated oxidative stress as a molecular switch for the temporal expression of genes ligated to the human heat shock promoter. Cancer Res. 2000, 60(6):1637-1644
32. Fidler IJ, Hart IR. Biological diversity in metastatic neoplasms: origins and implications. Science. 1982, 217(4564):998-1003
33. Beyer DC. Brachytherapy for recurrent prostate cancer after radiation therapy. Semin Radiat Oncol. 2003, 13(2):158-165
34. Wheeler JA, Zagars GK, Ayala AG. Dedifferentiation of locally recurrent prostate cancer after radiation therapy. Evidence for tumor progression. Cancer. 1993, 71(11):3783-3787

Chapter 3. The Applicability of HVJ-E to Accelerator-based BNCT and the Development of a Setup for in vivo and in vitro Studies

The second chapter indicated that HVJ-E is capable of being useful for low-molecular weight drug delivery. HVJ-PDT was highly effective at achieving therapeutic drug concentrations. I therefore applied HVJ-E to Boron Neutron Capture Therapy (BNCT).

In theory, BNCT provides a way to selectively destroy malignant cells while sparing normal cells. It is based on the nuclear capture and fission reactions between boron-10 (^{10}B) and thermal neutrons. ^{10}B is a nonradioactive constituent of natural elemental boron. The reaction cross section is exceptionally large, i.e., ~3800 b at thermal neutron energy. ^{10}B thus captures thermal neutrons very efficiently and produces energetic α particles (^{4}He) and recoiling lithium-7 (^{7}Li) nuclei via a ^{10}B (n, α)-^{7}Li reaction (Figure 3-1). These particles have high reactive biological effectiveness (RBE) and a range of less than 10 μm in tissue[1]. Because the high linear energy transfer (LET) particles have limited path lengths in tissue, the destructive effects of these high-energy particles are limited to boron-containing cells. The dose to normal tissue is limited by the drug specificity and control of the irradiated area. An affected site near a vital organ can be cured by BNCT because the physical distance has little to do with the side effects. As boron is accumulated selectively, as in chemotherapy, BNCT has curative properties against small infiltrating cancers. It also decreases the risk of recurrence.

The theory of BNCT was advanced by Locher in 1936[2]. Clinical trials of BNCT were started in 1951 at Brookhaven National Laboratory by Sweet[3] and Javid, Javid et al.[4], and Farr et al.[5]. However, the trials were discontinued after the treatment of 17 glioblastoma cases at the Massachusetts Institute of Technology in 1960–1961 due to the discouraging clinical results. Interest in BNCT was renewed by Hatanaka in Japan, who had worked at Massachusetts General Hospital with the BNCT team headed by Sweet. Hatanaka modified the procedure developed by Sweet at MGH in 1960–1961 by introducing ^{10}B-sodium-mercaptoundecahydrododecaborate (^{10}B-$Na_2B_{12}H$-SH). Between 1968 and 1992, 120 patients with 119 intracranial tumors and 1 extracranial nerve-related tumor were treated by the current standard BNCT technique. The clinical results for Grade 3–4 glioma patients treated before March 1985 were reported in comparison with those for control patients[6]. Japan is therefore in a position to build on this success and lead this field. To date, clinical studies on BNCT for head and neck cancer have been conducted using the Kyoto University Reactor or Japan Research Reactor No. 4. However, BNCT is now receiving attention around the world, and clinical studies have begun in Italy and Argentina. The implementation status of BNCT at home and overseas is described in Table 3-1 and Table 3-2.

Neutron sources for BNCT are currently limited to nuclear reactors, which is one of the biggest reasons for the limited understanding and slow spread of this technique. 1.0×10^9 n·cm^{-2}·s^{-1} thermal neutrons are needed for BNCT using current standard protocols, and only reactors can achieve this rate. There is no reactor specialized for BNCT. Research reactors present obstacles to treatment, with insufficient medical settings and legal restrictions. Furthermore, reactors are generally installed in suburban areas, and it is difficult to build them adjoining hospitals. The construction and operational costs are also very high.

To overcome these difficulties and make BNCT a useful modality for the treatment of cancer, accelerator-based BNCT has been suggested. Accelerators can also be used to produce neutrons, and accelerator-based neutron sources are being developed in several countries [7-13]. These sources are also compact enough to be sited in hospitals, thereby allowing more effective but technically more complicated BNCT procedures to be carried out. However, to date, various engineering problems have precluded accelerator-based

therapy. Developing effective accelerator-based BNCT is thus important for both experimental study and therapy.

The dose of BNCT is provided mainly via the ^{10}B (n, α)-^{7}Li reaction. The absorbed dose is thus proportional to the product of thermal neutron fluence and ^{10}B concentration. Therefore, if the drug concentration can be increased, the accelerator load can be decreased substantially. High accumulation and selective delivery of boron compounds into tumor tissue and cancer cells are therefore most important for achieving effective BNCT while keeping the concentration as low as possible in adjacent healthy cells.

Some novel drugs have already been reported to accumulate to levels 10–20 times higher than those of ordinary drugs. For example, Suzuki et al. reported the efficacy of administering a lipiodol emulsion of sodium mercaptoundecahydro-closo-dodecaborate (BSH), producing a boron concentration in liver tumors of 197.3 [ppm][14]. Kahl et al. reported that in tumor-bearing rats receiving boronoporphyrins (BOPP) by convection-enhanced delivery (CED), CED of 1.5 mg BOPP produced an average tumor boron level of 519 [ppm][15].

The 2 most promising boron compounds to emerge from investigations of hundreds of low-molecular-weight boron-containing chemicals were [(L)-4-dihydroxy-borylphenylalanine], based on arylboronic acids and called BPA[14], and another compound based on a newly discovered polyhedral borane anion called BSH[17]. The mechanism of accumulation is not clear but is related to the amino acid transport system. Various amino acid transporter activities are enhanced in rapidly multiplying cells, and L-amino acid transporter-1 (LAT-1) imports BPA into cells and may play a major role in the efficacy of BPA-based BNCT. BSH is a small, lipophilic compound with a cage-like structure and is the boron carrier most commonly used for BNCT for glioblastoma. Clinical experience[18] and the results of studies dedicated to the investigation of BSH pharmacokinetics and boron biodistribution[19-22] encouraged the European collaboration on BNCT to proceed toward clinical use of BNCT. While BSH is unable to pass the intact blood-brain-barrier (BBB), it has been to selectively penetrate the BBB at tumor sites because of damage to the BBB by the infiltrating malignant cells[23]. BSH consists of 12 ^{10}B atoms and has been under investigation for the treatment of glioblastoma.

A boron concentration of ~20 μg/g can be achieved in tumor tissue. This value is too low for treatment with accelerator-based neutron sources. Therefore, the boron concentration must be increased using Drug Delivery System (DDS) technology. If the ^{10}B concentration could be centuplicated, even a small, weak neutron source that generates a hundredth part of the thermal neutrons produced by a nuclear reactor would be effective. In the present study, fundamental BNCT experiments were conducted with a combination of the Intense 14 MeV Neutron Source Facility, OKTAVIAN, of Osaka University and novel boron agents (HVJ-E and B-Liposomes), which are anticipated to further progress in boron localization. The OKTAVIAN facility generates 14 MeV neutrons via the Deuterium-Tritium (D-T) reaction. The generated neutrons must be moderated to the thermal range for use in BNCT.

In the first section, I confirmed the feasibility of formulating a setup for verifying the logic described above. The neutron transportation rates, fluxes, and spectra were calculated using simulation calculations using Monte Carlo N-Particle Transport Code: MCNP5[24]. The size of the sample area was decided first, and then the rough geometry was designed. The materials for the reflector and modulator were selected and the optimal size was calculated by comparing the neutron fluxes.

In the following section, the anti-tumor effects of accelerator-based BNCT were determined *in vivo* and *in vitro* using the setup built in the first section. The intracellular boron concentration and the cytotoxicity of the novel agent were measured

after the experimental conditions were set.

Finally, I will discuss the *in vivo* experiments. The BNCT effect was not detected in the *in vitro* experiments described in the second section, which is suspected to be due to the affinity of HVJ-E for the LLC cell line. Therefore, a cell line meeting the requirements for measuring the BNCT effect was chosen and the setup was improved by the use of deuterium water.

Figures

Table 3-1. Implementation status in Japan as of 2009

Reactor	Organization	Brain	Skin	Other	Total	Term
HTR	Hitachi, Ltd.	13	0	0	13	1968-1974
JRR-3	Japan Atomic Energy Agency	1	0	0	1	1969
MuITR	Musashi Institute of Technology	99	9	0	108	1977-1989
KUR	Kyoto University Research Reactor Institute	47	14	0	61	1974,87,90-95
KUR-M	Kyoto University Research Reactor Institute	97	8	105	210	1996-2006
JRR-2	Japan Atomic Energy Agency	33	0	0	33	1990-1996
JRR-4	Japan Atomic Energy Agency	62	2	35	99	1999-2007
Total		352	33	140	525	-

Table 3-2 Implementation status of the world as of 2008

Country	Reactor	Range	Cases	Region	Term
United States of America	Brookhaven's Graphite Research Reactor	thermal	28	brain	1951～58
	Brookhaven Medical Research Reactor	thermal	17	brain	1959～61
		epithermal	54	brain	1994～99
	MIT Nuclear Research Reactor	thermal	18	brain	1959～61
		epithermal	24	brain skin	1994～
Netherlands	The High Flux Reactor (HFR) Petten	epithermal	22	brain	1997～
Finland	Finland Research Reactor	epithermal	150	brain	1999～
Czech Republic	LVR-15 research reactor	epithermal	2	brain	2000～
Sweden	R2-0	epithermal	52	brain	2001～05
Italia	Research Reactor	epithermal	2	liver	2002～
Argentina	Research Reactor	epithermal	7	melanoma	2003～

thermal: En < 0.5 eV, epithermal: 0.5 eV < En < 10 keV

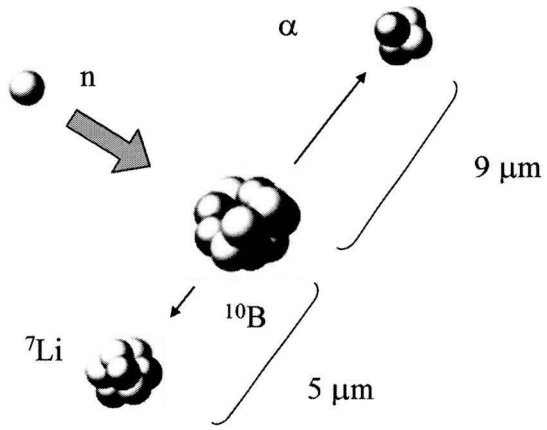

Figure 3-1. Concept of BNCT. ^{10}B captures thermal neutron efficiently and produce □ and ^{7}Li ray. They have high reactive biological effectiveness and the range of □□and Li rays are 9 μm and 5 μm, respectively.

References

1. Kobayashi T. The Present Status and the Future Prospects of Neutron Capture Therapy : A Viewpoint of Radiation Medical Phys-ics and Engineering, Japanese Journal of Radiological Technology. 2000, 56[6], 780-791
2. Locher, G.L., "Biological effects and therapeutic possibilities of neutrons," Am. J. Roentgenol. Radium Ther, 1936, 36: 1-13
3. Sweet WH, Javid M. The possible use of neutron-capturing isotopes such as boron-10 in the treatment of neoplasms. I. Intracranial tumor. J. Neurosurg. 1952;9: 200–209
4. Hayakawa Y, Inada T, Harasawa S, Hatanala H. Chapter XXI. A system for simultaneous monitoring of thermal and epithermal neutron flux during boron-neutron capture therapy. In: Hatanaka H editors. Boron-neutron capture therapy for tumors. Niigata: Nishimura; 1986, 283–292
5. Farr LE, Sweet WH, Robertson JS, Foster CG, Locksley HB, Sutherland DL, et al. Neutron capture therapy with boron in the treatment of glioblastoma multiforme. Am. J. Roentgenol. 1954, 71: 279–293
6. Hatanaka H, Kamano S, Amano K, Hojo S, Sano K, Egawa S, et al. Chapter XXV. Clinical experience of boron-neutron capture therapy for gliomas—A comparison with conventional chemo-immuno-radiotherapy. In: Hatanaka H editors. Boron-neutron capture therapy for tumors. Niigata: Nishimura; 1986, 349-379
7. Beynon T, Forcey KS, Green S, Cruickshank G, JamesN. Statusof the Birmingham accelerator based BNCT facility. In: M.W. Sauerwein, R. Moss and A. Wittig, editors. Research and Development in Neutron CaptureTherapy, Bologna: Monduzzi Editore, Interna-tional ProceedingsDivision; 2002, 225-228
8. Burlon A, KreinerA,Valda A, et al. Optimization of a neutron production target and beam shaping assem-bly based on the $^{7}Li(p.n)^{7}Be$ reaction. In:M.W.Sauerwein, R. Moss and A.Wittig, editors. Research and Development in Neutron CaptureTherapy, Bologna: Monduzzi Editore, International ProceedingsDivision. 2002, 229-234
9. Kononov O, Kononov V, Koroveynikov V, et al. Investigations of using near-threshold $^{7}Li(p.n)^{7}Be$ reaction forNCT basedonin-phantomdose distribution. In: M.W. Sauerwein, R. Moss and A.Wittig, editors. Research and Development in Neutron Capture Therapy, Bologna: Monduzzi Editore, International Proceedings Division. 2002, 241-246
10. Blackburn B,YanchJ, Klinkowstein R.Development of a high-power water cooled beryllium target for use in accelerator-based boron neutron capture therapy. Med Phys. 1998, 10: 1967-1974
11. Hawk A, BlueT,WoolardJ, Gupta N. Effectsof target thickness on neutron field quality for an ABNS.Research and development in neutron capture therapy. In: M.W. Sauerwein, R. Moss and A.Wittig, editors. Research and Development in Neutron Capture Therapy, Bologna: Monduzzi Editore, International ProceedingsDivision. 2002, 253-257
12. SakuraiY, Kobayashi T, Ono K. Study on accelerator-base neutron irradiation field aiming for wider application in BNCTKspectrum shift and regional filtering. In: M.W. Sauerwein, R. Moss and A.Wittig, editors. Research and Development in Neutron Capture Therapy, Bologna: Monduzzi Editore, International Proceedings Division. 2002, 259-263
13. Giusti V, Esposito J. Neutronic feasibility study of an accelerator-based thermal neutron irradiation cavity. In:M.W. Sauerwein, R.Moss and A.Wittig, editors. Research and Development in Neutron Capture Therapy, Bologna: Monduzzi Editore, International Proceedings Division. 2002, 305-308
14. Suzuki M, Masunaga S, Kinashi Y, Nagata K, Sakurai Y, Nakamatsu K, Nishimura Y, Maruhashi A, Ono K. Intra-arterial administration of sodium borocaptate

(BSH)/lipiodol emulsion delivers B-10 to liver tumors highly selectively for boron neutron capture therapy: experimental studies in the rat liver model. Int J Radiat Oncol Biol Phys. 2004, 59(1): 260-266
15. Ozawa T, Afzal J, Lamborn KR, Bollen AW, Bauer WF, Koo MS, Kahl SB, Deen DF. Toxicity, biodistribution, and convection-enhanced delivery of the boronated porphyrin BOPP in the 9L intracerebral rat glioma model. Int J Radiat Oncol Biol Phys. 2005, 63(1): 247-252
16. Snyder HR, Reedy AJ, Lennarz WJ. Synthesis of aromatic boronic acids, aldehydo boronic acids and a boronic acid analog of tyrosine. J Am Chem Soc 1958;80:835–8
17. Soloway AH, Hatanaka H, Davis MA. Penetration of brain and brain tumor. VII. Tumor-binding sulfhydryl boron compounds. J Med Chem 1967, 10: 714
18. Hatanaka H, Kamano S, Amano K, Hojo S, Sano K, Egawa S, Yasukochi H: Clinical experience of boron-neutron capture therapy for gliomas: A comparison with conventional chemoimmuno-radiotherapy, in Hatanaka H (ed):Boron Neutron Capture Therapy for Tumors. Niigata, Japan, Nishimura, 1986, 349-378
19. Haritz D, Gabel D, Huiskamp R: Clinical phase I study of $Na_2B_{12}H_{11}SH$ (BSH) in patients with malignant glioma as precondition for boron neutron capture therapy (BNCT). Int J Radiat Oncol Biol Phys. 1994, 28: 1175-1181
20. Haselsberger K, Radner H, Gössler W, Schlagenhaufen C, Pendl G: Subcellular boron-10 localization in glioblastoma for boron neutron capture therapy with $Na_2B_{12}H_{11}SH$.J Neurosurg. 1994, 81: 741-744
21. Haselsberger K, Radner H, Pendl G: Boron neutron capture therapy: Boron biodistribution and pharmacokinetics of $Na_2B_{12}H_{11}SH$ in patients with glioblastoma. Cancer Res. 1994, 54: 6318-6320
22. Stragliotto G, Fankhauser H: Biodistribution of boron sulfhydryl for boron neutron capture therapy in patients with intracranial tumors. Neurosurgery. 1995, 36: 285-293
23. A Barth RF, Yang W, Rotaru JH, Moeschberger ML, Boesel CP, Soloway AH, Joel DD, Nawrocky MM, Ono K, Goodman JH. Boron neutron capture therapy of brain tumors: enhanced survival and cure following blood-brain barrier disruption and intracarotid injection of sodium borocaptate and boronophenylalanine. Int J Radiat Oncol Biol Phys. 2000, 47(1): 209-18
24. X-5 Monte Carlo Team,RMCNP A GeneralMonte Carlo N-Particle Transport Code,Version 5, SLA-UR-03-1987. 2003

Section 1. Development of thermal neutron field with D-T neutron source aiming at in vitro experiment for BNCT

I. Introduction

Recently the number of cancer cases has been increasing. In addition because of aging of the population and diversification of values among the people, less-invasive and high-QOL (quality of life) treatment for tumors has been required. Boron Neutron Capture Therapy (BNCT) is known to be a less-invasive tumor therapy based on a reaction between boron (^{10}B) and thermal neutron. ^{10}B captures a thermal neutron very efficiently (in an exceptionally high probability) and produces energetic α and ^{7}Li particles by the next nuclear reaction.

$$^{10}B + {}^{1}n \rightarrow {}^{7}Li + {}^{4}He(\alpha) + 2.31\ MeV \quad (1)$$

They have high reactive biological effectiveness (RBE) and the range of them is less than 10 μm in tissue[1,2].

However there are some problems to be solved on BNCT. One of the severest problems is in the following: The number of patients treated is limited because a nuclear reactor is required as a neutron source. The number of nuclear reactors available for BNCT is only two in Japan. Moreover they are not specialized for medical use. There are no plans to construct new nuclear reactors for BNCT. Various studies thus started so far to realize accelerator-based neutron source for BNCT[3,4], because it makes easy to access accelerator-based irradiation facilities near urban hospitals. And the accelerator can reduce construction and operational cost. However, such kinds of accelerators are not yet constructed because of various engineering problems; decay heat removal capability on target, stable control of high beam current, radioactivities produced in such facilities[5-7].

The effectiveness of BNCT is estimated by making the product of ^{10}B concentration, the cross section of ^{10}B and the thermal neutron flux intensity[8]. If the concentration could be increased, the accelerator load could be decreased substantially. Aiming at high accumulation of boron compounds into tumor tissues, drug delivery system (DDS) is widely studied as an attractive intelligent technology to achieve the selective delivery of medicine as well as boron. So far, several new efficient agents have been proposed[9-14]. Especially Ozawa et al. reported about tumor bearing rats receiving boronoporphyrins (BOPP) by convection-enhanced delivery (CED). CED of 1.5 mg BOPP produced an average tumor boron level of 519 ppm[10].

These novel boron agents realize accelerator based BNCT with even a little weak neutron source like a D-T neutron source. To confirm a possibility of BNCT with a low neutron flux combined with a high boron concentration, a fundamental research is indispensable.

In this study, we focus on the D-T neutron source as an accelerator-based thermal neutron source. As for the D-T neutron source, there were some facilities available worldwide. Because the D-T neutron source technology is already well established, the performance is stable and the source can be utilized to various applications quite easily. Also, it becomes simple to design a neutron moderator because the D-T neutron is monoenergetic. In addition it is advantageous in design that in the D-T reaction no gamma-rays are generated. However D-T neutrons have to be moderated and the contribution of fast neutrons must be reduced since the incident energy is very high. And the source neutron intensity is a little weak for BNCT.

Under these considerations, we aim at design and construction of a thermal neutron field for fundamental BNCT experiments using a D-T neutron source. The constructed thermal neutron field would be used to irradiate cultured cells or mice combined with efficient boron agents to discuss possibility of the use of D-T neutron sources for BNCT. Thus in this study, a thermal neutron field, not an epi-thermal field

is constructed first for fundamental researches for BNCT. When studying the effect of BNCT using cultured cells or mice, a pure thermal neutron field is preferred. However clinical facilities should utilize epithermal neutrons because tumors are normally located in deeper places. In the next step, an epi-thermal field will be planned to be designed and constructed aiming at researches for practical applications for man.

The present neutron field should meet the following three design conditions. Considering a necessary BNCT dose of a few Gy-Eq (equivalent dose), uniform irradiation environment (temperature, humidity and so on) and use of mice (mice should not be fixed for a long period), the exposure time must be limited to be shorter than 2 hours (Design Requirement 1). The BNCT dose should be as high as possible. If this is set to be several Gy-eq, the thermal neutron flux has to be more than 1×10^6 n/sec/cm^2 even if achieving a boron concentration being 10 times higher than before (Design Requirement 2). Finally, it is obviously necessary to reduce the fast neutron contribution as low as possible (Design Requirement 3), because fast neutrons, which have cytotoxicity, don't have selectivity.

In this study, simulation calculations are carried out to design a thermal neutron field meeting the 3 requirements described above using a D-T neutron source. The results are used to construct a thermal column for experiments with small animals. As a D-T neutron source, the Intense 14 MeV Neutron Source Facility, OKTAVIAN, of Osaka University, Japan is utilized. The constructed thermal neutron field is characterized and the obtained results are compared with the predicted values. We then examine whether *in vivo* BNCT experiments would be possible using novel boron agents in the present experimental setup. Finally, we discuss the future possibility of using D-T neutron-based thermal neutron sources for actual BNCT in hospitals.

II. Design Calculation

1. Neutron Transport Calculation

In order to estimate the thermal (< 0.5 eV) and fast (> 0.01 MeV) neutron flux at the irradiation area, simulation calculations were performed using MCNP-5 (A General Monte Carlo N-Particle Transport Code)[15]. ENDF/B-VI was used as a neutron cross section library[16]. Track length estimator (F4) tally was used for calculating thermal and fast neutron spectra. Reaction rates for ^{197}Au (n, γ) positioned in several places in a box for irradiation of mice were calculated for comparison with the experimental results. The calculation was performed using a virtual pure gold foil with the tally multiplier card, FM, for the reaction type of (n, γ), i.e., MT = 102. The number of histories was 1×10^7, by which the statistical error can be reduced downto less than 5%. The absorbed dose per source neutron from fast neutrons and photons was scored using an energy deposition (F6) tally.

2. Neutron Source

As a neutron source, Intense 14 MeV Neutron Source Facility, OKTAVIAN, of Osaka University was used. The OKTAVIAN facility is a Cockcroft Walton type accelerator and generates 14 MeV neutrons by ^{3}H (d, n) ^{4}He reaction. The stably produced maximum neutron source intensity is $\sim 1 \times 10^{11}$ n/sec at present. Though the value is a little weak for BNCT, it is sufficient to be used to fundamental researches.

3. Assumed Size of Irradiation Area

We designed a thermal insulation equipment using a styrofoam box for upcoming *in vitro* irradiation experiment and small animal holding fixture for upcoming *in vivo* experiment. The holding fixture can hold 12 mice, which is sufficient value for fundamental *in vivo* experiments. The calculation was carried out with the idea of using them. To put this equipment, the space of $20 \times 20 \times 20$ cm^3 was kept inside the thermal

neutron field. In the simulations the mice were assumed as water phantom containing a small amount of salt.

4. Moderator and Reflector

The optimum amounts of moderator and reflector materials surrounding the irradiation area were investigated by simulation calculations. Figure 3-1-1 shows basic arrangement before the design calculations. The irradiation position (the distance from the neutron source) and the thickness of carbon reflector were varied.

As a moderator high density polyethylene was put between the neutron source and the irradiation area to moderate 14 MeV neutrons. Polyethylene has a high density of 0.95 and consists of only carbon and hydrogen. And it has a high hydrogen atomic number density. Because their absorption cross sections are low and hydrogen thus has an excellent moderation performance for neutron, polyethylene is selected as a neutron moderator.

Also, neutrons leaking from the moderator have to be reflected to improve the neutron flux intensity at the irradiation area. In this study graphite blocks were used as the reflector. The thicknesses of the polyethylene and graphite reflector were determined to meet the optimum condition by checking the thermal and fast neutron flux intensities in the irradiation area.

In addition, a beryllium block was put between the polyethylene and the tritium target for neutron multiplication by the Be (n, 2n) reaction. This reaction is available only near the neutron source because it is a threshold reaction. Behind the sample area, concrete and polyethylene blocks were put to shield and reflect neutrons passing through the irradiation area.

III. Design of Thermal Neutron Field

Simulation calculations were performed to design an irradiation field so as to meet the Design Requirement 1-3 in Chap. 1. Calculated thermal and fast neutron fluxes at the irradiation area are shown in Figure 3-1-2 as a function of moderator thickness. The error in the calculation was 0.5% to 3.3%. The fast neutron flux decreases with the thickness of polyethylene. The thermal neutron flux shows its maximum value at 5 cm, and decreases if it becomes more than 5 cm. The ratio of thermal to fast neutron fluxes is increasing as the moderator becomes thicker. Thickness of 65 cm is the highest in the case of OKTAVIAN. However thickness of 65 cm is not acceptable because the thermal neutron flux is too low. Finally, in this study the thickness of 20 cm was selected considering the thermal neutron flux intensity. The nearer position seems to be surely better from the standpoint of thermal neutron flux intensity, however, the fast neutron dose becomes too high at positions nearer than 20 cm.

The thermal and fast neutron fluxes at the irradiation area are shown in Figure 3-1-3 as a function of the reflector thickness. As the reflector becomes thicker, the thermal neutron flux increases; meanwhile the fast neutron flux is constant. Because the thermal neutron flux intensity slowly saturates for thickness more than 30 cm, 40 cm thick graphite reflector was adopted considering that it is actually difficult to construct a bigger one than a 40 cm thick reflector.

In the case of 20 cm thick moderator and 40 cm thick reflector, the neutron spectrum in the irradiation area is shown in Figure 3-1-4. Neutrons are moderated adequately and Maxwellian distribution in the energy region of about 0.025 eV is observed. The fast, epi-thermal and thermal neutron flux per source neutron were 5.4×10^{-5} n/cm^2/source neutron (s.n), 3.9×10^{-5} n/cm^2/s.n and 1.6×10^{-4} n/cm^2/s.n, respectively. There is negligibly small difference in the thermal neutron flux between in the front and back sides of the irradiation area.

IV. Neutron Irradiation Experiment

1. Neutron Flux Measurement

A thermal column as described in Figure 3-1-5 and 3-1-6 was built in the heavy irradiation room of OKTAVIAN, and irradiation experiments were performed to compare with the simulation calculation. In the experiment, the moderator thickness was decided to be 20 cm. The fast and thermal neutron flux intensities were monitored with activation foils. Niobium foils and gold foils were used for fast neutrons and thermal neutrons, respectively. Niobium absorbs fast neutron via (^{93}Nb(n,2n)^{92m}Nb) reaction, which has an energy threshold of 9.1 MeV. Gamma rays of 934 keV were emitted from ^{92m}Nb. Niobium foils of 100 μm thickness were put in front of the tritium target for D-T neutron, in the moderator and in the irradiation area. The dimensions of the niobium foils for the three positions were 1 × 1 cm^2, 5 × 5 cm^2 and 3 × 10 cm^2, respectively. Gold foils of 50 μm thickness and 1 × 1 cm^2 were setup along the beam axis. Also cadmium covers of 1 mm thickness were used together to determine the so-called cadmium ratio. 934 keV and 412 keV γ rays for niobium and gold foils, respectively, were measured using a high-purity germanium detector (HpGe) (GMX-15185-p, SEIKO EG & G, Japan). Also, signals from a proportional counter were recorded in an MCS mode to monitor the time-dependent neutron intensity and in order accurately to estimate the amount of activation.

2. Radiation Dose Calculation

In this study we had assumed that 12 mice are irradiated. The BNCT dose (D_{BNCT}) at the irradiation area was calculated to evaluate the performance of the constructed thermal neutron field. The equivalent dose of BNCT, D_{BNCT}, was calculated using the following equation:

$$D_{BNCT} = (R_N \times K_N + R_B \times K_B \times C_B) \times \phi_{thermal} \times T + D_f + D_\gamma \quad (2)$$

where, K_N and K_B are the doses per unit fluences from nitrogen (2% in weight of mouse cell) and from boron (per 1 ppm)[8], respectively. Nitrogen captures a thermal neutron like as boron and produces a proton (^{14}N (n, p) ^{14}C). This reaction occurs as side reaction in thermal neutron field because the reaction isn't threshold reaction. To calculate the equivalent dose, the RBE 3.2 and 3.8 (R_N and R_B) for D_N (the dose from nitrogen reaction) and D_B (the dose from boron reaction) were used, respectively[1]. C_B, $\phi_{thermal}$ and T are the intracellular boron concentration, the thermal neutron flux and the irradiation time, respectively. The irradiation time was assumed to be 2 hours. Activation foils were used to estimate intensities of the generated 14 MeV neutrons and thermal neutrons ($\phi_{thermal}$). And D_f and D_γ are the equivalent dose from fast neutrons and the dose from gamma ray, respectively. They were estimated by MCNP-5 calculation and the measured value of the generated 14 MeV neutrons. In the calculation, the areas in which there are mice were replaced with a cylindrical water phantom and it was assumed that there is a tumor on the surface of a mouse. The RBE of 2.3 was used[17]. K_N and K_B are derived from the following equation.

$$K_i = N_A \times Q_i \times \sigma_I \quad (3)$$

where, Na is Avogadro's number, Q is the energy released per nuclear reaction, i.e., 0.6 and 2.31 MeV for ^{14}N(n, p) and ^{10}B(n, α) reactions, respectively and σ is the cross-sections of 1.75 barn for ^{14}N(n, p) and 3837 barn for ^{10}B(n, α) reactions (the representative value for thermal neutron). The boron concentration of the tumor tissue was assumed to be 300 ppm and that of the healthy tissue is 5 ppm. Although the concentration is about 10 times higher than those expected in general BNCT cases, it was reported in some papers[10-12] that it could be surely achieved. In this case the ratio of tumor dose / normal dose is 53.

V. Results and Discussion

1. Comparison Between Calculation and Measurement

Neutron irradiation was performed at the OKTAVIAN facility and the fast and thermal neutron fluxes were measured with niobium and gold foils. The 14 MeV neutron source intensity was 4.1 ($\pm$0.4) $\times$ 10^{10} n/s. The fast and thermal neutron fluxes at the sample area were 1.9 $\times$ 10^{6} ($\pm$0.03) n/cm^2/s and 6.5 $\times$ 10^{6} ($\pm$0.01) n/cm^2/s, respectively. These results were compared with the calculation values as in Figure 3-1-7 as a function of the distance from the tritium target. Table 3-1-1 compares the reaction rate of foils in the sample area. The measured neutron fluxes were in good agreement with the calculation results in the whole region (the ratio between simulation and irradiation experiment of fast and thermal neutron fluxes were from 0.95 to 1.2, 0.85 to 1.0). Though there is a tiny difference, it is small enough to discuss the dose of BNCT. It was determined by the MCNP simulation that the neutrons in the irradiation area were moderated adequately and the neutron energy distribution is Maxwellian in the energy region of about 0.025 eV. Thus the thermal neutron flux can be measured correctly by gold foil activation. On the other hand, the activation of Niobium with fast neutron has an energy threshold of 9.1 MeV. The threshold may lead to an underestimation of fast neutron flux because the fast neutron in the energy region from 0.01 to 9.1 MeV cannot be measured.

From the comparison, it was confirmed that the simulation calculation worked correctly. The irradiation dose could be hence estimated appropriately and the fast and thermal neutron spectra can be quantified without measurement if only the time-dependent neutron intensity of OKTAVIAN would be accurately monitored.

The irradiation dose of each sample could also be estimated from the calculated results even if there are many samples (cells and/or mice) arranged in the irradiation area. The thermal neutron flux was thus found to be constant in the irradiation area within a difference less than 10%. It means the radiation doses can be kept constant. So we can arrange many samples at a time in the same condition.

2. Irradiation Dose of BNCT

Equivalent doses were derived for cultured cell or small animals from the MCNP calculation and the measured result. The equivalent doses were evaluated and summarized in Table 3-1-2.

According to Makinodan, bone marrow death did not occur at doses of 5 Gy-eq[18]. Hsue-Yin Hsua made sure that marrow stem cell survived 100 % under 2 Gy-eq of dose[19]. For these reasons, the normal tissue dose should be limited below 2 Gy-eq. When the sample is positioned at 20 cm from the source, the equivalent dose of normal tissue was confirmed to become much less than 2 Gy-eq. The toxicity for normal cell was very low and mice would not be injured by fast neutrons.

It was reported that 3.7 Gy-eq dose shrinks the tumor of rats[20] and that tumors disappeared by 23 Gy-eq dose[21]. As is Table 3-1-2, the dose to the tumor tissue is 5.0 Gy-eq, which is enough large to confirm the anti-tumor effect in *in vivo* experiments. Therefore the neutron flux from our setup is sufficient for BNCT experiments using cultured cell or mice. Now we are making a start on the experiment with cultured cells[22].

Also if 1 $\times$ 10^{11} n/s neutrons, which is the currently achievable neutron source intensity at OKTAVIAN, are generated for 2 hours, the equivalent dose of tumor tissue achieved 12 Gy-eq, which is effective value to treat tumor. On the other hand, the small animals would be irradiated across the entire body and the dose is calculated in 1.0 Gy-eq. This value is adequately low to damage their health[12,19,23] and 1.0 Gy-eq dose can't affects lipids peroxides in mouse serum[24]. It can be expected that it would become possible to carry out more precise experiments.

3. Feasibility of BNCT in a hospital with D-T neutron source

To realize a D-T based BNCT in a hospital, some existing problems should be solved. The first one is to develop an epithermal neutron field, because the epithermal neutron field is generally the best. The point is that the energy is too high to be moderated keeping necessary epi-thermal neutron intensity and suppressing high energy neutron contribution. However, thermal neutron fields using a D-T neutron source is intensively under investigation[25-27]. There are thus sufficient possibilities to overcome the problem in the near future.

Next, higher epithermal neutron flux of 10^9 n/cm^2/s is needed according to IAEA[28]. In our approach, ~10^8 n/cm^2/s thermal or epithermal neutron field should thus be needed with efficient boron agents. Generally D-T neutron sources can generate ~1 × 10^{12} n/sec using a rotating tritium target or gas target. The OKTAVIAN facility can generate 3 × 10^{12} n/s, which is the full spec of the facility. The thermal neutron flux would thus be ~10^8 n/cm^2/s at the irradiation area from the presently obtained result. It means from the present results that BNCT with thermal neutrons for man could be realized using the novel boron agents and a D-T neutron source.

Finally, careful handling of tritium, which is a radioisotope, is required. The history of D-T neutron source goes back quite a long way[29]. The handling method has been studied for nuclear fusion reactors[30-32]. And tritium behavior in human body was studied for years to control doses at OKTAVIAN facility[33]. With these proven techniques and careful treatments of tritium, there would be a possibility that BNCT in hospitals would be realized.

VI. Conclusion

In this study, we designed and constructed a thermal neutron field with a D-T neutron source to carry out basic BNCT experiments with cultured cell or small animals with help of new boron agents. The neutron field was designed through simulation calculations and verified with irradiation experiments. In the experiment, the 14 MeV neutron source intensity was 4.1 × 10^{10} n/s and the thermal neutron flux at the irradiation area was about 6.5 × 10^6 n/cm^2/s. The BNCT dose is 5.0 Gy-eq for 2 hour irradiation and the ratio between MCNP simulation and irradiation experiment of fast and thermal neutrons were from 0.95 to 1.2, 0.85 to 1.0. In this case, fast neutron and gamma ray doses were suppressed to be 0.31 Gy-eq and 0.023 Gy, respectively. It was confirmed that the anti-tumor effect of BNCT could be observed in *in vivo* experiment using novel boron agents at the present neutron filed.

The series study showed a possibility of the D-T-based BNCT if the source neutron intensity would be larger than ~10^{12} n/s.

Figures

Table 3-1-1. Comparison of the foil reaction rate in the sample area (the distance from the tritium target was 35 cm) between the calculation and experiment

	niobium foil (fast) [/cm³/s]	gold foil (thermal) [/cm³/s]
calculation	6.8E+04	3.1E+07
experiment	6.0E+04	2.8E+07
C/E	1.1	1.1

Table 3-1-2 Equivalent doses for small animals. The equivalent dose of BNCT was calculated. The boron concentrations of normal and tumor tissue were assumed 5 and 300 ppm, respectively. The RBE 3.8, 3.2 and 2.3 for DB, DN and Df, respectively. The irradiation time was assumed to be 2 hours.

	D_B [Gy-eq]	D_N [Gy-eq]	D_f [Gy-eq]	D_γ [Gy]	D_{BNCT} [Gy-eq]
normal tissue	7.8e-2	1.1e-2	3.1e-1	2.3e-2	4.2e-1
tumor tissue	4.7e+0	1.1e-2	3.1e-1	2.3e-2	5.0e+0

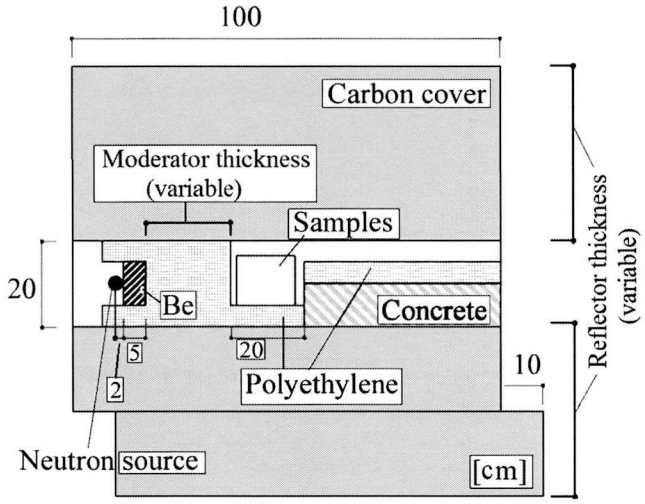

Figure 3-1-1 Basic arrangement for simulation calculations. Polyethylene blocks (dotted area) were placed between tritium target and sample area to moderate 14 MeV neutrons and graphite blocks (gray area) cover them to reflect neutrons. The moderator and reflector thicknesses were variable.

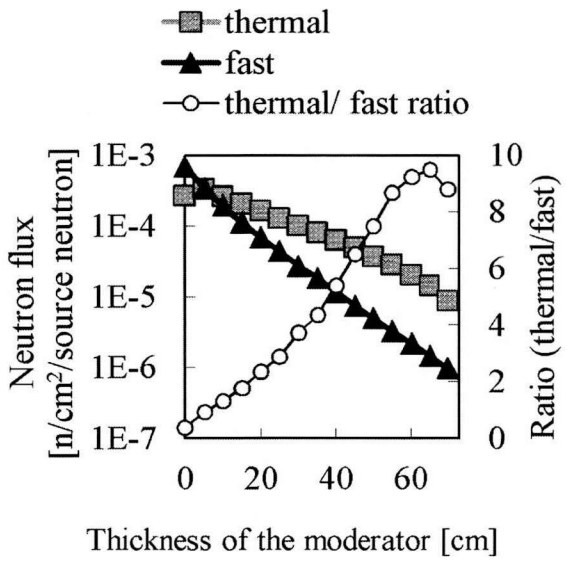

Figure 3-1-2 Thermal and fast neutron fluxes and their ratio against the thickness of polyethylene moderator. The error in the calculation was 0.5% to 3.3%

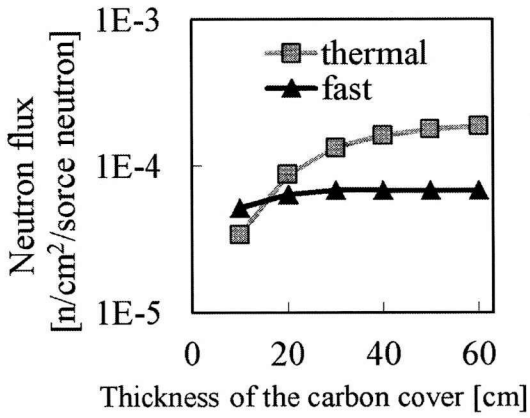

Figure 3-1-3 Thermal and fast neutron fluxes against the thickness of reflector graphite.

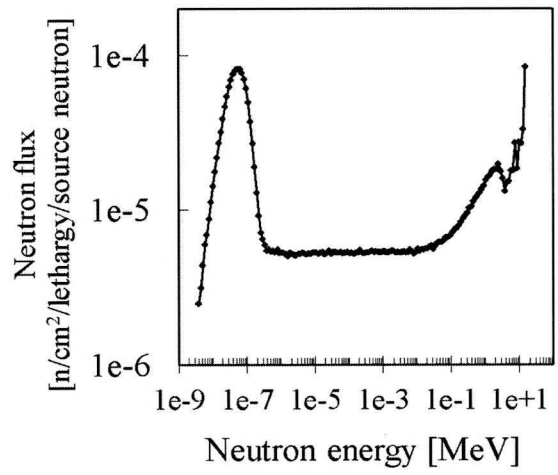

Figure 3-1-4 Neutron spectrum in the irradiation field.

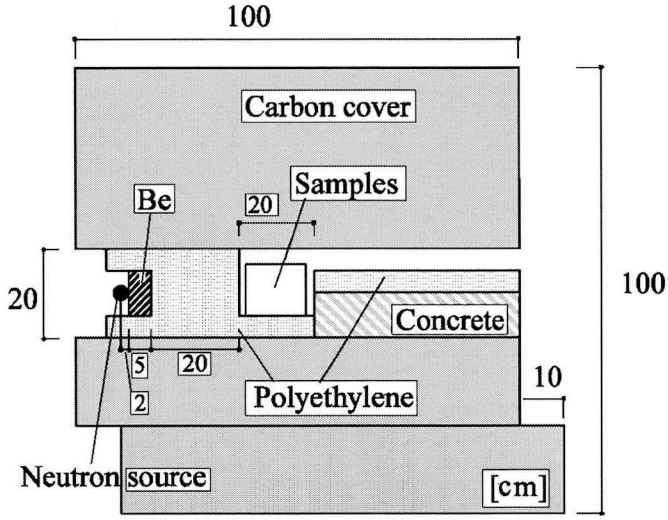

Figure 3-1-5 Vertical cross-section of the final experimental setup for neutron irradiation.

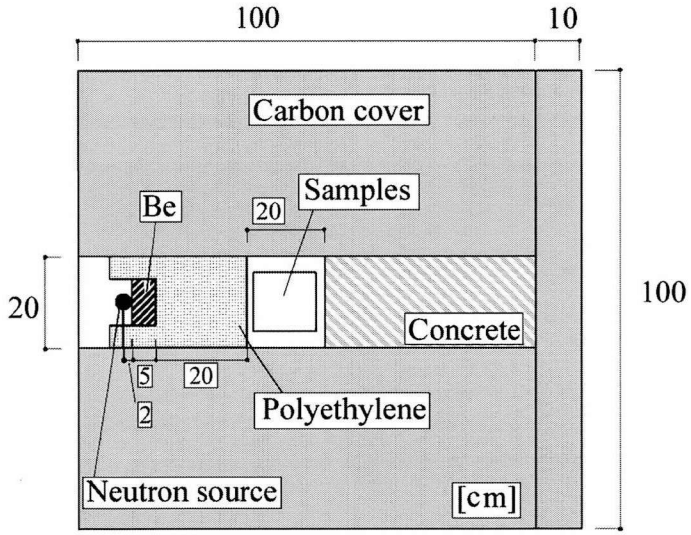

Figure 3-1-6 Horizontal sectional view of the final experimental setup for neutron irradiation.

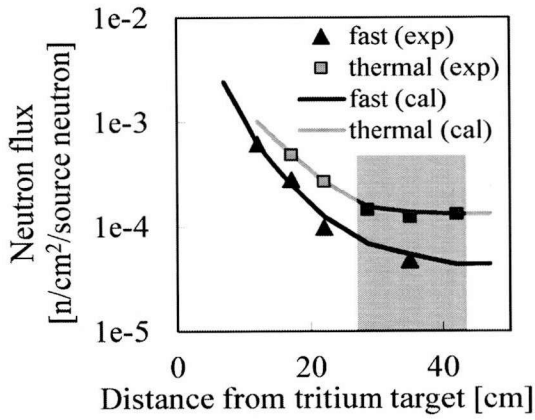

Figure 3-1-7 Calculated thermal and fast neutron distributions in the assembly compared with the experimental results. (Gray area (27 ~ 42 cm) shows the irradiation area. Lines are calculations. Gray square and black triangle symbols are neutron fluxes for thermal and fast energy regions, respectively.).

References

1. Coderre JA, Makar MS, Micca PL, Nawrocky MM, Liu HB, Joel DD, Slatkin DN, Amols HI. Derivations of relative biological effectiveness for the high-let radiations produced during boron neutron capture irradiations of the 9L rat gliosarcoma in vitro and in vivo. Int J Radiat Oncol Biol Phys. 1993, 27(5): 1121-1129
2. Takahashi H. Towardi the 21st century nuclear-science technology. Prog. in Nuc. Ener. 2005, 47: 53-60
3. Kobayashi T, Kanda K. Analytical calculation of boron- 10 dosage in cell nucleus for neutron capture therapy. Radiat Res. 1982, 91(1): 77-94
4. Blue TE, Yanch JC. Accelerator-based epithermal neutron sources for boron neutron capture therapy of brain tumors. J Neurooncol. 2003, 62(1-2): 19-31
5. Tanaka K, Yokobori H, Endo S, Kobayashi T, Bengua G, Saruyama I, Nakagawa Y, Hoshi M. Characteristics of proton beam scanning dependent on Li target thickness from the viewpoint of heat removal and material strength for accelerator-based BNCT. Appl Radiat Isot. 2009, 67(2): 259-265
6. Takenaka N. Nio D. Kiyanagi Y. Mishima K. Kawai M. Furusaka, M. Thermal hydraulic design and decay heat removal of a solid target for a spallation neutron source. Journal of Nuclear Materials. 2005, 343(1-3): 169-177
7. Tooru K. Bengua G. Nakagawa Y. Tanaka K. Masaharu H. A POSSIBILITY OF BNCT IRRADIATION SYSTEMS USING ACCELERATORS, The 1st Annual Meeting of Particle Accelerator Society of Japan and the 29th Linear Accelerator Meeting in Japan, Aug. 4-6, Funabashi Japan. 2004, 180-182 [in Japanese]
8. Nakagawa Y, Pooh K, Kobayashi T, Kageji T, Uyama S, Matsumura A, Kumada H. Clinical review of the Japanese experience with boron neutron capture therapy and a proposed strategy using epithermal neutron beams. J Neurooncol. 2003, 62(1-2): 87-99
9. Suzuki M, Masunaga S, Kinashi Y, Nagata K, Sakurai Y, Nakamatsu K, Nishimura Y, Maruhashi A, Ono K. Intra-arterial administration of sodium borocaptate (BSH)/lipiodol emulsion delivers B-10 to liver tumors highly selectively for boron neutron capture therapy: experimental studies in the rat liver model. Int J Radiat Oncol Biol Phys. 2004, 59(1): 260-266
10. Ozawa T, Afzal J, Lamborn KR, Bollen AW, Bauer WF, Koo MS, Kahl SB, Deen DF. Toxicity, biodistribution, and convection-enhanced delivery of the boronated porphyrin BOPP in the 9L intracerebral rat glioma model. Int J Radiat Oncol Biol Phys. 2005, 63(1): 247-252
11. Mima H, Tomoshige R, Kanamori T, Tabata Y, Yamamoto S, Ito S, Tamai K, Kaneda Y. Biocompatible polymer enhances the in vitro and in vivo transfection efficiency of HVJ envelope vector. J Gene Med. 2005, 7(7): 888-897
12. Pan XQ, Wang H, Shukla S, Sekido M, Adams DM, Tjarks W, Barth RF, Lee RJ. Boron-containing folate receptor-targeted liposomes as potential delivery agents for neutron capture therapy, Bioconjug Chem. 2002, 13(3): 435-442
13. Kojima C. Design of stimuli-responsive dendrimers. Expert Opin Drug Deliv. 2010, 7(3): 307-319
14. Yanagie H, Ogata A, Sugiyama H, Eriguchi M, Takamoto S, Takahashi H. Application of drug delivery system to boron neutron capture therapy for cancer. Expert Opin Drug Deliv. 2008, 5(4): 427-443
15. X-5 Monte Carlo Team,RMCNP A GeneralMonte Carlo N-Particle Transport Code,Version 5, SLA-UR-03-1987. 2003
16. Rose PF (Ed.). Cross Section Evaluation Working Group, ENDF/B-VI Summary Document, Report BNL-NCS-17541, fourth ed.,(ENDF-201). 1991
17. CARTER RE, BOND VP, SEYMOUR PH. The relative biological effectiveness of fast neutrons in mice. Radiat Res. 1956, 4(5): 413-423

18. MAKINODAN T. Immunology of bone marrow transplantation. J Cell Physiol Suppl. 1957, 50(Suppl 1): 327-351
19. Hsu HY, Yang JJ, Ho YH, Lin CC. Difference in the effects of radioprotection between aerial and root parts of Lycium chinense. J Ethnopharmacol. 1999, 64(2): 101-108
20. Yoshida F, Yamamoto T, Nakai K, Kumada H, Shibata Y, Tsuruta W, Endo K, Tsurubuchi T, Matsumura A. Combined use of sodium borocaptate and buthionine sulfoximine in boron neutron capture therapy enhanced tissue boron uptake and delayed tumor growth in a rat subcutaneous tumor model. Cancer Lett. 2008, 263(2): 253-258
21. Maruyama K, Ishida O, Kasaoka S, Takizawa T, Utoguchi N, Shinohara A, Chiba M, Kobayashi H, Eriguchi M, Yanagie H. Intracellular targeting of sodium mercaptoundecahydrododecaborate (BSH) to solid tumors by transferrin-PEG liposomes, for boron neutron-capture therapy (BNCT). J Control Release. 2004, 98(2): 195-207
22. Sakai M. Fujimoto N. Ishii K. Murata I. Awazu K. Thermal neutron field with D-T neutron source for BNCT, Progress in NUCLEAR SCIENCE and TECHNOLOGY. 1 2011, 513-516
23. LINDOP PJ, ROTBLAT J. The age factor in the susceptibility of man and animals to radiation. I. The age factor in radiation sensitivity in mice. Br J Radiol. 1962, 35: 23-31
24. Yamamoto G. Lipid peroxides (TBA reactive substances) and Fatty Acid Compositions in Mouse Serum with Whole-body Irradiation and in Tumor-bearing Mouse Serum with Local Iradiation, Bull. Sch. Health Sci. Okayama Univ. 1990, 1: 29-37
25. Cerullo N. Esposito J. Leung KN. Custodero S. An irradiation facility for Boron Neutron Capture Therapy application based on a radio frequency driven DT neutron source and a new beam shaping assembly, Review of Scientific Instruments. 2002, 73: 3614-3619
26. Montagninia B. Cerullob N. Espositoa J. Giustia V. Mattiodac F. Varonec R. Spectrum shaping of accelerator-based neutron beams for BNCT, Nuclear Instruments and Methods in Physics Research Section A. 2002, 476(1-2): 90-98

Section 2. In vitro and in vivo investigation of accelerator BNCT using a non-viral vector; hemagglutinating virus of Japan envelope

I. Introduction

In the first section, I assembled a setup that achieved a thermal neutron flux of 6.5×10^6 n·s^{-1}·cm^{-2} in the sample area. In this section, I describe the determination of the *in vivo* and *in vitro* effects of BNCT using low neutron flux with the same setup.

I first made HVJ-E-BSH, which is HVJ-E containing mercaptoundecahydro-closo-dodecaborate (BSH). BSH accumulates selectively in brain cancers due to the impaired function of the blood-brain-barrier (BBB)[1]; the selectivity is not higher than that of the other commonly used drug, (L)-4-dihydroxy-borylphenylalanine, called BPA[2]. However, the low selectivity is not a problem when using HVJ-E, which would extend the use of BSH to other cancers. Although it cannot accumulate to as high an osmotic pressure, BSH, which has many boron atoms, is also suitable.

In general, cells are seeded in culture plates for *in vitro* experiments. Six-well (wide-space) culture plates were not appropriate for these experiments, as they require a great deal of boron solution and produce a heterogeneous distribution of thermal neutrons. However, if 96-well (small-space) culture plates were used, the number of pre-seeded cells was quite low, diminishing the accuracy of the results. Therefore, I used microtubes for irradiation. The adherent cells were trypsinized and suspended in a buffer solution with boron agent. Because the conditions of the conjugate were stressful for the cells, the time for which the cells remained healthy under these stresses was measured and the irradiation time was set at 2 hours. The treated cells were maintained in culture for 5 days to determine the magnitude of cell death during the days following the irradiation. An appropriate number of pre-seeded cells was determined before the experiment.

After the optimal conditions for the *in vitro* experiments were determined, the intracellular boron concentration and the anti-tumor effect of BNCT using HVJ-E-BSH were measured. After the *in vitro* experiments, *in vivo* experiments were conducted. Cancer-bearing mice were produced and treated with BNCT using HVJ-E-BSH. The tumor size and the survival time were measured and compared with those of untreated mice.

II. Material and Method

1. D-T Neutron Source and Thermal Neutron Field:

The intense 14 MeV neutron source facility OKTAVIAN of Osaka University was used as a D-T neutron source. And set-up to make thermal neutron field was built based on simulation calculation (Fig. 3-1-4). The detail was expressed in present study[3]. Briefly 20 cm of high density polyethylene was used for moderator and 40 cm width of graphite cover the moderator and sample area.

2. Neutron Flux Mesurement:

For D-T neutrons niobium foils were used and gold foils were for thermal neutrons. Niobium foils of 100 [μm] thickness were put in front of the tritium target, in the moderator and in the sample box. The areas of the niobium foils for the three positions were 1 x 1 [cm^2], 5 x 5 [cm^2] and 3 x 10 [cm^2] respectively. Gold foils of 50 [μm] thicknesses and 1 x 1 [cm^2] were set up along the beam axis and the line perpendicular to the axis to measure 2-dimensional flux distribution. Also cadmium covers of 1 [mm] thickness were used together to determine the so-called cadmium ratio. 934 [keV] and 412 [keV] γ rays for niobium and gold foils, respectively, were counted using a high-purity germanium detector (HpGe) (GMX-15185-p, SEIKO EG & G, Japan). The

absolute efficiency of the detector was measured with standard gamma-ray sources. Also, signals from a proportional counter were recorded in an MCS mode to accurately estimate the amount of activation of the activation foils.

The neutron flux was calculated from the measurement result of HpGe using following formula.

$$\phi = \lambda \times N.C./\left[\sigma \times N \times \left\{1-(\frac{1}{2})^{\frac{t_I}{T_{1/2}}}\right\} \times S.A. \times \left\{(\frac{1}{2})^{\frac{C.T.}{T_{1/2,}}} - (\frac{1}{2})^{\frac{C.T.+L.T.}{T_{1/2,}}}\right\}\right] \quad (1)$$

where ϕ: neutron flux, λ: decay constant, $N.C.$: number of measured γ-ray, σ: cross-section, N: number of atom of foil, t_I: irradiation time, $T_{1/2}$: half-life time of the isotope, $S.A.$: self- absorption factor of foil, $C.T.$: cooling time and $L.T.$: live time

The self-absorption factor of foil is

$$\mu = \frac{1-\exp(A \times \rho \times d)}{A \times \rho \times d} \quad (2)$$

where A: absorption rate of γ-ray, ρ: density and d: thickness. The value of A was calculated from data base of National Institute of Standard and Technology using interpolation method.

3. Cell Culture:

A549 human lung cancer (adenocarcinoma) cell line and mouse lung cancer cell line LLC were used for these studies. A549 cells were cultured in RPMI1640 (Sigma-Aldrich Inc., MO) containing 10% serum (fetal calf serum, BioWest Inc., France), and antibacterial agent (100 units/mL penicillin, and 0.1 mg/mL streptomycin (Nacalai Tesque, Japan)). LLC cells were cultured in Dulbecco's Modified Eagle's Medium (DMEM) (Sigma-Aldrich Inc., MO) containing 10 % FBS, 100 units/mL penicillin, and 0.1 mg/mL streptomycin. The cells were cultured at 37°C and 5 % CO_2.

4. Synthesis of HVJ-E-BSH:

HVJ was inactivated by UV irradiation (99 mJ/cm^2) using UV cross-linker (Spectro Linker XL-1000 UV cross-linker, Spectronic Corp.). Inactivated HVJ (3 x 10^{10} parti-cles) was mixed with 15 μL of 1% protamine sulfate/ TE buffer (QIAGEN), 110.7 μL of 3% BSH (STELLA PHARMA CORPORATION) and 40 μL of 3% TWEEN 80 (Nacalai Tesque) and incubated 5 minutes at 4°C. The suspension centrifuged (15,000 x g) for 5 minutes at 4°C. The supernatant liquid was removed and the pellet remained was washed with BSS (Balanced Salt Solution, 10 mM Tris-Cl, pH 7.5, 137 mM NaCl and 5.4 mM KCl). After this the suspension was centrifuged (15,000 x g) for 5 minutes at 4°C and the supernatant liquid was removed.

5. Preparation of CG-HVJ-E-BSH:

3 x 10^{10} particles of HVJ-E-BSH was mixed with 125 mL of 40 mg/mL cationized gelatin (CG) polymer solution (Figure 3-2-1) and incubated for 10 minutes at 4°C. The suspension was centrifuged (15,000 x g) for 5 minutes at 4°C and the supernatant liquid was removed.

6. Determination of Administration Time with HVJ-E:

300 μL (2 x 10^5 cells/mL) of A549 cell was plated in a 24-well Plate (costar(R) 3526, Corning Inc.). 24 hours later, when the cells had adhered to the plate, 25 μL of HVJ-E added red fluorescent dye (PKH26-Red Fluorescent Cell Linker Kit for Phagocytic Cell Labeling, Sigma-Aldrich Inc.) conjugate were injected to each well. After 0.5 - 4 hours incubation, HVJ-E conjugation was removed and washed with Phosphate Buffered

Saline solution (PBS) (pH 7.4, Sigma-Aldrich Inc.). And the fluorescence of PKH26-Red (excitation: 551 nm, fluorescence: 567 nm) was observed with fluorescent microscopy (BIOREVO BZ-9000, KEYENCE).

7. Concentration of Boron uptake by cells with HVJ-E-BSH, CG-HVJ-E-BSH, B-liposome:

200 μL (1 x 10^6 cells/well) of A549 cell was plated in a 24-well Plate. Four hours later, when the cells had adhered to the plate, 100 μL of 100 ppm B boron compounds (BSH, HVJ-E-BSH, CG-HVJ-E-BSH and B-liposome) were added to each well. Two hours later, the supernatant was removed and the cells were washed three times thoroughly with phosphate buffered saline solution (PBS, pH 7.4, Sigma), and lysed with 1 mL of 0.1% sodium dodecyl sulfate solution at 37°C for 20 minutes. After this the suspension was diluted by adding 5 mL water and the intracellular uptake of boron was quantified using ICP-AES (Inductively Coupled Plasma - Atomic Emission Spectrometry, ICP-7500, Shimadzu Corp.).

8. Evaluation of the antitumor activity of BNCT in vitro:

100 μL of each of 100 ppm B boron agents (BSH, HVJ-E-BSH, CG-HVJ-E-BSH, B-Liposome) was added to 100 μL of A549 cell suspension (1 x 10^5 cells/mL). After 2 hours incubation, the cells were subjected to neutron irradiation for 2 hours. After neutron irradiation, the boron agents were replaced with complete growth medium and cultured with 6-well plate (microplate 6-well with Lid. code 3810-006, IWAKI, Japan). After 5 days, the number of cells was counted to evaluate their sensitivity to BNCT. Trypan blue (Wako Pure Chemical Industries, Ltd., Japan) staining methods was used to determine cell viability in this experiment.

9. The Boron Concentration in Tumor Tissue

Six-week-old male C57BL6J mice were purchased from Hamaguchi Laboratory Animals. 1 x 10^6 LLC cells were injected subcutaneously in the dorsum of each mouse. Seven days after cell injection, either 3.48 mg of BSH or 129 μg of BSH/ 5000 HAU of HVJ-E-BSH was administered intravenously or via local infusion respectively. Thirty minutes or 2 hors later, the tumors were isolated and freeze dried. One hundred mg of freeze dried samples were burned with nitric acid (30%, 3 mL). The residues were dissolved to nitric acid (6%, 10 mL). The boron concentration was measured using ICP-AES.

10. Evaluation of Anti-tumor Effect of BNCT in vivo:

To determine tumor volume, the greatest longitudinal diameter (length) and the greatest transverse diameter (width) from each tumor were determined using an external caliper. Each tumor's volume, based on the caliper measurements, was calculated using the following formula: tumor volume = length × $\text{width}^2 \times 0.5$[4]. Seven days after the injection of A431 cells, mice were randomized into four groups of at least 12 animals per group for the following treatments: (i) no treatment; (ii) neutron irradiation without boron agent; (iii) 3.48 mg of BSH and BNCT performed or (iv) 129 μg of HVJ-E-BSH and BNCT performed. After treatment, the mice were monitored daily and their tumor volume was measured thrice a week.

III. Results

1. Chronological change of intracellular fluorescent dye:

The fluorescent images of PKH26-RED were shown in Figure 3-2-2. The fluorescent intensity was brightened up with time to 2 hours. After 2 hours, the intensity became stable.

2. Intracellular Boron Concentration:
The relationship between the boron agent and its intracellular uptake is shown in Figure 3-2-3. The value using BSH was lower than limit of determination. The value using HVJ-E, CG-HVJ-E-BSH or B-Liposome was 1.00, 0.85 or 0.68 $\mu g/10^6$ cells respectively. The novel boron agents decupled the boron concentration comparing with BSH.

3. Measurement of fast and thermal neutron at the sample box:
The fast neutron flux was 3.76 (±0.18) x 10^5 $n/cm^2/sec$. The thermal neutron flux was 1.69 (±0.37) x 10^6 $n/cm^2/sec$ and Cd ratio was 5.03 (±1.05).

4. Evaluation of the antitumor activity of BNCT *in vtro*:
The cytocidal effects of BNCT were evaluated for each boron agent. The results are described in Figure 3-2-4. The figure shows the proportion of cell number compared with untreated cell number. Only when using HVJ-E-BSH, the cytotoxicity of BNCT was observed with significant differences.

5. Boron concentration in tumor tissue:
Figure 3-2-5 showed the result of boron concentration in tumor tissue. The concentration using HVJ-E was less than the concentration using BSH.

6. Evaluation of the antitumor activity of BNCT *in vivo*:
The antitumor activity of BNCT was evaluated in *in vivo* experiment. The tumor size modification and Kaplan-Meier survival curve of BNCT was shown in Figure 3-2-6 and 3-2-7 respectively. Any difference was observed.

IV. Discussion
As shown in Fig. 3-2-4, BNCT cytotoxicity was observed when HVJ-E-BSH was used. I hypothesize that the increased intracellular boron concentration was responsible for the anti-tumor effect. The equivalent dose of BNCT can be estimated from the product of neutron fluence and boron concentration.

Currently, nuclear reactors are used as the neutron sources for BNCT. Various problems with this system have been described. Accelerator-based neutron sources for BNCT have been developed in several countries[5-10]. However, to date, such kinds of accelerators are not yet realized because of weakness of accelerator-based neutron source. Development of effective accelerator-based BNCT is important for both experimental study and therapy. I therefore proposed low-neutron-flux BNCT with a combination of an accelerator neutron source and high intracellular boron concentration obtained with a drug delivery system.

The time for transition of contents from HVJ-E into cells was observed using HVJ-E containing red fluorescent dye (Fig. 3-2-3). The fluorescence increased notably between 0.5–2 hours but little between 2–4 hours. Therefore, it seems that HVJ-E requires less than 2 hours to deliver the drug. In this study, the transition time was assumed to be 2 hours.

The experiments measuring intracellular boron concentration demonstrated that the novel boron agents (HVJ-E, CG-HVJ-E, and B-liposomes) increase boron concentration more than 10-fold over that obtained with BSH alone (Fig. 3-2-4). CG adds a positive charge to the HVJ-E surface and thus increases its association with the cell surface[11], which is negatively charged. However, this effect was not observed in this experiment. Therefore, the usefulness of the electrostatic attraction between CG-HVJ-E-BSH and the cell surface should be reconsidered.

The anti-tumor effect of BNCT was measured using the MTT assay (Fig. 3-2-5).

The magnitude of the effected correlated with the boron concentration. It is not known whether the cytotoxicity is affected by the mode of uptake. Although the cellular uptake levels of CG -HVJ-E-BSH and HVJ-E-BSH were almost the same, the cytotoxicity of CG-HVJ-E-BSH was less. In contrast, B-Liposomes produced the same cytotoxicity as HVJ-E despite delivering a lower boron concentration. The different subcellular localization of the drug may produce different effects on the DNA, subcellular organelles, or cytokine production related to the induction of cell death[12,13]. CG-HVJ-E-BSH and B-Liposomes exhibited cytotoxicity even in the absence of neutron irradiation. This drug toxicity may also interact with the BNCT effect.

In the neutron irradiation experiments, the equivalent dose of BNCT was calculated with the RBE values of α rays and Li rays equal to 3.0[14] (Table 3-2-1). The fast neutron flux was 3.76×10^5 n/cm^2/s, the equivalent dose of fast neutrons calculated with LET was $7.44 \times 10\text{-}14$ J/kg/(n/cm^2), and the RBE of recoil nucleus = 2.3[15] was 4.47×10^{-4} Gy-Eq. These values are not effective for killing cancer cells. However, the equivalent doses of novel boron agents were adequately high and produced sufficient BNCT effect for the cytotoxicity to be detectable.

The relationship between the dose and the cytotoxicity was same in previous studies[16,17] that is, sufficient to observe the cytocidal effects but insufficient for actual therapy. The equivalent dose in the present case was not sufficient for actual therapy. However we know that the stably produced maximum neutron intensity for a D-T neutron source such as OKTAVIAN is on the order of 10^{12} n/s. In addition, in our previous work, the use of HVJ-E-BSH achieved intracellular boron concentrations of up to 100 ppm. Considering these facts and the presently obtained cytocidal effects, it should be possible to use a D-T neutron source as a thermal neutron source for BNCT.

In the *in vivo* experiments, no growth inhibition of tumor tissue or survival advantage was observed due to the failure of HVJ-E-BSH to enhance the boron concentration. Fig. 3-2-6 shows the results for the boron concentration in tumor tissue. Contrary to my expectations, the boron concentration produced using HVJ-E-BSH was less than that produced using standard BSH. Delivery of BSH by HVJ-E did not achieve a sufficiently high boron concentration in the tumors to support BNCT treatment. However, the concentration was sustained 2 hours after injection, which is an advantage of HVJ-E.

I hypothesize that the low affinity of LLC cells for HVJ-E is the reason for the low boron concentration of HVJ-E-treated tumor tissue. HVJ-E binding to the cell surface is mediated by an acetyl-type sialic acid recognized by the HN protein on the vector[18] but LLC cells express little sialic acid at the cell surface. In the HVJ-PDT experiment (Section 2-1), the LLC cell line took up less photosensitizer than did the other cell lines despite their high growth rate. In general, human cancer cells strongly express sialic acid. Therefore, the BNCT effect produced by HVJ-E-BSH should be measured in a cell line that expresses sialic acid similarly to human cancer cells.

Figures

Table 3-2-1. Equivalent dose (RBE-Gy) of BNCT

	BSH	HVJ-E-BSH	CG-HVJ-E-BSH	B-Liposome
Dose (± SD) [Gy-Eq]	< 0.19	3.4 (± 0.07)	2.9 (± 0.13)	2.3 (± 0.04)

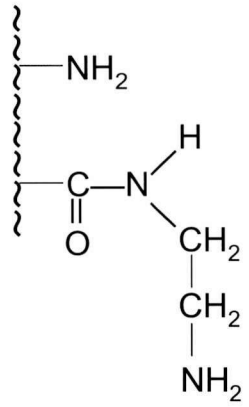

Figure 3-2-1. Chemical structure of cationized gelatin.

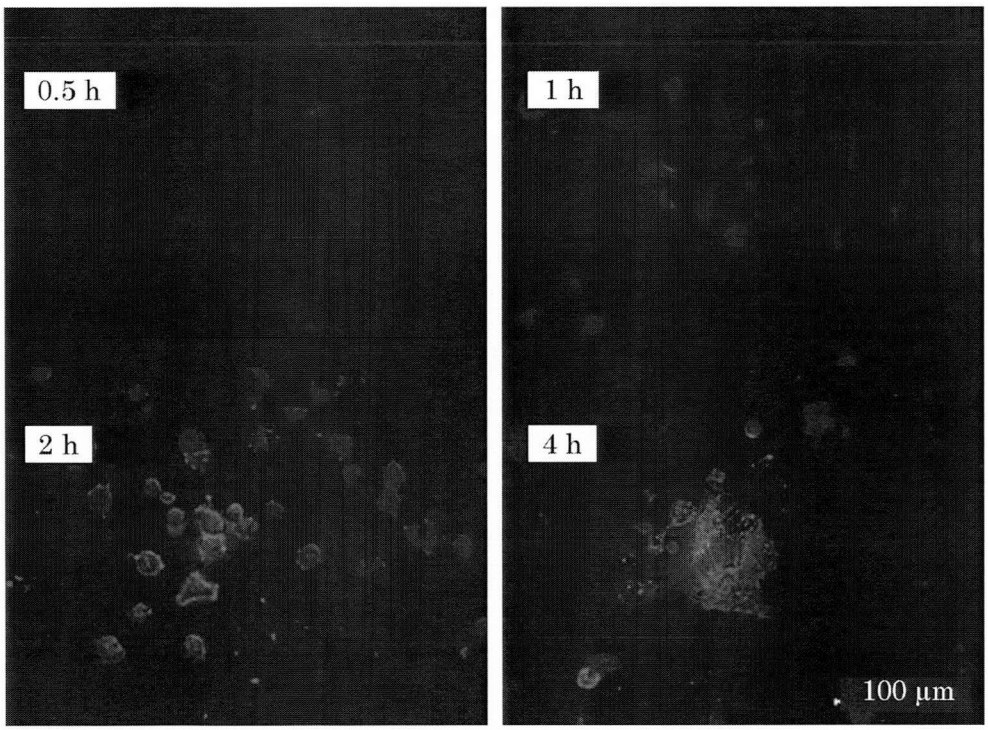

Figure 3-2-2. Fluorescence microscopic images of A549 with PKH26-RED. Images of PKH26-RED obtained at 0.5, 1, 2, 4 hours after the addition of the probes. Bar = 100 μm.

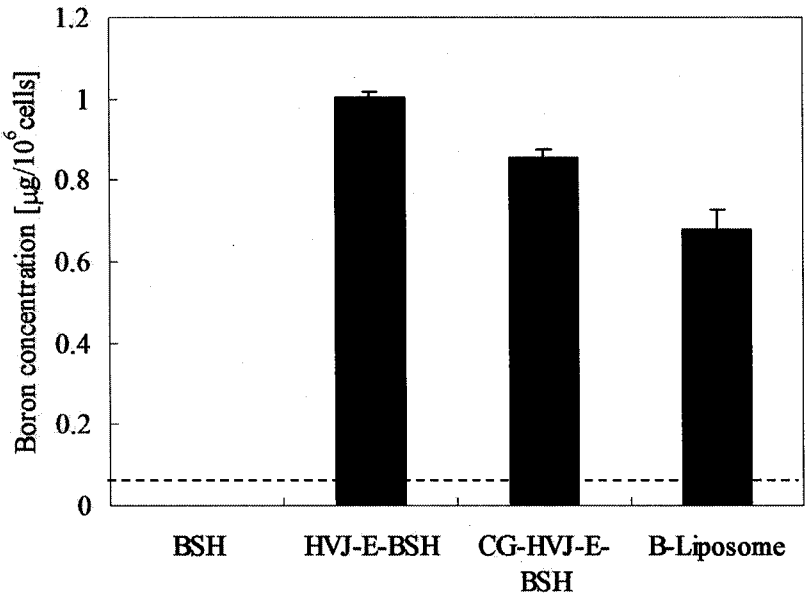

Figure 3-2-3 Intracellular uptake of Boron. Intracellular concentration of boron is expressed against boron compound. The broken line indicates quantification limits (0.06 mg/10^6 cells).

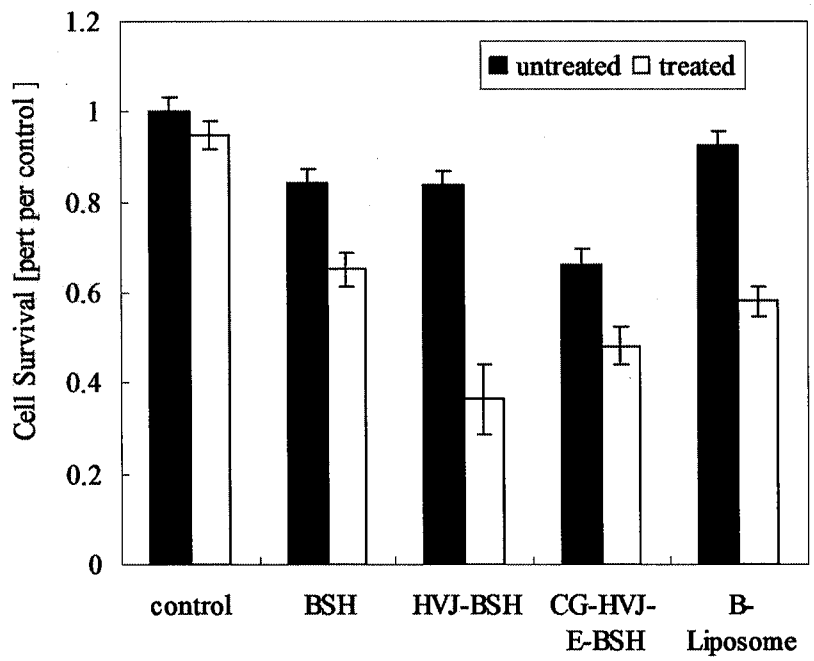

Figure 3-2-4. Antitumor effect of BNCT measure by trypan blue dyeing. The cell survival rate (%) compared with the cell number of B-negative and neutron-negative sample is expressed.

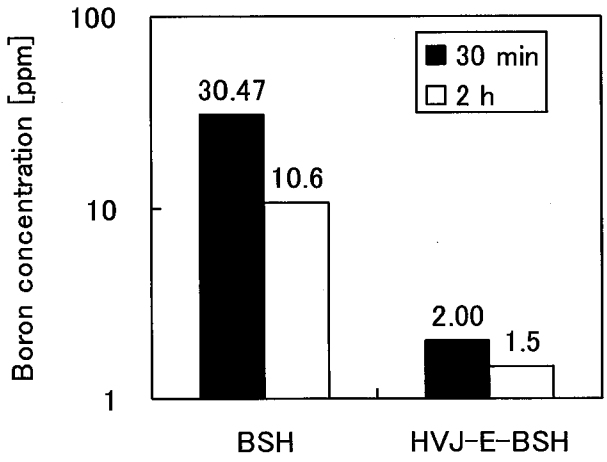

Figure 3-2-5. Boron concentration in tumor tissue.

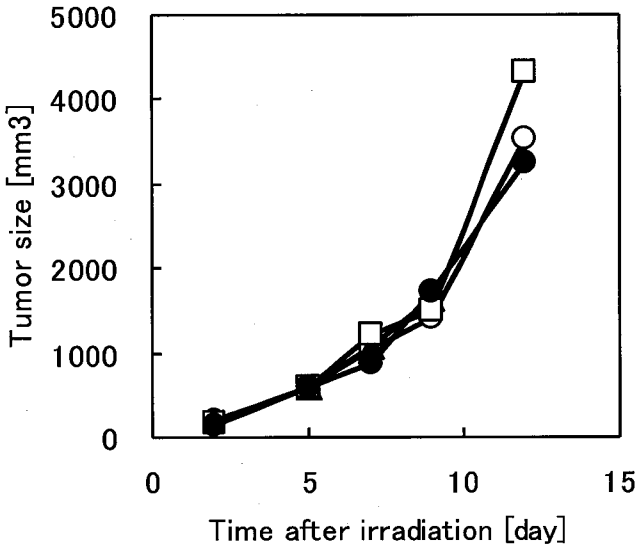

Figure 3-2-6. The tumor growth mediated BNCT in LLC tumor. The tumor volume is expressed against elapsed days. The symbol indicates: ●; no treatment, □; neutron irradiation without boron agent, △; 3.48 mg of BSH and BNCT performed and ○; 129 μg of HVJ-E-BSH and BNCT performed.

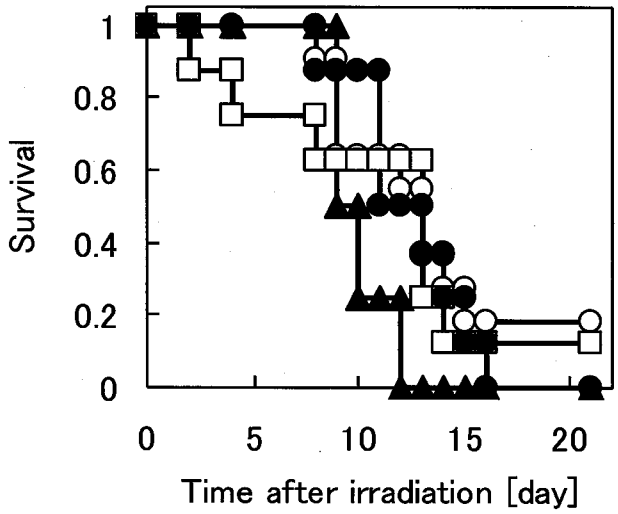

Figure 3-2-7. An analysis using a Kaplan-Meier survival curve of BNCT in LLC tumors. The symbol indicates: ●; no treatment, □; neutron irradiation without boron agent, △; 3.48 mg of BSH and BNCT performed and ○; 129 μg of HVJ-E-BSH and BNCT performed.

References

1. Barth RF, Yang W, Rotaru JH, Moeschberger ML, Boesel CP, Soloway AH, Joel DD, Nawrocky MM, Ono K, Goodman JH. Boron neutron capture therapy of brain tumors: enhanced survival and cure following blood-brain barrier disruption and intracarotid injection of sodium borocaptate and boronophenylalanine. Int J Radiat Oncol Biol Phys. 2000, 47(1): 209-218
2. Capala J, Makar MS, Coderre JA. Accumulation of boron in malignant and normal cells incubated in vitro with boronophenylalanine, mercaptoborane or boric acid. Radiat Res. 1996, 146(5):554-560
3. Sakai M, Fujimoto N, Murata I, Awazu K. Development of thermal neutron field with D-T neutron source aiming at in vivo and in vitro experiments for BNCT. Housyasen. 2012,
4. Yoshida J, Mizuno M, Yagi K. Secretion of Human β-Interferon into the Cystic Fluid of Glioma Transfected with the Interferon Gene. Journal of Clinical Biochemistry and Nutrition. 1991, 11(2): 123-128
5. Hawk AE, Blue TE, Woollard JE. A shielding design for an accelerator-based neutron source for boron neutron capture therapy. Appl Radiat Isot. 2004, 61(5): 1027-1031.
6. Lee DJ, Han CY, Park SH, Kim JK. An accelerator-based epithermal neutron beam design for BNCT and dosimetric evaluation using a voxel head phantom. Radiat Prot Dosimetry. 2004, 110(1-4): 655-660
7. Bayanov B, Kashaeva E, Makarov A, Malyshkin G, Samarin S, Taskaev S. A neutron producing target for BINP accelerator-based neutron source. Appl Radiat Isot. 2009, 67(7-8 Suppl): S282-284
8. Tanaka H, Sakurai Y, Suzuki M, Masunaga S, Mitsumoto T, Fujita K, Kashino G, Kinashi Y, Liu Y, Takada M, Ono K, Maruhashi A. Experimental verification of beam characteristics for cyclotron-based epithermal neutron source (C-BENS). Appl Radiat Isot. 2011, 69(12): 1642-1645
9. Bergueiro J, Igarzabal M, Sandin JC, Somacal HR, Vento VT, Huck H, Valda AA, Repetto M, Kreiner AJ. Development of high intensity ion sources for a Tandem-Electrostatic-Quadrupole facility for Accelerator-Based Boron Neutron Capture Therapy. Appl Radiat Isot. 2011, 69(12): 1676-1679
10. Terlizzi R, Colonna N, Colangelo P, Maiorana A, Marrone S, Rainò A, Tagliente G, Variale V. Design of an accelerator-based neutron source for neutron capture therapy. Appl Radiat Isot. 2009, 67(7-8 Suppl): S292-295
11. Fujii H, Matsuyama A, Komoda H, Sasai M, Suzuki M, Asano T, Doki Y, Kirihata M, Ono K, Tabata Y, Kaneda Y, Sawa Y, Lee CM. Cationized gelatin-HVJ envelope with sodium borocaptate improved the BNCT efficacy for liver tumors in vivo. Radiat Oncol. 2011, 20(6): 8
12. Haselsberger K, Radner H, Gössler W, Schlagenhaufen C, Pendl G. Subcellular boron-10 localization in glioblastoma for boron neutron capture therapy with Na2B12H11SH. J Neurosurg. 1994, 81(5): 741-744
13. Bennett BD, Mumford-Zisk J, Coderre JA, Morrison GH. Subcellular localization of p-boronophenylalanine-delivered boron-10 in the rat 9L gliosarcoma: cryogenic preparation in vitro and in vivo. Radiat Res. 1994, 140(1): 72-78
14. Coderre JA, Makar MS, Micca PL, Nawrocky MM, Liu HB, Joel DD, Slatkin DN, Amols HI. Derivations of relative biological effectiveness for the high-let radiations produced during boron neutron capture irradiations of the 9L rat gliosarcoma in vitro and in vivo. Int J Radiat Oncol Biol Phys. 1993, 27(5): 1121-1129
15. Cho T, Uehara S, Yoshinaga H. Contribution of Recoiled Nuclei in 14.1 MeV Neutron Irradiation. Memoirs of Kyushu University Scool of Health Sciences. 1975, 2: 35-41

16. Nitsche M, Christiansen H, Hermann RM, Lucke EM, Peters K, Rave-Frank M, Schmidberger H, Pradier O. The combined effect of fludarabine monophosphate and radiation as well as gemcitabine and radiation on squamous carcinoma tumor cell lines in vitro. Int J Radiat Biol. 2008, 84(8): 643-657
17. Bromley R, Oliver L, Davey R, Harvie R, Baldock C. Predicting the clonogenic survival of A549 cells after modulated x-ray irradiation using the linear quadratic model. Phys Med Biol. 2009, 54(2): 187-206
18. Kaneda Y, Saeki Y, Morishita R. Gene therapy using HVJ-liposomes: the best of both worlds?. Mol Med Today. 1999, 5(7): 298-303

Section 3. Development of the in-vitro experiment of BNCT

I. Introduction

In this section, I describe strategies for correcting the problems of the previous *in vivo* experiments. In the previous section, no effect of BNCT was observed in tumor-bearing small animals. This poor result was thought to be due to the lack of affinity of LLC cells for HVJ-E.

Because HVJ-E-BSH (HVJ-E containing mercaptoundecahydro-closo-dodecaborate (BSH)) was administered via local infusion, the affinity of the tumor cells for HVJ-E is important[1,2]. In section 1 of chapter 2, the intracellular concentrations of photosensitizer in each cell line were compared, and some differences were observed. LLC took up less photosensitizer than did the other cell lines. The lower uptake may lead to less accumulation. Inclusions enter the excretory pathway independently. BSH is impervious to molecular degradation. The BSH uptake abilities of each cell line should also be compared.

The setup was also improved by the use of deuterium water. The importance of deuterium water was indicated in section 1. It is highly possibility that this allows the thermal neutron flux in the sample area to be increased without increasing the fast thermal neutron flux. A reservoir was made from high-density polyethylene, and neutron transport was simulated when this reservoir was filled with deuterium water.

II. Material and Method.

1. Synthesis of HVJ-E-BSH

HVJ was inactivated by UV irradiation (99 mJ/cm^2) using UV cross-linker (Spectro Linker XL-1000 UV cross-linker, Spectronic Corp.). Inactivated HVJ (3 x 10^{10} parti-cles) was mixed with 15 μL of 1% protamine sulfate/ TE buffer (QIAGEN), 110.7 μL of 3% BSH (STELLA PHARMA CORPORATION) and 40 μL of 3% TWEEN 80 (Nacalai Tesque) and incubated 5 minutes at 4°C. The suspension centrifuged (15,000 x g) for 5 minutes at 4°C. The supernatant liquid was removed and the pellet remained was washed with BSS (Balanced Salt Solution, 10 mM Tris-Cl, pH 7.5, 137 mM NaCl and 5.4 mM KCl). After this the suspension was centrifuged (15,000 x g) for 5 minutes at 4°C and the supernatant liquid was removed.

2. Cell culture

The cell lines used in this study were the human lung cancer cell line A549, the murine melanoma cell line B16 the mouse colon carcinoma cell line CT26 and the mouse Lewis lung adenocarcinomas cell line LLC. The A549 cells were cultured in RPMI-1640 medium (Sigma-Aldrich Inc.) containing 10 % fetal bovine serum (FBS, Biowest Inc., France), 100 units/mL penicillin, and 0.1 mg/mL streptomycin (Nacalai Tesque, Japan). The B16, CT26 and LLC cells were cultured in Dulbecco's Modified Eagle's Medium (DMEM) (Sigma-Aldrich Inc.) containing 10% FBS, 100 units/mL penicillin, and 0.1 mg/mL streptomycin. The cells were cultured at 37°C and 5% CO_2.

3. Concentration of Boron uptake by cells with HVJ-E-BSH, CG-HVJ-E-BSH, B-liposome

200 μL (1 x 10^6 cells/well) of A549 cell was plated in a 24-well Plate. 4 hours later, when the cells had adhered to the plate, 100 μL of 100 ppm B boron compounds (BSH, HVJ-E-BSH, CG-HVJ-E-BSH and B-liposome) were added to each well. Two hours later, the supernatant was removed and the cells were washed three times thoroughly with phosphate buffered saline solution (PBS, pH 7.4, Sigma), and lysed with 1 mL of 0.1% sodium dodecyl sulfate solution at 37°C for 20 minutes. After this the suspension was diluted by adding 5 mL water and the intracellular uptake of boron was quantified

using ICP-AES (Inductively Coupled Plasma - Atomic Emission Spectrometry, ICP-7500, Shimadzu Corp.).

4. Neutron Transport Calculation

In order to estimate the thermal and fast neutron flux at the irradiation position, simulation calculations were performed using MCNP-5[3] (A General Monte Carlo N-Particle Transport Code). ENDF/B-VI[4] was used as a neutron cross section library. Track length estimator tally, F4, was used for calculating thermal and fast neutron spectra. Reaction rates for ^{197}Au (n, γ) positioned in several places in a box for irradiation of mice were calculated for comparison with the experimental results. The calculation was performed using a virtual pure gold foil with the tally multiplier card, FM, for the reaction type of (n, γ), i.e., MT = 102. The number of histories was $1x10^7$.

5. D-T Neutron Source and Thermal Neutron Field

The intense 14 MeV neutron source facility OKTAVIAN of Osaka University was used as a D-T neutron source. And set-up to make thermal neutron field was built based on simulation calculation (Figure 3-3-1).

6. Neutron Flux Mesurement

FFor D-T neutrons niobium foils were used and gold foils were for thermal neutrons. Niobium foils of 100 μm thickness were put in front of the tritium target, in the moderator and in the irradiation position. The areas of the niobium foils for the three positions were 1 x 1 cm^2, 5 x 5 cm^2 and 3 x 10 cm^2 respectively. Gold foils of 50 μm thickness and 1 x 1 cm^2 were set up along the beam axis and the line perpendicular to the axis to measure 2-dimensional flux distribution. Also cadmium covers of 1 mm thickness were used together to determine the so-called cadmium ratio. 934 keV and 412 keV γ rays for niobium and gold foils, respectively, were counted using a high-purity germanium detector (HpGe) (GMX-15185-p, SEIKO EG & G, Japan). The absolute efficiency of the detector was measured with standard gamma-ray sources. Also, signals from a proportional counter were recorded in an MCS mode to accurately estimate the amount of activation of the foils.

7. Radiation Dose Calculation

In this study we had assumed that 12 mice are irradiated. The BNCT dose (D_{BNCT}) at the irradiation area was calculated to evaluate the performance of the constructed thermal neutron field. The equivalent dose of BNCT, D_{BNCT}, was calculated using the following equation:

$$D_{BNCT} = (R_N \times K_N + R_B \times K_B \times C_B) \times \phi_{thermal} \times T + D_f + D_\gamma \quad (2)$$

where, K_N and K_B are the doses per unit fluences from nitrogen (2% in weight of mouse cell) and from boron (per 1 ppm)[5], respectively. Nitrogen captures a thermal neutron like as boron and produces a proton (^{14}N (n, p) ^{14}C). This reaction occurs as side reaction in thermal neutron field because the reaction isn't threshold reaction. To calculate the equivalent dose, the RBE 3.2 and 3.8 (R_N and R_B) for D_N (the dose from nitrogen reaction) and D_B (the dose from boron reaction) were used, respectively[6]. C_B, $\phi_{thermal}$ and T are the intracellular boron concentration, the thermal neutron flux and the irradiation time, respectively. The irradiation time was assumed to be 2 hours. Activation foils were used to estimate intensities of the generated 14 MeV neutrons and thermal neutrons ($\phi_{thermal}$). And D_f and D_γ are the equivalent dose from fast neutrons and the dose from gamma ray, respectively. They were estimated by MCNP-5 calculation and the measured value of the generated 14 MeV neutrons. In the calculation, the areas in which there are mice were replaced with a cylindrical water phantom and it was assumed that there is a tumor on the surface of a mouse. The RBE

of 2.3 was used[17]. K_N and K_B are derived from the following equation.

$$K_i = N_A \times Q_i \times \sigma_I \quad (3)$$

where, Na is Avogadro's number, Q is the energy released per nuclear reaction, i.e., 0.6 and 2.31 MeV for $^{14}N(n, p)$ and $^{10}B(n, \alpha)$ reactions, respectively and σ is the cross-sections of 1.75 barn for $^{14}N(n, p)$ and 3837 barn for $^{10}B(n, \alpha)$ reactions (the representative value for thermal neutron). The boron concentration of the tumor tissue was assumed to be 300 ppm and that of the healthy tissue is 5 ppm. Although the concentration is about 10 times higher than those expected in general BNCT cases, it was reported in some papers[7-9] that it could be surely achieved. In this case the ratio of tumor dose / normal dose is 53.

III. Result

1. Intracelluler Boron Concentration

The relationship between the boron agent and its intracellular uptake is shown in Figure 3-3-2. When the concentration of HVJ-E-PPIX suspension was over 50 μM, the B16 cells took up more PPIX than the other cells especially LLC.

2. Estimated Value of Simulation Calculation

Monte Calro simulation was operated to estimate the fast and thermal neutron flux. The value predicted by the calculation was 4.4×10^{-5} n/cm^2/source neutron and 2.9×10^{-4} n/cm^2/source neutron respectively. Though the predicted fast neutron flux was increased, the rate was small. On the other hand the thermal neutron flux was expected to improve two times higher than current set-up.

3. Comparison between Calculation and Measurement:

Neutron irradiation was performed at the OKTAVIAN facility and the fast and thermal neutron fluxes were measured with niobium and gold foils (Table 3-3-1, Figure 3-3-3). The 14 MeV neutron source intensity was 3.2×10^{10} n/s. The fast and thermal neutron fluxes were 6.1×10^5 and 8.9×10^6 n/s/cm2 respectively and Cd ratio was 6.7. The measured neutron fluxes were in good agreement with the calculation results in the whole region.

IV. Discussion

The intracellular boron concentration of each cell line was measured, with B16 cells found to take up the most boron. Although the difference in uptake rates between B16 and LLC cells was not large, the difference would be magnified in *in vivo* experiments because the uptake need not take place as quickly *in vitro*. In the tumor tissue of small animals, HVJ-E moves through with the flow of blood, making its ability to adhere to tumor cells even more important. While the *in vitro* experiments reported herein did not allow me to evaluate the tumor accumulation of the boron agent, it is highly possible that the accumulation was in fact improved.

The setup was also improved by the use of deuterium water, which increased the thermal neutron flux. Rat tumors have been reported to shrink after a radiation dose of 3.7 Gy-eq[10] and disappear after a dose of 23 Gy-eq[11] Boron concentrations of 120 ppm and 1050 ppm would be required to achieve the equivalent doses with the thermal neutron flux produced by this experiment. Although it is not known whether HVJ-E can deliver such concentrations, it seems likely, as it has been reported that the boron level produced by CG-HVJ-E-BSH (a HVJ-E BSH-spiked cationized gelatin) was 35 times higher than that produced by BSH alone. There are also other boron agents that have already reached a concentration of 519 ppm boron[7]. Therefore, these novel boron agents could be used to conduct *in vivo* experiments on accelerator-based BNCT.

Figures

Table 3-3-1. Results of the measurement of the □ rays from the activation foil.

	Experimental value	C/E
generated 14 Mev neutron	3.2×10^{10}	-
fast neutron in sample area	6.1×10^{5}	2.3×10^{0}
thermal neutron in samaple area	8.9×10^{6}	1.1×10^{0}
Cd ratio	6.8	-

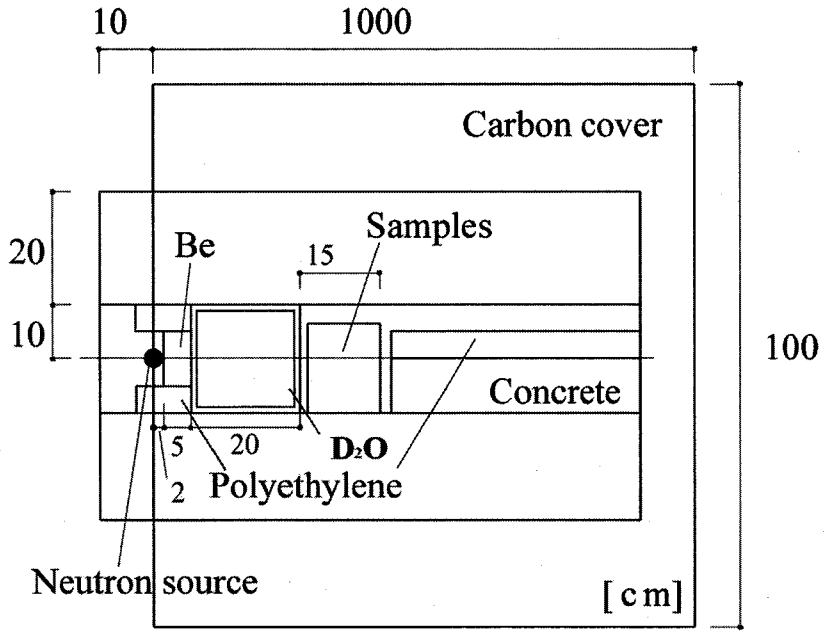

Figure 3-3-1. Experimental set-up for neutron irradiation. Deuterium water was placed between tritium target and sample area to moderate 14 MeV neutrons.

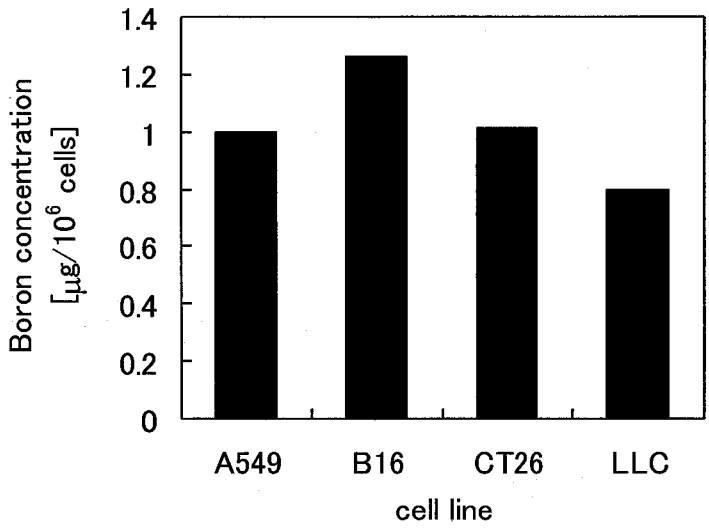

Figure 3-3-2. Intracellular uptake of boron. Intracellular concentration of boron in each cell line is expressed. The value of B16 was the highest.

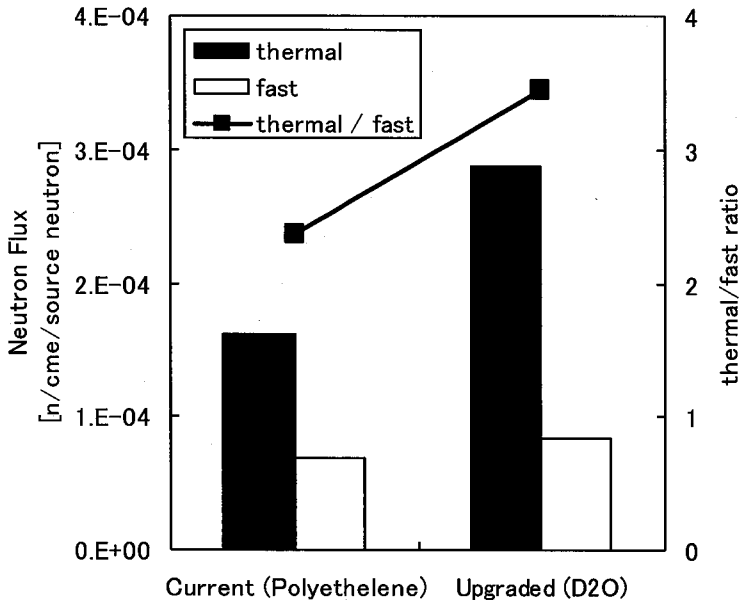

Figure 3-3-3 Flux of the thermal and fast neutron and the ratio of thermal/ fast in the sample box using different moderator calculated by MCNP-5; polyethylene (PE) and heavy water (D_2O).

References

1. Saga K, Tamai K, Kawachi M, Shimbo T, Fujita H, Yamazaki T, Kaneda Y. Functional modification of Sendai virus by siRNA. J Biotechnol. 2008, 133(3): 386-394
2. Mima H, Yamamoto S, Ito M, Tomoshige R, Tabata Y, Tamai K, Kaneda Y. Targeted chemotherapy against intraperitoneally disseminated colon carcinoma using a cationized gelatin-conjugated HVJ envelope vector. Mol Cancer Ther. 2006, 5(4): 1021-1028
3. X-5 Monte Carlo Team,RMCNP A GeneralMonte Carlo N-Particle Transport Code,Version 5, SLA-UR-03-1987. 2003
4. Rose PF (Ed.). Cross Section Evaluation Working Group, ENDF/B-VI Summary Document, Report BNL-NCS-17541, fourth ed.,(ENDF-201). 1991
5. Nakagawa Y, Pooh K, Kobayashi T, Kageji T, Uyama S, Matsumura A, Kumada H. Clinical review of the Japanese experience with boron neutron capture therapy and an a propsed strategy using epithermal neutron beams. J Neurooncol. 2003, 62(1-2): 87-99
6. Coderre JA, Makar MS, Micca PL, Nawrocky MM, Liu HB, Joel DD, Slatkin DN, Amols HI. Derivations of relative biological effectiveness for the high-let radiations produced during boron neutron capture irradiations of the 9L rat gliosarcoma in vitro and in vivo. Int J Radiat Oncol Biol Phys. 1993, 27(5): 1121-1129
7. Ozawa T, Afzal J, Lamborn KR, Bollen AW, Bauer WF, Koo MS, Kahl SB, Deen DF. Toxicity, biodistribution, and convection-enhanced delivery of the boronated porphyrin BOPP in the 9L intracerebral rat glioma model. Int J Radiat Oncol Biol Phys. 2005, 63(1): 247-252
8. Pan XQ, Wang H, Shukla S, Sekido M, Adams DM, Tjarks W, Barth RF, Lee RJ. Boron-containing folate receptor-targeted liposomes as potential delivery agents for neutron capture therapy, Bioconjug Chem. 2002, 13(3): 435-442
9. Mima H, Tomoshige R, Kanamori T, Tabata Y, Yamamoto S, Ito S, Tamai K, Kaneda Y. Biocompatible polymer enhances the in vitro and in vivo transfection efficiency of HVJ envelope vector. J Gene Med. 2005, 7(7): 888-897
10. Yoshida F, Yamamoto T, Nakai K, Kumada H, Shibata Y, Tsuruta W, Endo K, Tsurubuchi T, Matsumura A. Combined use of sodium borocaptate and buthionine sulfoximine in boron neutron capture therapy enhanced tissue boron uptake and delayed tumor growth in a rat subcutaneous tumor model. Cancer Lett. 2008, 263(2): 253-258
11. Maruyama K, Ishida O, Kasaoka S, Takizawa T, Utoguchi N, Shinohara A, Chiba M, Kobayashi H, Eriguchi M, Yanagie H. Intracellular targeting of sodium mercaptoundecahydrododecaborate (BSH) to solid tumors by transferrin-PEG liposomes, for boron neutron-capture therapy (BNCT). J Control Release. 2004, 98(2): 195-207

Chapter 4. DNA Damage from High LET Radiation Using *Escherichia coli*

In Chapter 3, equivalent dose was calculated to evaluate the boron neutron capture therapy (BNCT) effect, and the value was compared with those from other studies on the same cell line. Although the RBE value of each nuclear reaction was determined in the previous study, some points remain unclear. To accurately calculate the dose and administer treatment with the least side effects, the radiological consequences need to be precisely assessed.

In PDT treatment, reactive oxygen species induce apoptosis or necrosis via cell membrane or organelle damage[1]. n the other hand, radiation damages DNA in BNCT treatment. DNA damage-induced cytotoxicity occurs via 2 pathways (indirect and direct effects)[2].

In the indirect effect, molecules except the target absorb radiation energy and produce active substances such as free radicals whose toxicity elicits a biological effect. In aqueous solution, radiation interacts with the external medium. It may break the bonds that hold the water molecule together, producing fragments such as hydrogen and hydroxyl ions. These fragments may recombine or may interact with other fragments or ions to form compounds, such as water, which is not harmful to the cell. However, they could combine to form toxic substances, such as hydrogen peroxide, which can contribute to the destruction of the cell[3]. Particularly, hydroxyl and hydroperoxy radicals readily react with DNA[4].

The interaction of radiation with the atoms of DNA or other cellular components critical to the survival of the cell is referred to as a direct effect. Such an interaction may affect the ability of the cell to reproduce and, thus, survive. If enough atoms are affected such that the chromosomes do not replicate properly, or if there is significant alteration in the information carried by the DNA molecule, then the cell may be destroyed by "direct" interference with its life-sustaining system. The position at which the radiation is absorbed does not necessarily correspond to the breakpoint. The absorbed energy is sometimes transported to other bonds or molecules, where it breaks weak bonds[5,6].

DNA is the most important material and serves as the master blueprint for the cell. There is considerable evidence suggesting that DNA is the primary target for cell damage from ionizing radiation. If a cell is exposed to radiation, the probability of the interaction between radiation and the DNA molecule is very small because these critical components make up a small part of the cell. However, cells are mostly composed of water. Therefore, there is a much higher probability of radiation interacting with the water. The proportion of direct effects depends on the radiation type and energy, and high linear energy transfer (LET) radiation produces more direct effects. Because indirect effects produce discrete lesions by random energy deposition of the diffusing radical, they are easy to repair. Direct effects produce closely spaced lesions forming clustered DNA damage. Clustered DNA lesions have been suggested to be more difficult to repair and are, in general, a form of DNA damage that is repair-resistant or non-repairable, with a high mutagenic potential. Therefore, they are highly significant biological endpoints[7,8].

BNCT involves a B (n, α)-Li reaction and mainly produces ion beams that damage cells. Ion beams generated by BNCT exhibit a Bragg peak and high LET. That leads high dose, low Oxygen Enhancement Ratio (OER) and high specificity. However, the RBE value of these ion beams remains unclear. For example, the value of the radiation weighting factor is 20[9]. Although this value is set slightly high from a radiation protection perspective, various values have been reported in BNCT studies and no consensus has been reached.

The major factor in the lack of a consensus is insufficient knowledge of clustered damage. If the absorbed dose is same value, clustered damage inhibits DNA repair and

increases the effects on the cell. Therefore, I examined the mechanisms underlying the cellular disorder induced by γ-rays and α-rays, which are generated in the BNCT reaction.

In this study, I used *Escherichia coli* (*E. coli*), a model organism used to investigate cellular responses to ionizing radiation. It possesses several repair pathways, such as base excision repair and homologous recombination, to cope with various types of radiation-induced DNA damage, which are relevant to the biological consequences of ionizing radiation[10].

E. coli is likely to mutate, which can be easily detected using various methods. I used phenyl-β-d-galactose (P-Gal), 5-bromo-4-chloro-indolyl-galactopyranoside (X-gal), and antibiotics. P-gal and X-gal detect mutations in the *lac* operon, which is a suite of genes whose products metabolize lactose. It consists of 3 adjacent structural genes: *lacZ*, *lacY*, and *lacA*. The *lac* operon is regulated by several factors, including the availability of glucose and lactose. In its natural environment, the *lac* operon allows for the effective digestion of lactose. The cell can use lactose as an energy source by producing the enzyme β-galactosidase, which digests lactose into glucose and galactose. However, it would be inefficient to produce the enzyme when there is no lactose available, or if there is a more readily available energy source, such as glucose. The *lacI* gene coding for the repressor lies near the *lac* operon and is always expressed. In the absence of lactose, the repressor binds very tightly to a short DNA sequence, called the *lac* operator [11] , downstream of the promoter near the beginning of *lacZ*. P-gal is a substrate for β-galactosidase, but does not inactivate the repressor and is, therefore, not an inducer. Because wild-type cells produce very little β-galactosidase, they cannot use P-Gal as a carbon and energy source. Mutants lacking the repressor are able to grow on P-Gal. Thus, minimal medium containing only P-Gal as a source of carbon and energy is selective for repressor and operator mutants[12] . X-gal is used together with isopropyl-β-d-thiogalactoside (IPTG), which is an inducer of the *lac* operon in physiological studies. Cells that express *lacZ* metabolize X-gal, and are dyed blue[13,14].

The antibiotics rifampicin and streptomycin were used in this study. Rifampicin inhibits RNA polymerase, which is responsible for binding to a strand of DNA and uses it as a template to construct a strand of mRNA[15]. Streptomycin is bactericidal in action. It inhibits protein synthesis by irreversibly combining with the 30S subunit of the70S ribosome. Specifically, it binds to the S12 protein involved in the initiation of protein synthesis. Cells harboring mutations in the binding protein can be detected using medium containing these antibiotics[16].

The radiation sensitivities of wild-type *E. coli* and each mutant were compared using survival and mutation frequency measurements. In section 1, the relationship between LET and DNA repair function is examined. Wild type and mutants were irradiated with X-rays or He-rays and the survival rate and mutation frequency were measured. In section 2, I examined the effect of medium on the radiation sensitivity observed in section 1. Because rich medium makes wild-type *E. coli* resistant to X-rays, the mechanism and relationship with LET were examined.

References

1. Buytaert E, Dewaele M, Agostinis P. Molecular effectors of multiple cell death pathways initiated by photodynamic therapy. Biochim Biophys Acta. 2007, ;1776(1): 86-107
2. Perez CA. Brady LW. Halperin EC. Schmidt-Ullrich R. Principles and Practice of Radiation Oncology. Philadelphia, PA. Lippincott Williams & Wilkins; Fourth Edition. 2003
3. Hutchinson F. Chemical changes induced in DNA by ionizing radiation. Prog Nucleic Acid Res Mol Biol. 1985, 32: 115-154
4. Yoshimura T, Matsuno K, Miyazaki T, Suzuki K, Watanabe M. Electron spin resonance studies of free radicals in gamma-irradiated golden hamster embryo cells: radical formation at 77 and 295 K, and radioprotective effects of vitamin C at 295 K. Radiat Res. 1993, 136(3): 361-365
5. Schulte-Frohlinde D, Opitz J, Gorner H, Bothe E. Model studies for the direct effect of high-energy irradiation on DNA. Mechanism of strand break formation induced by laser photoionization of poly U in aqueous solution. Int J Radiat Biol Relat Stud Phys Chem Med. 1985, 48(3): 397-408
6. Goodhead DT, Munson RJ, Thacker J, Cox R. Mutation and inactivation of cultured mammalian cells exposed to beams of accelerated heavy ions. IV. Biophysical interpretation. Int J Radiat Biol Relat Stud Phys Chem Med. 1980, 37(2): 135-167
7. Ward JF. Some biochemical consequences of the spatial distribution of ionizing radiation-produced free radicals. Radiat Res. 1981, 86(2): 185-195.
8. Goodhead DT. Initial events in the cellular effects of ionizing radiations: clustered damage in DNA. Int J Radiat Biol. 1994, 65(1): 7-17
9. International Commission on Radiological Protection. 1990 recommendations of the International Commission on Radiological Protection. Oxford, England: Pergamon, 1991. ICRP publication 60
10. Friedberg EC. Walker GC. Siede W. Wood RD. Shultz RA. Ellenberger T. DNA Repair and Mutagenesis, ASM Press, Washington, DC, USA, 2nd edition, 2006
11. Beckwith JR. Regulation of the lac operon. Recent studies on the regulation of lactose metabolism in Escherichia coli support the operon model. Science. 1967, 156(3775): 597-604
12. Miller JH. A short course in bacterial genetics, Cold Spring Harbor Laboratory Press, 1992
13. Hansen LH, Knudsen S, Sorensen SJ. The effect of the lacY gene on the induction of IPTG inducible promoters, studied in Escherichia coli and Pseudomonas fluorescens. Curr Microbiol. 1998, 36(6): 341-347
14. Joung JK, Ramm EI, Pabo CO. A bacterial two-hybrid selection system for studying protein-DNA and protein-protein interactions. Proc Natl Acad Sci U S A. 2000, 97(13): 7382-7387
15. Acocella G. Clinical pharmacokinetics of rifampicin. Clin Pharmacokinet. 1978, 3(2): 108-127
16. Schatz A, Bugie E, Waksman SA. Streptomycin, a substance exhibiting antibiotic activity against gram-positive and gram-negative bacteria. 1944. Clin Orthop Relat Res. 2005, (437): 3-6

Section 1. Difference of radiation effective depending on LET

I.Introduction

There are many types of radiation and each has its own mechanism of action. Especially, the effects of high-linear energy transfer (LET) radiation are different from those of X-rays or γ-rays. High-LET radiation tends to inflict great damage on DNA via direct effects and the damage is easily clustered. Because clustered DNA damage is difficult to repair, high-LET radiation has a significant impact on cells[1].

To determine the difference, I compared the effects of He-ray and x-ray. Wild-type *Escherichia coli* (*E. coli*) and its mutants were used, because *E. coli* lacking the gene for DNA repair can be easily generated from wild-type cells. Table 4-1-1 shows the genes, the protein products of the genes, and the repair mechanisms associated with the genes used in this study. The mechanisms described in Table 1 are the main DNA repair systems in *E. coli*.

Nucleotide excision repair (NER) is a highly versatile and sophisticated DNA damage removal pathway that counteracts the deleterious effects of a multitude of DNA lesions, including the major types of damage induced by environmental sources. The most relevant lesions subject to NER are cyclobutane pyrimidine dimers and 6,4-photoproducts, the 2 major kinds of injury produced by the shortwave UltraViolet (UV) component of sunlight[2].

DNA mismatch repair (MMR) is a repair system that removes erroneous insertions, deletions, and mis-incorporation of bases during DNA replication, usually in the newly synthesized strand[3,4].

Homologous recombination is the exchange or replacement of a DNA region by its homologous DNA sequence from the homologous chromosome or the sister chromatid[5]. Homologous recombination is the major process for repairing double-strand breaks (DSB) in bacterial DNA[6,7].

The SOS response is a set of inducible physiological reactions that enable cells to survive after treatment with various DNA-damaging agents[8,9]. RecA and LexA, which are the products of the *recA* and *lexA* genes, respectively, regulate the induction of the SOS response in cells after exposure to genotoxic stress. LexA is a repressor that binds to a motif called the SOS box located upstream of the regulated genes[10]. RRecA is essential for homologous recombination because it binds to single-stranded DNA, which is generated when the replication fork encounters replication-blocking lesions or after exonucleolytic processing of DSBs, and forms a nucleofilament to facilitate the search for a homologous sequence[11]. RecA also has a regulatory role: it becomes activated after binding to DNA, and in its activated form degrades LexA. Null mutants of *recA* show no SOS response[10]. The *lexA3* strain, which produces a mutant *lexA* that is resistant to degradation by RecA, also does not exhibit an SOS response.

DNA helicase I (TraI) is a bifunctional protein encoded by the F-plasmid[12] and contains 3 functional domains essential for the transfer of bacterial genes during conjugation[13-15]. F-plasmid transfer is initiated by endonucleolytic cleavage of the DNA strand. This origin-specific nicking event is modulated by the product of *traI*[16,17]. If the nick is produced near a single-strand breakpoint, it may behave like clustered DNA damage.

In this study, mutations were generated in the above-mentioned DNA repair genes. To reveal the effect of high-LET radiation, wild-type *E. coli* and its mutants were irradiated with X-rays or He-rays and their sensitivities were measured. The survival rate and mutation frequency produced by the irradiation were compared.

II. MATERIALS AND METHODS

1. Bacterial strains:

The wild-type strain CSH100 and strains SMR6318, JW5855-2, CSH115, CC104, JW3996-1, and DM49 were obtained from the *E. coli* Genetic Stock Center, Yale University. CSH100*traI* was constructed by transducing a *traI*::Chm allele from strain SMR6318 using P1 phage. CSH100*recQ* was constructed by transducing a *recQ*::Kan allele from strain JW5855-2, CSH100*mutS* was constructed by transducing a *mutS*::Tet allele from strain CSH115*mutS*, and CSH100*uvrA* was constructed by transducing a *uvrA*::Chm allele from strain cc104*uvrA* using P1 phage. CSH100*recA* was constructed by transducing a *recA*::CmR allele from strain AJW807 using P1 phage. AJW807 was a kind gift from Dr. A. J. Wolfe. CSH100*lexA3* was constructed in 2 steps. First, *lamB::Kan*^{r} from JW3996-1 was transduced into DM49. Second, the *lexA3* allele was co-transduced with *lamB::Kan*^{r} into CSH100 via P1 transduction. The transfer of the *lexA3* allele was verified by PCR amplification and subsequent *Msp*I digestion of the *lexA* locus[18].

2. Growth of cells

Cells were grown in minimal medium (10.5 g/L of K_2HPO_4, 4.5 g/L of KH_2PO_4, 1 g/L of $(NH_4)_2SO_4$, 0.5 g/L of sodium citrate, 1 mM $MgSO_4$, 5×10^{-4}% thiamine hydrochloride, and 0.2% glucose). For irradiation, cells were prepared according to the protocol of Maezawa[19]. Briefly, logarithmic cells were prepared by diluting an overnight culture 50-fold followed by incubation for several hours at 37°C to obtain a cell density of approximately 4×10^8 cells/mL. Logarithmic cells were washed and resuspended in saline solution (0.15 M NaCl), and were placed on a nitrocellulose membrane (GSWP01300; Millipore, Co. Ltd).

3. X-ray irradiation

X-rays were generated using Soft X-ray generator with a tungsten target (SOFTEX M-150WE; SOFTEX Co., Ltd). The peak electrical voltage was set at 150 kVp and the current was set at 6 mA. The dose rate was 27.9 Gy/min, which was determined using a Fricke dosimeter.

4. He-ion irradiation

The energy of He ions (50 MeV) generated by the AVF cyclotron at Takasaki Ion Accelerators for Advanced Radiation Application was reduced by placing an Ni filter of 300-μm thickness in front of the sample. The average LET of the sample, estimated using ELOSS code, a modified OSCAR code[20], and was 889 keV/μm. To calculate the absorbed dose, particle fluence was measured using a CR39 plastic dosimeter (HARZLAS TD-1; Fukuvi Chemical Industry Inc., Japan). The dose rate was 8–10 Gy/sec.

5. Measurement of survival and mutation frequency of cells

After irradiation, cells were collected and suspended in saline solution and a fraction was immediately plated on minimal or selection plates containing 15 g/L agar. The number of survivor colonies was determined and divided by the number of non-irradiated colonies to determine the survivor fraction. We selected *lacI* mutants on minimal medium containing 0.2% P-gal as the sole carbon source, as described elsewhere[21]. After exposure to X-ray irradiation, cell suspensions were plated on minimal plates containing 100 mg/mL streptomycin or rifampicin. After incubation at 37°C for 40 h, the streptomycin- or rifampicin-resistant colonies were enumerated. Each experiment was repeated at least 3 times using independent cultures.

6. Increment in mutation frequency with time

After irradiation, cells were collected and suspended in saline solution and a fraction was immediately plated on minimal or selection plates containing 15 g/L agar. After 40–88 h, the number of survivor colonies was determined and divided by the number of non-irradiated colonies to determine the survivor fraction. We selected *lacI* mutants on minimal medium containing 0.2% P-gal as the sole carbon source, as described elsewhere[21].

III. RESULTS

1. Isolation of repair-defective strain

The DNA of antibiotic-selected mutants was amplified and the insertion was determined by agarose gel electrophoresis. A DNA fragment of the expected size was detected (date not shown).

2. Increase in mutation frequency of *traI*

The temporal changes in the mutation frequencies of wild type and *traI* were determined (Figure 4-1-1 C). The survival and mutation frequencies of wild-type and *traI* cells were not significantly different at 40 h after irradiation, (Figure 4-1-1 A, B). The mutation frequency of both strains increased with time. There was no significant difference in the time course.

3. Survival of *E. coli* cells after X-ray irradiation

The survival of wild-type, *uvrA*, *mutS*, *recQ*, *recA*, and *lexA3* cells exponentially decreased with increasing dose of X-rays (Figure 4-1-2A).Compared to the other cell lines (Group I), *recA* and *lexA3* (Group II) were significantly sensitive. The survival rates of Groups I and II were not significantly different.

4. Survival of *E. coli* cells after He-ion irradiation

The survival of wild-type, *uvrA*, *mutS*, *recQ*, *recA*, and *lexA3* cells exponentially decreased with increasing dose of He ions (Figure 4-1-3B). The survival of Group II was lower than that of Group I, as seen in the case of X-ray irradiation. However, the difference was less than that seen with X-ray irradiation.

5. Mutation frequency of *E. coli* cells after X-ray irradiation

Cells were plated on P-gal selection medium immediately after irradiation. In the case of X-ray irradiation, the *lacI* mutation frequency of the wild type did not significantly increase above the level of spontaneous mutation with the dose of 256 Gy, but increased with increasing dose over 256 Gy (Figure 4-1-3). The *lacI* mutation frequencies of *uvrA* and *recQ* were similar to that seen with X-ray irradiation. The *lacI* mutation frequency of *mutS* was very high compared with that of the other types. The mutation frequencies of *recA* and *lexA3* appeared to be independent of the radiation dose, and they both remained very low at the level of spontaneous mutations.

6. Mutation frequency of *E. coli* cells after He-ion irradiation

In the case of He-ion irradiation, the mutation frequencies of wild-type, *recA*, and *lexA3* cells did not increase significantly above the level of spontaneous mutations, and were dose-independent. The value of *uvrA* was the same as that observed with X-ray irradiation, and the values of *mutS* and *recQ* were higher than the corresponding values observed with X-ray irradiation. Munson and Bridges reported that the mutagenic effect steadily decreased with increasing LET[22]. Our results are consistent with their findings. On the other hand, Tokarova et al. observed a clear increase in mutation frequency after exposure of stationary cells to heavy ions[23]. This discrepancy is most

likely due to the fact that the 2 experiments used cells in different growth phases.

IV. DISCUSSION

To observe the effect of He-rays, *E. coli* and its variant strains were used. They were irradiated with X-rays or He ions and their survival and mutation frequencies were measured.

First, I focused on DNA nicking. F-plasmid transfer is initiated by endonucleolytic cleavage of the DNA strand. This origin-specific nicking event is modulated by the product of *traI*[166,17]. If the nick is produced near the single-strand breakpoint, it may behave like clustered DNA damage and may mask the effects of radiation-induced clustered DNA damage. Therefore, survival, mutation frequency, and the time course of mutation frequency were measured. No significant differences were noted between the 2 strains. Therefore, cells with an intact *traI* gene were used in subsequent experiments.

In the case of X-ray irradiation, survival of the wild-type, *uvrA*, *mutS*, and *recQ* strains (Group I) were higher than those of the *recA* and *lexA3* strains (Group II) (Fig. 4-1-2A). RecA and LexA, the products of the *recA* and *lexA* genes, respectively, are closely linked to the SOS response. Consistent with previous results[23-25], *recA* and *lexA3* cells were much more sensitive than the wild-type cells. The increased sensitivity of *recA* or *lexA3* can be explained by their lack of an SOS response.

To compare the sensitivity of each strain, $D_{0.01}$, which is determined as the dose (Gy) required to reduce the surviving fraction to 1%, was calculated on the basis of the survival curves (Table 4-1-1). The ratios of sensitive *recA* and *lexA3* to wild type were 3.0 and 2.9, respectively. Although *uvrA* was a little sensitive than wild type, no significant difference was observed in the Group I strains.

UV light irradiation induces the formation of cyclobutane pyrimidine dimers between adjacent pyrimidines[26,27]. UvrA, which is the product of *uvrA*, is one of the key *E. coli* proteins involved in removing DNA damage during the process of NER[28]. UvrA is important for repairing pyrimidine dimers because *uvrA*-defective strains are sensitive to UV irradiation[29,30]. The antitumor agent cis-diamminedichloroplatinum (II) (DDP) produces DNA intrastrand, interstrand, and DNA-protein crosslinks[31]. *E. coli* cells that are *uvrA* deficient are more sensitive to DDP than wild-type cells, indicating that Uvr endonuclease-mediated excision repair contributes to the repair of DDP-induced DNA damage[32-34]. RecQ helicase is a key component of the RecF pathway in *E. coli* for initiation of homologous recombination[35,36]. RecQ is not important for repairing DNA defects induced by γ-rays or UV irradiation in nuclease-deficient strains because RecA and RecBCD can regulate homologous recombination[37]. On the other hand, *recQ*-deficient strains are sensitive to camptothecin[38]. Camptothecin prevents DNA re-ligation and therefore causes DNA damage, which results in apoptosis. Thus, X-ray or He-ion irradiation does not appear to elicit DNA damage because there were no differences between the wild type, *uvrA*, and *recQ* strains in my study.

The mutation frequency of *mutS* was much higher than that if wild type, although the survival of *mutS* was not different. The MutS protein initiates MMR and reduces DNA replication errors in *E. coli*[39]. Therefore, *mutS* displays elevated spontaneous mutation rates because of a deficiency in the postreplicative mismatch correction process[40]. Thus, it may be difficult to make a fair comparison between *mutS* and the other strains. Given that the survival of *mutS* was affected to the same extent as the X-ray-irradiated strains, MMR requiring MutS is unusual or it may be repaired via a different pathway. It is well known that some DNA repair systems complement the function of other repair systems[41-44]. Precisely for this reason, the rate of DNA mutations may be underestimated.

Group II was also more sensitive to He-ion irradiation than Group I. This indicates that the SOS response is important to repair not only X-ray -induced damage

but also He-ion-induced damage. The relative biological effectiveness (RBE) of He ions relative to X-rays was calculated from $D_{0.01}$, which was calculated from Fig. 4-1-2 (Table 4-1-1). The RBE values were approximately 3.0 and 2.9 for *recA* and *lexA*, respectively. The value for *mutS* was high (1.7), compared with that of previous studies[45]. Therefore, more experiments are warranted. The values for the other Group I strains were approximately 1.3, which is almost the same as that of previous studies[45]. It has been reported that the RBE of 40 MeV He ions is about 1[46]. The increase in RBE appears to be due to high LET (not the radiation type). The RBE values for *recA* and *lexA3* were less than 1. It seems like the decrease of the RBE versus LET curve at LET values above more than 100 keV/μm[47]. This effect has been interpreted as an "overkill effect," where the density of ionizations within a single cell is greater than the 2 events needed for the inactivation of that cell. This is, in effect, a wasted dose. In the cases of *recA* and *lexA3* in the present study, the same effect may have occurred. Of course, the value cannot be used to calculate the dose for BNCT treatment, because the DNA repair systems in *E. coli* and humans are different.

The mutation frequencies of both wild-type and *recA* cells did not significantly increase above the level of spontaneous mutations, and were independent of dose. This suggests that the damage induced by He-ion irradiation is easy to repair or the damaged cells did not survive or both. The difference in the sensitivities of wild-type and Group II cells to He-ion irradiation was small compared with that of X-ray irradiation. Thus, the contribution of the SOS response may be minimal in response to He-ion irradiation. The SOS response is an error-prone repair system[48] and its minimal contribution may explain the low mutation frequencies.

The *lacI* mutation frequency of the *recQ* strain in response to He-ion irradiation was higher than that of X-ray irradiation. RecQ helicase is a key component of the RecF pathway in *E. coli* for initiation of homologous recombination[35,36]. The repair system using the RecF pathway may be important for recovery from He-ion-induced damage. The *lacI* mutation frequency of the *mutS* strain was different from that observed with X-ray irradiation. However, the values at 0 Gy were quite different. Thus, the *mutS* strain needs to be further investigated.

These results are useful and fundamental to the studies of DNA repair and dose calculation. However, various types of mutations should be examined to determine the different types of radiation-induced DNA damage. The attempts to use streptomycin, rifampicin, and X-gal were unsuccessful. Therefore, the accuracy of the analyzing system should be improved or an alternative method should be used to detect significant differences.

Figures

Table 4-1-1 Genes, their protein products, and the associated repair mechanisms examined in this study

gene	protein	repair mechanism
uvrA	UvrA	Nucleotide excision repair
mutS	MutS	mismatch repair
recQ	RecQ	homologous recombination
recA	RecA	homologous recombination and SOS response
lexA3	variant LexA	SOS response

Table 4-1-2. $D_{0.01}$ of each strain for X-ray and He-ion irradiation and the RBE values

	Wild type	*mutS*	*uvrA*	*recQ*	*recA*	*lexA3*
X-ray	552	573	456	518	181	194
He ray	421	353	356	404	217	196
RBE	1.3	1.6	1.3	1.3	0.84	0.97

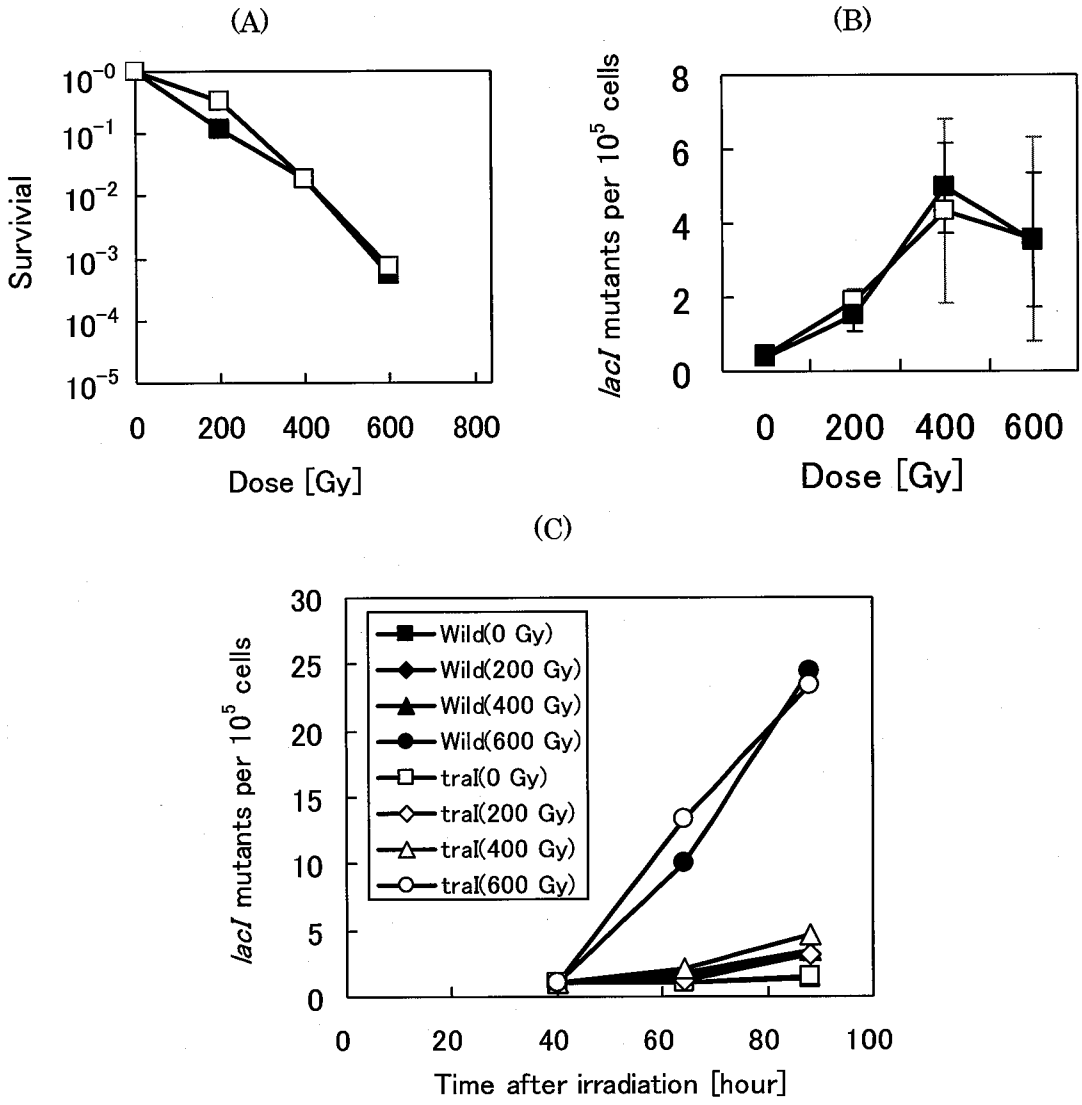

Figure 4-1-1. Survival (A) and mutation frequency (B) of cells plated immediately after X-irradiation and counted at 40 hours after irradiation. (C) Time course of mutation frequency after X-ray irradiation. (A, B): Wild type (solid symbols), *traI* (open symbols). (C) Wild type (solid symbols), *traI* (open symbols), 0 Gy (■, □), 200 Gy (◆, ◇), 400 Gy (▲, △), 600 Gy (●, ○).

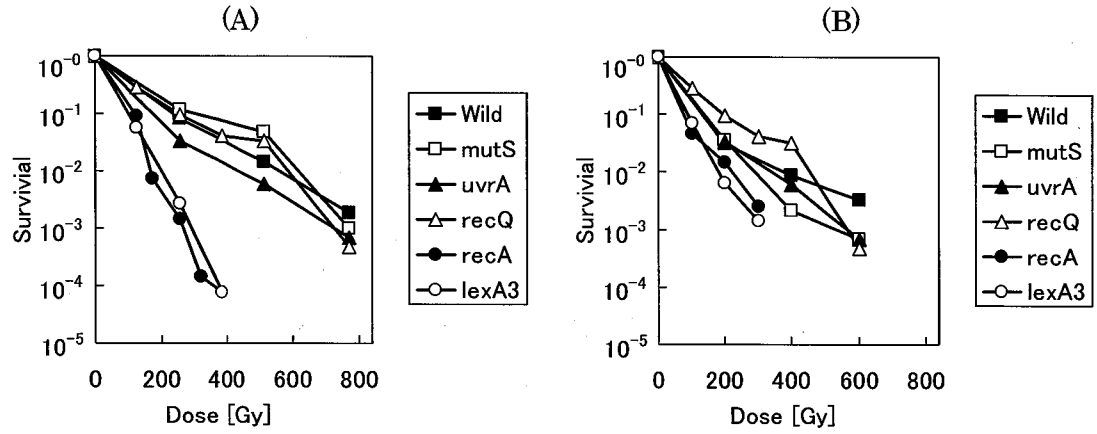

Figure 4-1-2. Survival of cells plated immediately after X-ray irradiation (A) and He-ion irradiation (B). Wild type (■), *mutS* (□), *uvrA* (▲), *recQ* (△), *recA* (●), *lexA3* (○).

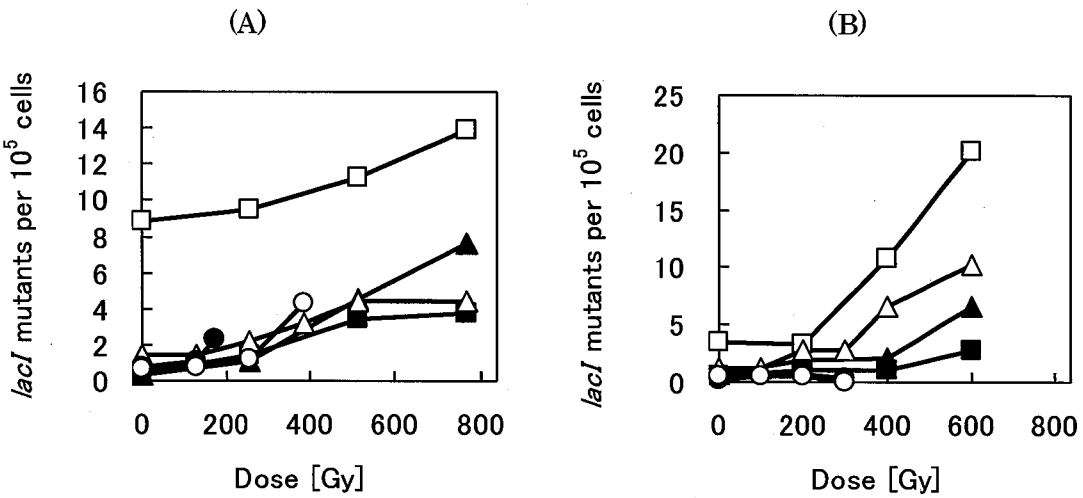

Figure 4-1-3. *lacI* mutation frequencies after X-ray irradiation (A) and He-ion irradiation (B). Wild type (■), *mutS* (□), *uvrA* (▲), *recQ* (△), *recA* (●), *lexA3* (○). The mutation frequency was measured by plating irradiated cells on P-gal selection medium immediately after irradiation. Mutation frequencies were not plotted when the number of mutants was less than 5 per plate because these data had large statistical errors.

References

1. Goodhead DT. Initial Events in the Cellular Effects of Ionizing Radiations: Clustered Damage in DNA. Int J Radiat Biol. 1994, 65(1): 7-17
2. de Laat WL, Jaspers NG, Hoeijmakers JH. Molecular mechanism of nucleotide excision repair. Genes Dev. 1999, 13(7): 768-768
3. Iyer RR, Pluciennik A, Burdett V, Modrich PL. DNA mismatch repair: functions and mechanisms. Chem Rev. 2006, 106(2): 302-23
4. Larrea AA, Lujan SA, Kunkel TA. SnapShot: DNA mismatch repair. Cell. 2010, 141(4): 730
5. Takehiko S. Functions of homologous DNA recombination. RIKEN Review 2001, 41
6. Kowalczykowski SC, Dixon DA, Eggleston AK, Lauder SD, Rehrauer WM. Biochemistry of homologous recombination in Escherichia coli. Microbiol Rev. 1994, 58(3): 401-465
7. Rocha EP, Cornet E, Michel B. Comparative and evolutionary analysis of the bacterial homologous recombination systems. PLoS Genet. 2005, 1(2): e15
8. Kuzminov A. Recombinational repair of DNA damage in Escherichia coli and bacteriophage lambda. Microbiol Mol Biol Rev. 1999, 63(4): 751-813
9. Janion C. Inducible SOS response system of DNA repair and mutagenesis in Escherichia coli. Int J Biol Sci. 2008, 4(6): 338-344
10. Nickoloff JA. Hoekstra MF. Totowa NJ. DNA Damage and Repair: DNA Repair in Prokaryotes and Lower Eukaryotes. Humana Press. 1998, 107-134
11. Shinohara A, Shinohara M. Roles of RecA homologues Rad51 and Dmc1 during meiotic recombination. Cytogenet Genome Res. 2004, 107(3-4):201-7
12. Geider K, Hoffmann-Berling H. Proteins controlling the helical structure of DNA. Annu Rev Biochem. 1981, 50: 233-260
13. Matson SW, Sampson JK, Byrd DR. F plasmid conjugative DNA transfer: the TraI helicase activity is essential for DNA strand transfer. J Biol Chem. 2001, 276(4): 2372-2379
14. Matson SW, Ragonese H. The F-plasmid TraI protein contains three functional domains required for conjugative DNA strand transfer. J Bacteriol. 2005, 187(2): 697-706
15. Willetts N, McIntire S. The exploitation of lambda tra transducing phages in the study of bacterial conjugation. Contrib Microbiol Immunol. 1979, 6: 137-145
16. Everett R, Willetts N. Characterisation of an in vivo system for nicking at the origin of conjugal DNA transfer of the sex factor F. J Mol Biol. 1980, 136(2): 129-150
17. Dostal L, Shao S, Schildbach JF. Tracking F plasmid TraI relaxase processing reactions provides insight into F plasmid transfer. Nucleic Acids Res. 2011, 39(7): 2658-2670
18. Markham BE, Little JW, Mount DW. Nucleotide sequence of the lexA gene of Escherichia coli K-12. Nucleic Acids Res. 1981, 9(16): 4149-4161
19. Maezawa H, Hieda K, Kobayashi K, Furusawa Y, Mori T, Suzuki K, Ito T. Effects of monoenergetic X-rays with resonance energy of bromine K-absorption edge on bromouracil-labelled E. coli cells. Int J Radiat Biol Relat Stud Phys Chem Med. 1988, 53(2): 301-308
20. Hata K. Baba H. OSCAR, a code for the calculation of the yield of radioisotopes produced by charged-particle induced nuclear reactions, JAERI-M. 1988, 88-184
21. Miller JH. A short course in bacterial genetics, Cold Spring Harbor Laboratory Press, 1992
22. Munson RJ, Bridges BA. The LET factor in mutagenesis by ionizing radiations. I. Reversion to wild type of a bacteriophage T4 amber mutant. Int J Radiat Biol Relat Stud Phys Chem Med. 1973, 24(3): 257-273
23. Tokarova B, Amirtayev KG, Kozubek S, Krasavin EA. Mutagenic action of heavy

ions on Escherichia coli cells. Mutat Res. 1989, 227(4): 199-205
24. Yatagai F, Matsuyama A. LET-dependent radiosensitivity of Escherichia coli K-12 rec and uvr mutants. Radiat Res. 1977, 71(1): 259-263
25. Krasavin EA. Amirtayev KG. Kozubek S. Tokarova B. Tcherevatenko AP. Role of DNA repair processes in the biological efficiency of heavy ions. Studia biophysica 1989, 133: 25-31
26. Gordon LK, Haseltine WA. Quantitation of cyclobutane pyrimidine dimer formation in double- and single-stranded DNA fragments of defined sequence. Radiat Res. 1982, 89(1): 99-112.
27. Wang, SY. Photochemistry and Photobiology of Nucleic Acids Vols 1, 2 Academic, New York. 1976
28. Goosen N, Moolenaar GF. Role of ATP hydrolysis by UvrA and UvrB during nucleotide excision repair. Res Microbiol. 2001, 152(3-4): 401-9
29. SETLOW RB, CARRIER WL. THE DISAPPEARANCE OF THYMINE DIMERS FROM DNA: AN ERROR-CORRECTING MECHANISM. Proc Natl Acad Sci U S A. 1964, 51: 226-231
30. BOYCE RP, HOWARD-FLANDERS P. RELEASE OF ULTRAVIOLET LIGHT-INDUCED THYMINE DIMERS FROM DNA IN E. COLI K-12. Proc Natl Acad Sci U S A. 1964, 51: 293-300
31. Roberts JJ, Thomson AJ. The mechanism of action of antitumor platinum compounds. Prog Nucleic Acid Res Mol Biol. 1979, 22: 71-133
32. Beck DJ, Brubaker RR. Effect of cis-platinum(II)diamminodichloride on wild type and deoxyribonucleic acid repair deficient mutants of Escherichia coli. J Bacteriol. 1973, 116(3): 1247-1252
33. Konishi H, Usui T, Sawada H, Uchino H, Kidani Y. Effects of anticancer platinum compounds on Escherichia coli strains with normal and defective DNA repair capacity. Gann. 1981, 72(4): 627-630
34. Fram RJ, Cusick PS, Marinus MG. Studies on mutagenesis and repair induced by platinum analogs. Mutat Res. 1986, 173(1): 13-18
35. Buljubašić M, Repar J, Zahradka K, Dermić D, Zahradka D. RecF recombination pathway in Escherichia coli cells lacking RecQ, UvrD and HelD helicases. DNA Repair (Amst). 2012, 11(4): 419-430
36. Nakayama K, Irino N, Nakayama H. The recQ gene of Escherichia coli K12: molecular cloning and isolation of insertion mutants. Mol Gen Genet. 1985, 200(2): 266-271
37. Ivanković S, Đermić D. DNA End Resection Controls the Balance between Homologous and Illegitimate Recombination in Escherichia coli. PLoS One. 2012, 7(6): e39030
38. Suzuki K, Kato A, Sakuraba Y, Inoue H. Srs2 and RecQ homologs cooperate in mei-3-mediated homologous recombination repair of Neurospora crassa. Nucleic Acids Res. 2005, 33(6): 1848-1858
39. Modrich P. Mechanisms in eukaryotic mismatch repair. J Biol Chem. 2006, 281(41): 30305-30309
40. Schaaper RM, Dunn RL. Spectra of spontaneous mutations in Escherichia coli strains defective in mismatch correction: the nature of in vivo DNA replication errors. Proc Natl Acad Sci U S A. 1987, 84(17): 6220-6224
41. Hansson J, Grossman L, Lindahl T, Wood RD. Complementation of the xeroderma pigmentosum DNA repair synthesis defect with Escherichia coli UvrABC proteins in a cell-free system. Nucleic Acids Res. 1990, 18(1): 35-40
42. Dianov G, Bischoff C, Piotrowski J, Bohr VA. Repair pathways for processing of 8-oxoguanine in DNA by mammalian cell extracts. J Biol Chem. 1998, 273(50): 33811-33816

43. Chow KH, Courcelle J. RecBCD and RecJ/RecQ initiate DNA degradation on distinct substrates in UV-irradiated Escherichia coli. Radiat Res. 2007, 168(4): 499-506
44. Sakai A, Cox MM. RecFOR and RecOR as distinct RecA loading pathways. J Biol Chem. 2009, 284(5): 3264-3272
45. Nikjoo H, Munson RJ, Bridges BA. RBE-LET relationships in mutagenesis by ionizing radiation. J Radiat Res. 1999 Dec;40 Suppl: 85-105.
46. DEERING RA. Mutation and killing of Escherichia coli WP-2 by accelerated heavy ions and other radiations. Radiat Res. 1963 May;19: 169-178.
47. Goodhead DT, Munson RJ, Thacker J, Cox R. Mutation and inactivation of cultured mammalian cells exposed to beams of accelerated heavy ions. IV. Biophysical interpretation. Int J Radiat Biol Relat Stud Phys Chem Med. 1980, 37(2): 135-167
48. Ishii Y, Kondo S. Comparative analysis of deletion and base-change mutabilities of Escherichia coli B strains differing in DNA repair capacity (wild-type, uvrA-, polA-, recA-) by various mutagens. Mutat Res. 1975, 27(1): 27-44

Section 2. Medium-dependent radiation sensitivity and mutagenesis with different qualities of radiation.

I. Introduction

Ionizing radiation is used extensively for various applications, such as food sterilization and mutational breeding to microorganisms, and medical radiography and cancer therapy to humans. Understanding of the details of the factors/conditions that affect radiation effects as well as their underlying mechanisms will be essential to evaluate the effects of radiation exposure in improving the effectiveness and/or the safeness of these applications. It has been known that the radiation sensitivity of a cell strongly depends on its physiological state, such as its level of stress or stage of growth[1].

Escherichia coli is a useful model to elucidate the effect of ionizing radiation, and the genetic basis as well as the cellular response to ionizing radiation has been extensively investigated. It possesses several repair pathways, such as base excision repair and homologous recombination, to cope with various types of radiation-induced DNA damage, which are relevant to the biological consequences of ionizing radiation[2]. *E. coli* has a cellular response, called the SOS response, that is induced by DNA damaging agents[3,4], and that involves more than 40 genes related not only to DNA repair but also to mutagenesis. The products of two of these genes, RecA and LexA, regulate the induction of the SOS response after cells are exposed to genotoxic stress. LexA is a repressor which binds to a motif called the SOS box located upstream of the regulated genes. RecA is essential for homologous recombination as it binds to single-stranded DNA, which is generated when the replication fork encounters replication-blocking lesions or after exonucleolytic processing of double-strand breaks (DSBs), and forms a nucleofilament to facilitate the search for a homologous sequence. RecA also has a regulatory role: it becomes activated after binding to DNA, and in its activated form degrades LexA. Null mutants of *recA* show no SOS response. Mutants of *lexA* that are resistant to degradation also show no SOS response.

Nutritional conditions directly influence the growth rate and gene expression profiles of *E. coli*[5-8], and thus, nutrients are considered to affect the physiological conditions of the cell. The radiation sensitivity of *E. coli* cells was found to depend on the culture media in which they were grown. Survival was higher for cells incubated in rich medium both pre- and post- irradiation than for cells grown in minimal medium both pre- and post- irradiation. Interestingly, the rich medium-dependent increase of survival is diminished when minimal medium was used either pre- or post-irradiation. Further, addition of the antibiotic rifampicin, a transcriptional inhibitor, also reduced the rich medium-dependent survival, indicating that *de novo* RNA (and protein) synthesis is required for the process. The idea that DNA repair plays an important role in the rich medium-enhanced survival is supported by two lines of evidence: (1) DSB repair was more efficient in rich medium than in minimal medium, and (2) DNA repair-deficient mutants, such as *recA*, *recB* or *lexA*, did not show any medium dependency[9-11]. Because the deficiency of RecA or LexA completely abolished the process, the SOS response is most likely involved in the rich medium-dependent increase of survival[9]. The mutagenesis of *E. coli* cells was also found to depend on the growth medium. Using arginine auxotrophic mutants, Grigg demonstrated that the reverse mutation frequency is higher when X-irradiated cells were grown in minimal medium supplemented with rich medium than when X-irradiated cells were grown in plain minimal medium[12].

Although medium dependence of survival after X-ray exposure has been studied in detail, the mechanism of medium-dependent mutagenesis, for instance, which gene(s) and cellular response(s) are responsible for the process, is still largely unknown. Further, to what extent the medium-dependent effect is affected by the ionizing density

of a radiation, which is usually related to the linear energy transfer (LET), remains unclear. Therefore, in this study, we used *E. coli* wild-type cells and *E. coli recA* and *lexA* mutants to determine how (1) the medium affects mutagenesis, and (2) radiation quality affects the medium-dependent radiation effects. We found that the mutagenesis was medium-dependent after X-irradiation and that this medium-dependent mutagenesis was dependent on RecA and LexA. Further, we found that the medium-dependent effects on both survival and mutation were less pronounced when the cells were irradiated with densely ionizing, high-LET He ions. These results should help to improve the efficiencies of radiation applications, especially for mutational breeding.

II. Materials and methods

1. Bacterial strains

Wild-type strain CSH100, and strains JW3996-1 and DM49 were provided from the *E. coli* Genetic Stock Center, Yale University. CSH100*recA* was constructed by transducing a *recA*::CmR allele from strain AJW807 by P1 phage. AJW807, was a kind gift from Dr. A. J. Wolfe. CSH100*lexA3* was constructed by two steps. Firstly, *lamB::Kan*^{r} from JW3996-1 was transduced to DM49. Secondly, the *lexA3* allele was co-transduced with *lamB::Kan*^{r} to CSH100 by P1 transduction. The transfer of the *lexA3* allele was verified by PCR amplification and subsequent *Msp*I (New England Biolabs, Ipswich, UK) digestion of the *lexA* locus[13].

2. Growth of cells

Minimal medium (containing 10.5 g/L of K_2HPO_4, 4.5 g/L of KH_2PO_4, 1 g/L of $(NH_4)_2SO_4$, 0.5 g/L of sodium citrate, 1 mM of $MgSO_4$, 5 x 10^{-4}% of thiamine hydrochloride and 0.2% of glucose) (Wako Pure Chemical Industries, Ltd., Osaka, Japan) and rich medium (LB broth Lennox (Becton, Dickinson and Company, NJ, USA)) were used for growing cells. For irradiation, cells were prepared according to the protocol of Maezawa[14]. In brief, logarithmic cells were prepared by diluting the overnight culture 50-fold (for minimal medium grown cells) or 100-fold (for rich-medium grown cells) by respective homologous medium and by subsequent incubation for several hr at 37 °C to reach a cell density of approximately 4 X 10^8 cells per ml. Logarithmic cells were washed and resuspended in saline (0.15M NaCl) (Wako Pure Chemical Industries, Ltd., Osaka, Japan), and were retained on a nitrocellulose membrane (MF-Millipore, GSWP01300, EMD Millipore Corporation, MA, USA). These membranes were placed on saline solid plates for irradiation.

3. X-ray irradiation

X-rays were irradiated using Soft X-ray generator with a tungsten target (SOFTEX M-150WE, SOFTEX Co., Ltd., Kanagawa, Japan) at room temperature. The peak electrical voltage was set at 150 kVp and the current was set at 6 mA. The dose rate was 27.9 Gy/min, which was determined by Fricke dosimeter.

4. He-ion irradiation

Cells were exposed to He ions, which were generated by the AVF cyclotron at Takasaki Ion Accelerators for Advanced Radiation Application, at room temperature. The energy of He ions (50MeV) was reduced by placing a Ni filter with 300 μm thickness in front of the sample. The average LET of the sample was estimated by ELOSS code, a modified OSCAR code[15], and was 89 keV/μm. The particle fluence was measured using CR39 plastic dosimeter (HARZLAS TD-1, Fukuvi Chemical Industry Inc., Fukui, Japan) to calculate the absorbed dose. The dose rate was 8~10 Gy/sec.

5. Measurement of survival and mutant frequency plated immediately after irradiation
After irradiation, cells were collected and suspended in saline solution and a fraction immediately plated to minimal, rich or selection plates (containing 15 g/L agar) (Bacto-agar, Becton, Dickinson and Company, NJ, USA). The number of survived colonies was counted and divided by the number of unirradiated colonies to determine the survived fraction. *lacI* mutants were selected on a minimal medium containing P-gal (0.2%) (Wako Pure Chemical Industries, Ltd., Osaka, Japan) as a sole carbon source, following the procedure as described elsewhere[16]. The mutant frequency was calculated by dividing the number of *lacI* mutants on P-Gal medium with the number of survived colonies on glucose minimal medium. Each experiment was repeated at least three times from independent cultures.

6. Measurement of medium-dependent sensitivity/mutagenesis of irradiated cells
The cells were pre-cultured in rich medium and were irradiated as describe above. After irradiation, cells were cultured in solution of either minimal or rich medium for 2 hr, to assay medium-dependent sensitivity/mutagenesis. After incubation, cells were washed with saline solution and plated on minimal, rich or selection plates to assess the effect of growth medium on the survival or mutation frequency. Each experiment was repeated at least three times from independent cultures.

III. Results
1. Survival of *E. coli* cells plated immediately after irradiation
The survival of wild-type, *recA*, and *lexA* after cells decreased exponentially with increasing dose of both X-rays (Figure 4-2-1A) and He ions (Figure 4-2-1B). The survival rates were not significantly different between the two types of radiation, except that, for wild-type cells, there was a medium-dependent increase of survival after X-irradiation but not after He ion radiation. Consistent with previous results[17-19], the *recA* and *lexA3* cell lines were much more sensitive than the wild type to both types of radiation. The increased sensitivity of *recA* or *lexA3* could be explained by their lack of an SOS response.

2. Mutation frequency of *E. coli* cells plated immediately after irradiation
Cells were grown in rich medium pre-irradiation and plated on P-gal selection medium immediately after irradiation. In the case of X-irradiation, the *lacI* mutation frequency of the wild type did not significantly increase above the level of spontaneous mutation with the dose of 256 Gy, but increased with increasing dose over 256 Gy (Figure 4-2-2). The mutation frequencies of *recA* and *lexA3* appeared to be independent of dose, and they both remained very low at the level of spontaneous mutations, confirming that the SOS response is required for low-LET radiation mutagenesis[20,21]. Induced mutations were also hardly observed when *recA* and *lexA3* cells were grown in minimal medium prior to irradiation (data not shown). In the case of He-irradiation, the mutation frequencies of all wild-type, *recA*, and *lexA3* cells did not increase significantly above the level of spontaneous mutation, and were independent of dose and the type of growth medium. Our results showing that high-LET radiation induces less mutations per dose than low-LET radiation are consistent with previous observations[22,23]. However, a clear increase of mutation frequency after exposing *E. coli* cells to several kinds of heavy ions have been observed[22,24-27]. One possible explanation for this discrepancy could be due to the fact that those experiments with increased mutation frequency exposed cells of stationary phase to ion particles.

3. Survival of cells incubated for 2 hr in liquid rich medium post-irradiation

To find out the duration that cells show medium-dependent radioresistance post-irradiation, we looked at the survival of cells incubated in liquid rich medium after irradation. Those cells were incubated in liquid rich medium pre-irradiation. The numbers of unirradiated wild-type, *recA*, and *lexA3* cells increased approximately 10-fold in liquid rich medium. The growth rate of each strain was reduced with increasing dose of radiation, probably due to both cell death and growth arrest after irradiation. Wild-type cells that were incubated for 2 hr post-irradiation of X-rays showed no enhancement of medium-dependent survival (Figure 4-2-3A). As expected, no enhancement was observed in either X-irradiated *recA* or *lexA3* cells (Figure 4-2-3B), and in wild-type cells after He-irradiation (Figure 4-2-3C).

4. Mutation frequency of cells incubated for 2 hr in liquid medium post-irradiation

Cells were incubated in liquid rich medium pre-irradiation and in either liquid minimal or rich medium for 2 hr post-irradiation, and then plated on solid P-gal medium to detect *lacI* mutants. The mutation frequencies of unirradiated wild-type cells (Figure 4-2-4A) and *recA* and *lexA3* cells did not change with or without the 2hr-incubation (Fig. 4-2-2, Fig. 4-2-4A and Figure 4-2-4B). Interestingly, for X-irradiated wild-type cells, the mutation frequencies plated after 2 hr post-irradiation incubation in both liquid rich and minimal medium were higher than the mutation frequencies in cells that were plated immediately after irradiation (Fig. 4-2-2 and Fig. 4-2-4A). More surprisingly, the mutation frequency after 2 hr post-irradiation incubation in liquid rich medium was significantly higher than that after 2 hr post-irradiation incubation in liquid minimal medium (Fig. 4-2-4A). This rich-medium-dependent increase of mutation frequency was not found in either *recA* cells or *lexA3* cells, as the mutation frequency stayed low at the level of spontaneous mutation in each cells (Fig. 4-2-4B). When wild-type cells were irradiated with He ions, there was no clear increase of the mutation frequency either with or without post-irradiation incubation (Fig. 2 and Figure 4-2-4C).

IV. Discussion

Using *E. coli* cells, we found that X-ray mutagenesis was significantly enhanced in rich medium and that the process was dependent on RecA and LexA. We did not observe the rich-medium-dependent enhancements of survival and mutation frequency with densely ionizing, high-LET radiation. Our results demonstrate that medium-dependent survival and mutagenesis are differently affected by exposures to different types of ionizing radiation.

Growth medium-dependent effects of X-irradiated *E. coli* cells

Our results confirm previous reports that *E. coli* cells have enhanced radiation resistance when grown on rich medium (LB) and that *recA* and *lexA3* cells do not share this medium-dependent sensitivity (Fig 4-2-1)[9]. These results strongly indicate that SOS response is involved in radiation resistance. It is noteworthy that the medium-dependent increase in survival was observed only when cells were incubated in rich medium both pre- and post-irradiation, and not when cells were grown in minimal medium either pre- or post-irradiation (data not shown). These results suggest that a specific physiological state induced by the rich medium is required prior and subsequent to irradiation to induce sufficient SOS response to enhance survival.

The *E. coli* strains used in this study have an F' plasmid, which harbors the *pro* gene that is required for growth only in minimal medium. Thus, the rich-medium-dependent increase of survival may be merely the result of rescuing cells that had lost the F' plasmid. However, this explanation is ruled out by the finding that the survival rates of wild-type cells, which were incubated in liquid rich medium for 2hr post-irradiation, on solid rich medium and on solid minimal medium did not differ (Fig.

4-2-3A). This indicates that the F' plasmid is not lost in rich medium post-irradiation. Several lines of evidence suggests that the rich medium is required immediately but only for 2 hr or less after irradiation to enhance survival: (1) a rich medium-dependent increase of survival was observed when cells were plated immediately on solid rich medium after irradiation (Fig. 4-2-1A), (2) such an increase was absent after cells were incubated in either rich or minimal medium for 2hr post-irradiation (Fig. 4-2-3A, data not shown). Because the survivals of *recA* and *lexA3* cells with post-irradiation incubation did not show any medium dependence (Fig. 4-2-3B), the efficiency with which DNA damage is repaired during the 2-hr incubation after X-irradiation is most likely enhanced by the SOS repair. The SOS response is at least partly functional in the minimal medium, since wild-type cells show higher survival than do *recA* and *lexA3* (Fig. 4-2-1). We assume that the 'extra' activity specifically expressed in rich medium is responsible for the medium-dependent increase of survival.

Interestingly, when X-irradiated wild-type cells were incubated in liquid medium for 2 hr after irradiation, the mutation frequency was increased compared to that of cells without post-irradiation incubation (Fig. 4-2-2 and Fig. 4-2-4A). The increase of mutation frequency of X-irradiated wild-type cells was significantly lager in cells incubated in liquid rich medium than in cells incubated in liquid minimal medium, indicating that the incubation of X-irradiated cells in rich medium strongly enhances mutagenesis (Fig. 4-2-2 and Fig. 4-2-4A). This medium-dependent enhancement of mutation frequency did not occur in *recA* cells or *lexA3* cells (Fig. 4-2-2 and Fig. 4-2-4B), indicating that the SOS response is involved in the mutagenic process and that the 'extra' activity of SOS response is likely responsible for the significant increase of mutation frequencies in rich medium. The mutations induced by the SOS response may have occurred at two different times: (1) during the 2 hr-incubation post-irradiation before plating on P-gal minimal medium, or (2) after plating on P-gal minimal medium by the process called 'adaptive mutation[28]. It is unclear at which time the mutants arose. In either case, the 2-hr incubation post-irradiation is sufficient to increase the frequency of mutations in *E. coli*.

Growth medium-dependent effects of He-irradiated *E. coli* cells

No medium-dependent increase of survival was found for He-irradiated wild-type, *recA* or *lexA3* cells (Fig. 4-2-1B). The medium-dependent resistance and mutagenesis after X-irradiation lead us to suggest that the 'extra' SOS response is inactive after He-irradiation. However, Kozubek et al., using a *sulA*/*lacZ* fusion gene, where *sulA* is an SOS-inducible gene, demonstrated that the SOS response is also efficiently induced by densely-ionizing heavy ions[29]. The most likely explanation for this apparent discrepancy is that although the SOS response is fully induced in rich medium, the induced 'extra' proteins cannot cope with some of the complex DSBs that were generated by He-irradiation. Exposure to high-LET radiation is known to result in spatial clustering of DNA damage, which, in turn, leads to reduced repair efficiency[30,31]. Datta et al. have shown that a complex DSB with DNA damage confined to the proximity of the break ends was induced by densely-ionizing ^{125}I decay[32,33], and was difficult to repair[34].

We also found that the mutation frequencies of wild-type cells irradiated with He ions did not increase significantly above the level of spontaneous mutation frequency (Fig. 4-2-2) and that the medium-dependent mutagenesis did not occur (Fig. 4-2-2 and Fig. 4-2-4C). Since translesion synthesis (TLS) induced as part of the SOS response is mainly responsible for mutagenesis after ionizing radiation exposure[2,20], we suggest that at least one of the following possibilities is responsible for the absence of medium-dependent increase of mutation frequency, as well as the low mutation frequencies of cells immediately plated after He-irradiation: (1) the polymerases for TLS

can replicate over He-damaged DNA, and do so in an error-free manner, (2) the polymerases for TLS cannot replicate over damaged DNA generated by He-irradiation, and thus the replication is blocked, or (3) there is only a small amount of DNA damage on double-stranded regions and that most of the DNA damage is gathered around complex DSBs. In the last case, we assume that complex DSBs have low mutagenicity if repaired, as exonucleases can remove damaged sites during homologous recombination[35,36].

V. Conclusions

We found that, in addition to medium-dependent sensitivity, there is medium-dependent mutagenesis in *E. coli* cells after ionizing radiation exposure, which requires an SOS response. Our results suggest that the incubation in rich medium before and after irradiation sets the physiological condition of a cell that results in medium-dependent effects. Thus, the physiological state of the cell plays an important role in determining the mutagenic consequences of X-irradiation. Furthermore, our finding that the medium-dependent effects are absent after exposure to high-LET radiation indicates that the higher level of clustering of DNA lesions is, at least partly, refractory to the SOS response. These results imply that both the physiological state of the cell and the radiation quality are important in determining the radiation effect to microorganisms, which gives valuable insights in radiation breeding, food sterilization and medical aplication.

Figures

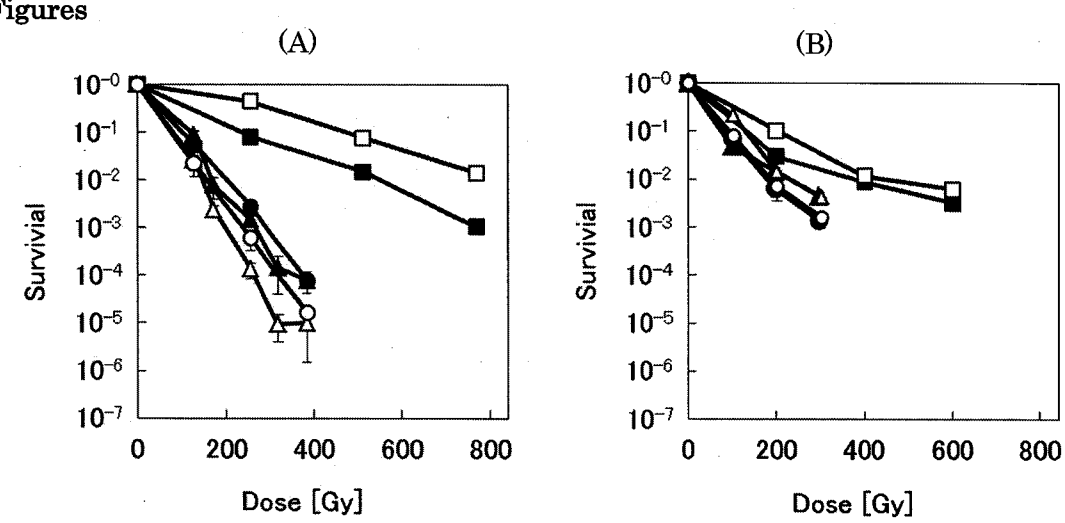

Figure 4-2-1. Survival of cells plated immediately after X-irradiation (A) and He-irradiation (B). Cells were grown pre- and post-irradiation in minimal (solid symbol) or rich (open symbol) medium. Wild type (■, □), *recA* (▲, △), *lexA3* (●, ○). Each data point represents the mean of at least three independent experiments, and the error bar denotes standard error. A data point without an error bar indicates that the error bar was smaller than the symbol.

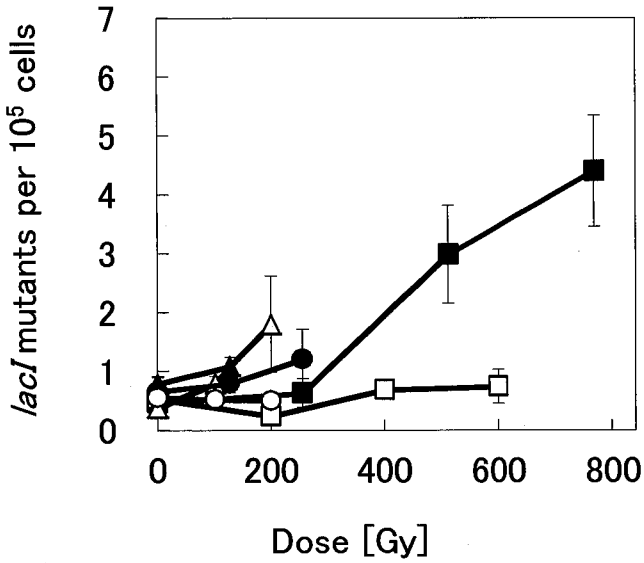

Figure 4-2-2. *lacI* mutant frequencies after X-irradiation (solid symbols) and He-irradiation (open symbols). Wild type (■, □), *recA* (▲, △), *lexA3* (●, ○). Cells were grown in liquid rich medium pre-irradiation. The mutant frequency was measured by plating irradiated cells on P-gal selection medium immediately after irradiation. Each data point represents the mean of at least three independent experiments, and the error bar denotes standard error. A data point without an error bar indicates that the error bar was smaller than the symbol. We did not plot mutant frequencies when the number of mutants was less than 5 per plate because these data had very large statistical errors. The data points that are not shown are: the mutant frequencies of X-irradiated *recA* (384 Gy), He-irradiated *recA* (300 Gy), X-irradiated *lexA3* (384 Gy), and He-irradiated *lexA3* (300 Gy).

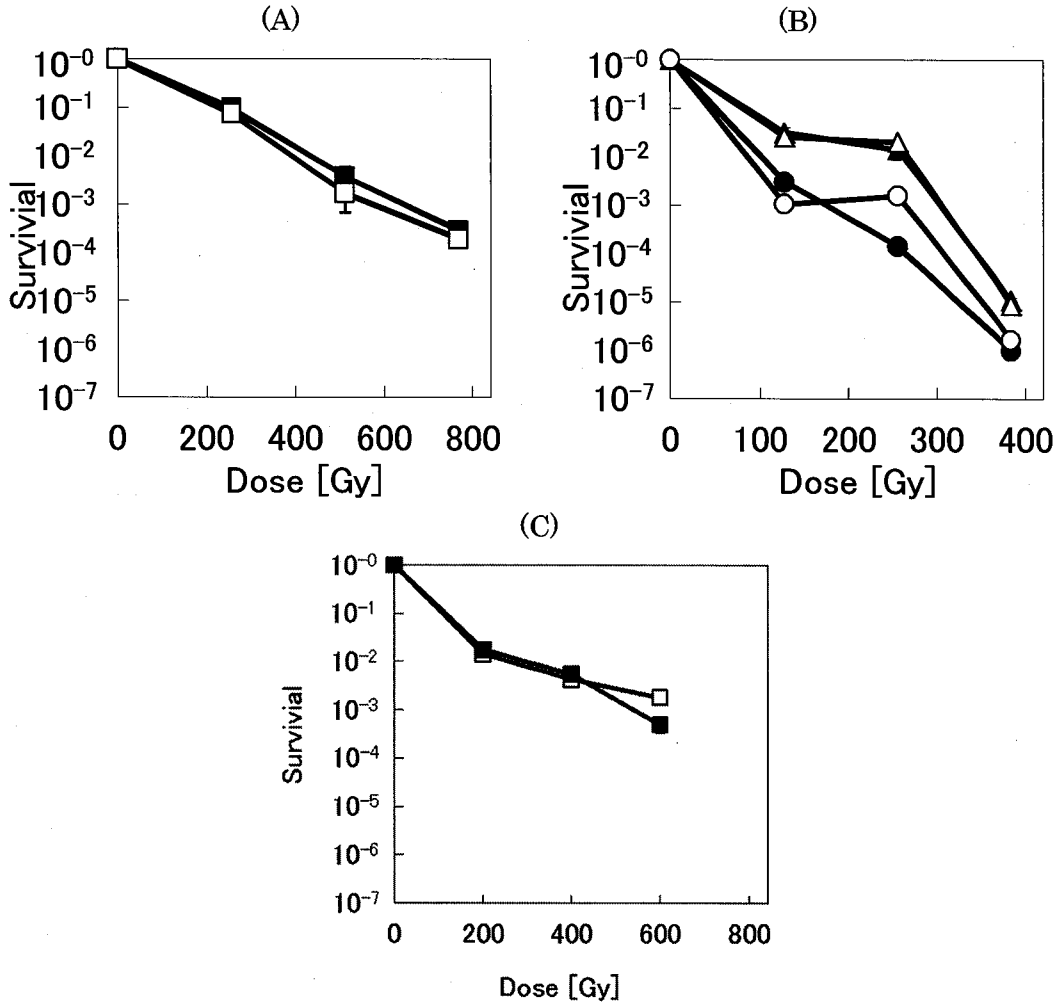

Figure.4-2- 3 Survival of cells incubated in liquid rich medium for 2 hr post-irradiation. Cells were grown in liquid rich medium pre-irradiation, and subsequently plated on solid minimal (solid symbols) or rich (open symbols) medium after post-irradiation incubation. (A) Wild-type cells incubated for 2 hr post X-irradiation (■, □), (B) *recA* (▲, △) and *lexA3* (●, ○) cells incubated for 2 hr post X-irradiation, (C) wild-type cells incubated for 2 hr post He-irradiation (■, □). Each data point represents the mean of at least three independent experiments, and the error bar denotes standard error. A data point without an error bar indicates that the error bar was smaller than the symbol.

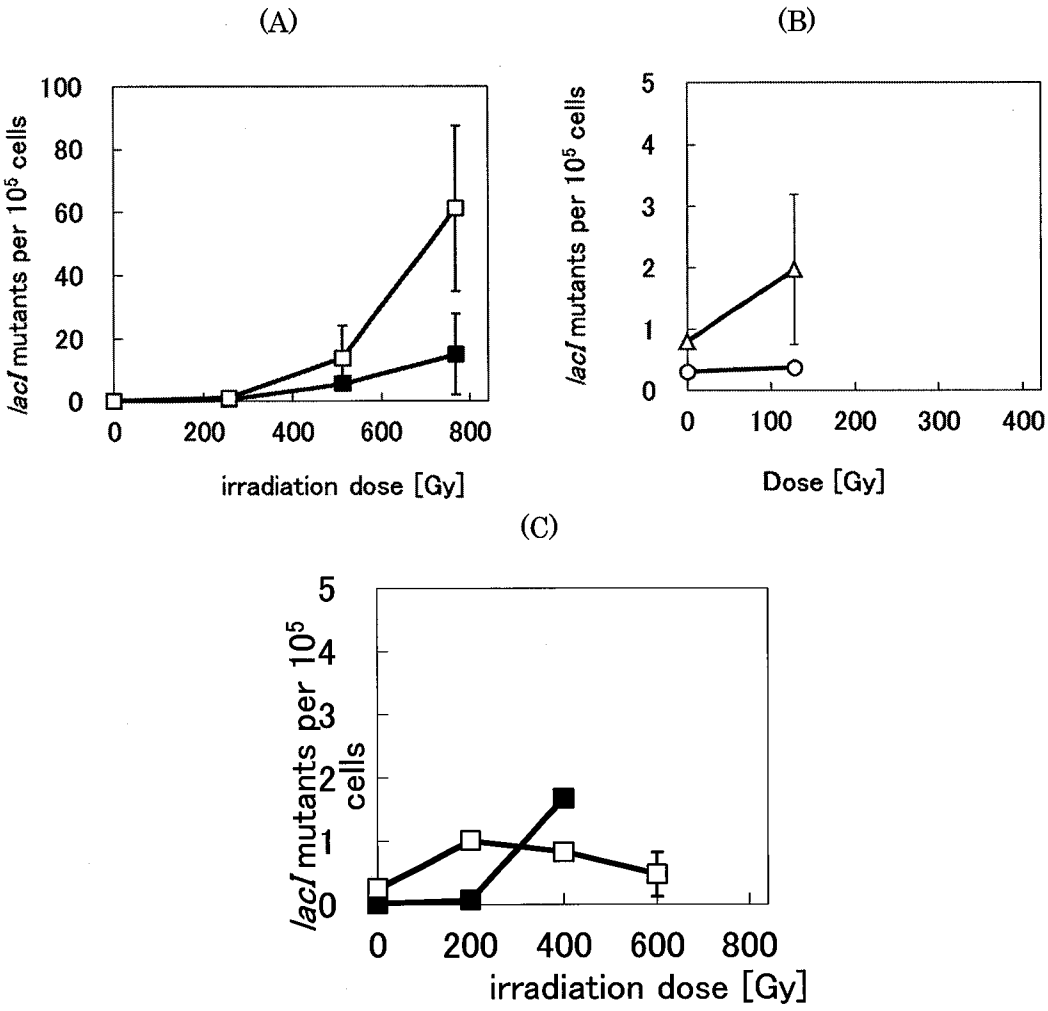

Figure 4-2-4. *lacI* mutant frequencies of cells incubated for 2 hr post-irradiation in liquid minimal (solid symbols) or rich (open symbols) medium. (A) Wild-type cells irradiated with X-rays (■, □), (B) *recA* (△) and *lexA3* (○) irradiated with X-rays, (C) Wild-type cells irradiated with He ions (■, □). Each data point represents the mean of at least three independent experiments, and the error bar denotes standard error. A data point without an error bar indicates that the error bar was smaller than the symbol. Due to low mutant frequencies with very large statistical errors, following data are not plotted: *recA* (256 and 384 Gy), *lexA3* (256 and 384 Gy), wild type irradiated with He ions and incubated for 2hr post-irradiation in liquid minimal medium (600Gy)

References

1. Bedford JS, Dewey WC. Radiation Research Society. 1952-2002. Historical and current highlights in radiation biology: has anything important been learned by irradiating cells? Radiat Res. 2002, 158(3): 251-259
2. Friedberg EC. Walker GC. Siede W. Wood RD. Shultz RA. Ellenberger T. DNA Repair and Mutagenesis, ASM Press, Washington, DC, USA, 2nd edition, 2006
3. Janion C. Inducible SOS response system of DNA repair and mutagenesis in Escherichia coli. Int J Biol Sci. 2008, 4(6): 338-344
4. Kuzminov A. Recombinational repair of DNA damage in Escherichia coli and bacteriophage lambda. Microbiol Mol Biol Rev. 1999, 63(4):751-813
5. Dong T, Kirchhof MG, Schellhorn HE. RpoS regulation of gene expression during exponential growth of Escherichia coli K12. Mol Genet Genomics. 2008, 279(3): 267-277
6. Dong T, Schellhorn HE. Control of RpoS in global gene expression of Escherichia coli in minimal media. Mol Genet Genomics. 2009 Jan;281(1):19-33.
7. Ferenci T. Hungry bacteria--definition and properties of a nutritional state. Environ Microbiol. 2001, 3(10): 605-611
8. Tao H, Bausch C, Richmond C, Blattner FR, Conway T. Functional genomics: expression analysis of Escherichia coli growing on minimal and rich media. J Bacteriol. 1999, 181(20): 6425-6440
9. Sargentini NJ, Diver WP, Smith KC. The effect of growth conditions on inducible, recA-dependent resistance to X rays in Escherichia coli. Radiat Res. 1983, 93(2): 364-380
10. Sargentini NJ, Smith KC. Growth-medium-dependent repair of DNA single-strand and double-strand breaks in X-irradiated Escherichia coli. Radiat Res. 1985 Oct;104(1):109-115
11. Sargentini NJ, Smith KC. Quantitation of the involvement of the recA, recB, recC, recF, recJ, recN, lexA, radA, radB, uvrD, and umuC genes in the repair of X-ray-induced DNA double-strand breaks in Escherichia coli. Radiat Res. 1986, 107(1): 58-72
12. Grigg GW. Radiation-induced reversion of transition mutants. Australian Journal of Biological Sciences. 1964, 17: 907-920
13. Markham BE, Little JW, Mount DW. Nucleotide sequence of the lexA gene of Escherichia coli K-12. Nucleic Acids Res. 1981, 9(16): 4149-4161
14. Maezawa H, Hieda K, Kobayashi K, Furusawa Y, Mori T, Suzuki K, Ito T. Effects of monoenergetic X-rays with resonance energy of bromine K-absorption edge on bromouracil-labelled E. coli cells. Int J Radiat Biol Relat Stud Phys Chem Med. 1988, 53(2): 301-308
15. Hata, K., and H. Baba. OSCAR, a code for the calculation of the yield of radioisotopes produced by charged-particle induced nuclear reactions. JAERI-M: 1988, 88-184
16. Miller JH. A short course in bacterial genetics. Cold Spring Harbor Laboratory Press 1992
17. Krasavin EA. Amirtayev KG. Kozubek S. Tokarova B. Tcherevatenko AP. Role of DNA repair processes in the biological efficiency of heavy ions. Studia biophysica. 1989, 133: 25-31
18. Tokarova B, Amirtayev KG, Kozubek S, Krasavin EA. Mutagenic action of heavy ions on Escherichia coli cells. Mutat Res. 1989, 227(4) :199-205
19. Yatagai F, Matsuyama A. LET-dependent radiosensitivity of Escherichia coli K-12 rec and uvr mutants. Radiat Res. 1977, 71(1): 259-263.
20. Sargentini NJ, Smith KC. Mutational spectrum analysis of umuC-independent and umuC-dependent gamma-radiation mutagenesis in Escherichia coli. Mutat Res.

1989, 211(2): 193-203
21. Wijker CA, Lafleur MV. Influence of the UV-activated SOS response on the gamma-radiation-induced mutation spectrum in the lacI gene. Mutat Res. 1998, 408(3): 195-201
22. DEERING RA. Mutation and killing of Escherichia coli WP-2 by accelerated heavy ions and other radiations. Radiat Res. 1963, 19: 169-178
23. Munson RJ, Bridges BA. The LET factor in mutagenesis by ionizing radiations. I. Reversion to wild type of a bacteriophage T4 amber mutant. Int J Radiat Biol Relat Stud Phys Chem Med. 1973, 24(3): 257-273
24. Horneck G, Krasavin EA, Kozubek S. Mutagenic effects of heavy ions in bacteria. Adv Space Res. 1994, 14(10): 315-329
25. Kozubek S, Horneck G, Krasavin EA, Ryznar L. Interpretation of mutation induction by accelerated heavy ions in bacteria. Radiat Res. 1995, 141(2): 199-207
26. Kozubek S, Ryznar L, Horneck G. Mutation induction by accelerated heavy ions in bacteria. Mutat Res. 1994, 309(1): 17-28
27. Tokarova B, Amirtayev KG, Kozubek S, Krasavin EA. Mutagenic action of heavy ions on Escherichia coli cells. Mutat Res. 1989, 227(4): 199-205
28. McKenzie GJ, Harris RS, Lee PL, Rosenberg SM. The SOS response regulates adaptive mutation. Proc Natl Acad Sci U S A. 2000, 97(12): 6646-6651
29. Kozubek S, Krasavin EA, Soska I, Drasil V, Amirtayev KG, Tokarova B, Bonev M. Induction of the SOS response in Escherichia coli by heavy ions. Mutat Res. 1989, 215(1): 49-53
30. Hada M, Georgakilas AG. Formation of clustered DNA damage after high-LET irradiation: a review. J Radiat Res. 2008, 49(3): 203-210
31. Shikazono N, Noguchi M, Fujii K, Urushibara A, Yokoya A. The yield, processing, and biological consequences of clustered DNA damage induced by ionizing radiation. J Radiat Res. 2009, 50(1): 27-36
32. Datta K, Jaruga P, Dizdaroglu M, Neumann RD, Winters TA. Molecular analysis of base damage clustering associated with a site-specific radiation-induced DNA double-strand break. Radiat Res. 2006, 166(5): 767-781
33. Datta K, Neumann RD, Winters TA. Characterization of complex apurinic/apyrimidinic-site clustering associated with an authentic site-specific radiation-induced DNA double-strand break. Proc Natl Acad Sci U S A. 2005, 102(30): 10569-10574
34. Datta K, Purkayastha S, Neumann RD, Pastwa E, Winters TA. Base Damage Immediately Upstream from Double-Strand Break Ends is a More Severe Impediment to Nonhomologous End Joining than Blocked 3'-Termini. Radiat Res. 2010 Nov 10. [Epub ahead of print]
35. DEERING RA. Mutation and killing of Escherichia coli WP-2 by accelerated heavy ions and other radiations. Radiat Res. 1963, 19: 169-178
36. Yeeles JT, Dillingham MS. The processing of double-stranded DNA breaks for recombinational repair by helicase-nuclease complexes. DNA Repair (Amst). 2010, 9(3): 276-285

Chapter 5. General overview and Summaries

This paper attempts to develop the novel cancer therapy; Photodynamic therapy (PDT) and Boron Neutron Capture Therapy (BNCT), by using Drug Delivery System. PDT and BNCT is one of the less invasive cancer treatments. They use quantum beam to excite the specific drug and the active oxygen or radiation produced by the excited drug make selective cytotoxicity.

The first, I determined the accumulation ability of HVJ-E using PDT (2-1). The accumulation with HVJ-E was 3 times higher than that with the photosensitizer alone and 20 times higher than that with ordinary method. In the study, the take-up ability was significantly different with cell line. In the result of detailed investigation, some subclones have different photosensitizer uptake ability and PDT sensitivity than the others, though they have same DNA and were differentiated from same cell (2-2). It shows that a small fraction of tolerant cells may actively grow and predominate after PDT, even though most of the non-tolerant cells in the original tumor tissue were selectively killed by the repeated treatment in clinical therapy. To effective treatment, enough cytotoxicity to kill the small function of cells is needed.

From the result of section 2-1, more than 1 x 10^6 n/sec/cm^2 of thermal neutron flux is thus needed for BNCT when HVJ-E is used. OKTAVIAN facility generates 14 MeV neutrons via D-T reaction. The produced 14 MeV neutrons have to be moderated to thermal neutron. And the stably produced neutron source intensity is $\sim$1 x 10^{10} n/sec at present. I carried out simulation calculations to design a thermal neutron field (3-1). With the result, the neutron flux at irradiation field was about 1.6 x 10^{-4} n/cm^2/source neutron using 20cm thickness of polyethylene moderator and there is possibility that the anti-tumor effect of BNCT can be observed using the novel boron agent in in-vitro experiment. After that, a thermal column was built in the heavy irradiation room of OKTAVIAN, and irradiation experiments were performed (3-2). The thermal neutron flux at the sample area achieved 1.6 x 10^6 n/cm^2/s, and the dose of BNCT was 3.4 Gy-eq for 2 hour irradiation. With the irradiation more than 50% of anti-tumor effect was observed in in-vitro experiment. However the anti-tumor effect was not observed in in-vivo experiment. The experimental method need to be improved.

In Chapter 3, equivalent dose was calculated to evaluate the BNCT effect, and the value was compared with those from other studies on the same cell line. Although the RBE value of each nuclear reaction was determined in the previous study, some points remain unclear. To accurately calculate the dose and administer treatment with the least side effects, the radiological consequences need to be precisely assessed. Then I studied the mechanism of cellular disorder comparing photon-ray and α-ray, which is generated in BNCT reaction (4-1). The relative biological effectiveness (RBE) of He ions relative to X-rays was calculated from $D_{0.01}$, which was calculated from Fig. 4-1-2 (Table 4-1-1). The RBE values were approximately 1.3 for Group I (wild-type, recQ and uvrA) and 3.0 for *recA* and *lexA*. The medium-dependent survival and mutagenesis were also observed (4-2). The SOS reaction was needed for medium dependency. From the result, it could be argued that cellular environment of tumor is considerable to effective treatment.

The summaries of each section were described below.

Section 2-1.
Photodynamic therapy (PDT) is a photochemical modality approved for cancer treatment. The accumulation of photosensitizers in cancer cells is necessary to enhance the therapeutic benefits of PDT; however, photosensitizers have a low uptake efficiency. To overcome this limitation, a drug delivery system (DDS), such as Hemagglutinating

virus of Japan envelope (HVJ-E) vector, is required. In this study, the combination of PDT and HVJ-E was investigated for enhancing the efficacy of PDT. The photosensitizers that were evaluated included 5-aminolaevulinic acid (5-ALA), protoporphyrin IX (PPIX), and HVJ-PPIX. The uptake of the photosensitizers as increased twenty-fold with the addition of HVJ-E. The cytotoxicity of conventional 5-ALA was enhanced by the addition of HVJ-E vector. In conclusion, HVJ-E vector improved the uptake of photosensitizers and the PDT effect.

Section 2-2
Photodynamic therapy (PDT) involves the administration of a photosensitizer, followed by local illumination of a tumor with a laser (of the appropriate wavelength) to activate a specific drug. However, the cells in a tumor tissue are heterogeneous, in terms of their morphologies and differentiation statuses, even if the tumor consists of progeny developed from a single neoplastic cell. It is not known how tumor cell heterogeneity affects their sensitivity to PDT. Here, I demonstrate that a single tumor cell has the potential to produce a progeny that is heterogeneous in terms of morphology, VEGF secretion, and PDT sensitivity, irrespective of intracellular photosensitizer amount. Understanding tumor cell heterogeneity for clinical applications of PDT will help in the design of new interventions and potentially improve long-term survival of PDT treated patients.

Section 3-1
BNCT is inefficient because nuclear reactor is used for neutron source. To improve BNCT, accelerator-based BNCT is needed. Though I tried to build the set up for BNCT experiment using culture cell or mice in accelerator facilities, it was difficult because of the weakness of accelerator-based neutron source. The effect of BNCT calculated from the product of boron concentration and thermal neutron flux. If the ^{10}B concentration could be increased, even a little weak neutron source would be available. These days various kinds of boron agents were developed and the concentration in tumor cells is approximately 10 times higher than that of a conventional way. In this study, I made an accelerator-based BNCT set up for novel boron agents using simulation calculations. In the result the neutron flux at irradiation field was about $1.6x10^{-4}$ [n/cm2/source neutron] and there is possibility that the anti-tumor effect of BNCT can be observed using the novel boron agent in in-vitro experiment. The series study showed the potential of the accelerator-based BNCT.

Section 3-2
BNCT (Boron Neutron Capture Therapy) is one of the effective treatments for cancers. However, BNCT is inefficient at present because nuclear reactor is required as a neutron source. Various studies started so far to realize accelerator-based neutron source. However, such kinds of accelerators are not yet realized because of weakness of accelerator-based neutron source. Recently, several studies proposed new efficient agents which can accumulate boron in tumor approximately 10 times higher than before. Even a little weak neutron source would be thus available with novel boron agents. In this study, I designed and constructed a thermal neutron field with a D-T neutron source to carry out basic BNCT experiments with cultured cell or small animals with help of new boron agents. In the experiment, the BNCT dose was 5.0 Gy-eq for 2 hour irradiation and fast neutron and gamma ray doses were suppressed to be 0.31 Gy-eq and 0.023 Gy, respectively. It was confirmed that the anti-tumor effect of BNCT could be

observed in in vivo experiment at the present neutron filed. And it was found that it would be possible to realize a D-T-based BNCT, if the source neutron intensity would be larger than ~10^{12} n/s.

Section 3-3
In the previous study, the effect of BNCT was not observed using small animals. The poor result was thought to be due to lack of affinity of LLC. The up-take abilities of each cell line were need to be compared using BSH. I compared the up-take abilities of four cell lines, and B16 cells have highest. The value was about twofold greater than LLC. The set-up was also improved, because deuterium water came to be used. The predominance of deuterium water was indicated in previous study. As the result, the thermal neutron flux at the sample area was increased to 8.9×10^{6} n/cm^2/sec. In the study, I could suggest a possible beneficial effect of in-vitro BNCT experiment.

Section 4-1
There are many types of radiation and each has its own mechanism of action. Especially, the effects of high-linear energy transfer (LET) radiation are different from those of X-rays or γ-rays. High-LET radiation tends to inflict great damage on DNA via direct effects and the damage is easily clustered. To determine the difference, I compared the effects of He-ray and x-ray using Wild-type *Escherichia coli* (*E. coli*) and its mutants. Though typical different damage was not observed, some new knowledge concerning DNA damages induced by high-LET radiation was obtained. It would lead to the discovery of the effect of high-LET radiation.

Section 4-2
The sensitivity to radiation depends on the physiological state of cells. For example, in *E. coli*, the survival of cells after irradiation is affected by the growth medium. In the present study, I analyzed *E. coli* cells to determine (1) the level of medium-dependent mutagenesis, and (2) the effects of the quality of radiation on medium-dependent survival and mutagenesis. Cells were exposed to low-linear energy transfer (LET) X-rays and then grown on rich and minimal media. I found that both survival and mutation frequencies were higher in the cells grown on rich medium. The increases of survival and mutation frequency were both strongly dependent on the function of RecA or LexA, suggesting that SOS repair is responsible for the medium-dependent sensitivity and mutagenesis. In contrast, high-LET He ions failed to demonstrate medium-dependent radiation resistance, and did not induce mutations. I suggest that the damage from He ions is too severe to stimulate survival or mutagenesis on rich medium and that SOS repair does not fully function after He ion-irradiation.

Acknowledgements

This research was carried out under the guidance of Dr. Kunio Awazu, Professor of Medical Beam Physics Laboratory, Division of Sustainable Energy and Environmental Engineering, Graduate School of Engineering, Osaka University. The author would like to express my deepest gratitude to Prof. Awazu whose comments and suggestions were innumerably valuable throughout the course of my study.

Special thanks also go to the reviewer of this thesis, Prof. Hiroshi Horiike, Division of Sustainable Energy and Environmental Engineering, Graduate School of Engineering, Osaka University, for their valuable advices. The author would like to express his appreciation to the reviewer of this thesis, Prof. Isao Murata Division of Electrical,Electronic and Information Engineering, Graduate School of Engineering, Osaka University, for their valuable advices.

The author would like to express his appreciation to Dr. Ishii and Dr. Hazama, Medical Beam Physics Laboratory, Division of Sustainable Energy and Environmental Engineering, Graduate School of Engineering, Osaka University, whose opinions and information have helped me very much throughout the production of this study.

The author wishes to express his heartily deeply thanks to Dr. Toshihiro Kushibiki, the department of Medical Engineering, National Defense Medical College, for cooperation and valuable advice in Chapter 2 of this manuscript.

The author wishes to express his heartily deeply thanks to Prof. Yasufumi Kaneda, Division of Gene Therapy Science, Graduate School of Medicine, Osaka University, and Hiroyuki Nakamura, Hiroyuki Nakamura, Department of Chemistry, Gakushuin University, for cooperation and valuable advice in Chapter 2 and 3 of this manuscript.

The author wishes to express my thanks to Dr. Lee Chun Man, Medical Center for Translational Research, Osaka University Hospital and Tomoyuki Nishikawa, Division of Gene Therapy Science, Graduate School of Medicine, Osaka University, for advice on the sample preparation and helpful discussion in Chapters 2 and 3 of this manuscript.

The author wishes to express my thanks to Dr. Yoko Akiyama, Division of Sustainable Energy and Environmental Engineering, Graduate School of Engineering, Osaka University, for advice on the boron measurement and helpful discussion in Chapters 3 of this manuscript.

The author wishes to express his heartily deeply thanks to Dr. Naoya Shikazono, Irradiated Cell Analysis Research Group, Medical and Biotechnological Application Division, Quantum Beam Science Directorate, Japan Atomic Energy Agency for cooperation and valuable advice in Chapter 4 of this manuscript.

The author wishes to express my thanks to Dr. Ken Akamatsu, and Dr. Momoko Takahashi, Irradiated Cell Analysis Research Group, Medical and Biotechnological Application Division, Quantum Beam Science Directorate, Japan Atomic Energy Agency, for advice on the sample preparation and helpful discussion in Chapter 4 of this manuscript.

The author is grateful to Drs. K. Fujii and A. Yokoya for useful discussions, Mr. S. Hanawa for his technical assistance and Dr. I. Narumi for his help with ion-irradiation experiments.

The author received generous support from Dr. Sachiko Suzuki-Yoshihashi and Mrs. Takako Tajiri, former staff of Professor Awazu's laboratory. The author would like to express his gratitude for their scientific cooperation, valuable advices and encouragement.

The author likes to take an opportunity to extend his heartily thanks to Ms. Masako Kudo, Secretary to Professor Awazu's laboratory.

The author is much indebted to Mr. Naohiro Fujimoto for his contribution to the present studies.

The author would like to express his appreciation to the students of Professor Awazu's laboratory and Dr. Murata's laboratory.

The author would like to thank Syoshisya scholarship for a grant that made it possible to complete this study.

Finally, the author would also like to express his gratitude to his family and friends for their moral support and warm encouragements.

Oct, 2012.
Osaka

Makoto Sakai

List of Research Achievement

Original article

酒井真理, 櫛引俊宏, 粟津邦男, 細胞形態の違いによる光線力学療法効果の違いの検討, 日本レーザー医学会誌, 30 (4), 405-414 (2010)

M. Sakai, N. Fujimoto, I. Murata, K. Awazu, Development of thermal neutron field with D-T neutron source aiming at in vitro experiment for BNCT, housyasen, in press (2012)

M. Sakai, N. Fujimoto, K. Ishii, M. E. El-Zaria, H. S. Ban, H. Nakamura, Y. Kaneda, K. Awazu, In vitro investigation of efficient Photodynamic Therapy using non-viral vector ; Hemagglutinating virus of Japan envelope, J. Biomed. Opt., 17(7), 079803 (2012)

N. Dwaikat, T. Iida, F. Sato, Y. Kato, I. Ishikawa, W. Kada, A. Kishi, M. Sakai, Y. Ihara, Study etching characteristics of a track detector CR-39 with ultraviolet laser irradiation, Nuclear Instruments and Methods in Physics Research Section A: Accelerators, Spectrometers, Detectors and Associated Equipment, 572(2), 826-830 (2007)

T. Kushibiki, M. Sakai, K. Awazu, Differential effects of photodynamic therapy on morphologically distinct tumor cells derived from a single precursor cell, Cancer Letters, 268(2), 244-251 (2008)

藤本尚弘, 酒井真理, 石井克典, M.E. El-Zaria, 潘鉉承, 中村浩之, 金田安史, 粟津邦男, 非ウイルスベクターを用いたがんに対する光線力学療法, 電気学会研究会資料, OQD-10-035 (2010)

International conference papers with peer review

M. Sakai, N. Fujimoto, K. Ishii, I. Murata, K. Awazu, Thermal neutron field with D-T neutron source for BNCT, Progress in NUCLEAR SCIENCE and TECHNOLOGY, 1, 513-516 (2011)

M. Sakai, N. Fujimoto, K. Ishii, I. Murata, C.M. Lee, Y. Kaneda, H. Nakamura, K. Awazu, Basic investigation of boron neutron capture therapy (BNCT) using novel boron agents and accelerator based neutron source, IFMBE Proceedings, 25(1), 638-641 (2009)

N. Honda, K. Ishii, A. Kimura, M. Sakai, K. Awazu, Determination of optical property changes by laser treatments using inverse adding-doubling method, Proceedings of SPIE, 7175: 71750Q (2009)

Conference presentation

酒井真理, 加田渉, 岸暖也, 井原陽平, 石川一平, DWAIKAT Nidal, 佐藤文信, 加藤裕史, 飯田敏行, 大気中ラドン測定用開放型比例計数管の試作,日本原子力学会 2007 年春の年会, 2007

酒井真理, 櫛引俊宏, 粟津邦男, 腫瘍細胞の形態による光線力学療法効果の違いに関する研究,日本光学会年次学術講演会 Optics and Photonics Japan 2007, 2007

酒井真理, 櫛引俊宏, 粟津邦男, 細胞形態の違いによる光線力学療法効果の違いの検討,第19回日本光線力学学会学術講演会, 2009

M. Sakai, N. Fujimoto, K. Ishii, I. Murata, K. Awazu, Thermal neutron field with D-T neutron source for BNCT, The Fifth International Symposium on Radiation Safety and Detection Technology (ISORD-5), 2009

M. Sakai, N. Fujimoto, K. Ishii, I. Murata, C.M. Lee, Y. Kaneda, H. Nakamura, K. Awazu, Basic investigation of boron neutron capture therapy (BNCT) using novel boron agents and accelerator based neutron source, World Congress on Medical Physics and Biomedical Engineering 2009 (WC 2009), 2009

酒井真理, 藤本尚弘, 石井克典, 浅野智之, 村田勲, 中村浩之, 李千萬, 金田安史, 粟津邦男, 加速器及び HVJ-E を用いたホウ素中性子捕獲療法の基礎的検討,日本原子力学会2009年春の年会, 2009

酒井真理, 藤本尚弘, 石井克典, 村田勲, 金田安史, 粟津邦男, Basic investigation of boron neutron capture therapy (BNCT) using HVJ-E and accelerator-based neutron source, 第49回日本生体医工学会大会, 2010

酒井真理, 鹿園直哉, 粟津邦男, 線質及び生育条件が放射線感受性に与える影響, 放射線影響学会第54回大会, 2011

酒井真理, 鹿園直哉, 粟津邦男, 線質及び生育条件が放射線感受性に与える影響, 第6回高崎量子応用研究シンポジウム, 2011

酒井真理, 鹿園直哉, 粟津邦男, 線質及び生育条件が放射線誘発突然変異に与える影響, 第7回高崎量子応用研究シンポジウム, 2012

岩本由美子、酒井真理、冨岡穣、櫛引俊宏、鈴木幸子、大島鉄朗、坂口裕和、沢美喜、大路正人、田野保雄、粟津邦男, 脈絡膜血管内皮細胞を用いた超短パルスレーザー励起インドシアニングリーンによる光線力学治療の検討, 第18回日本光線力学学会, 2007

木村彰紀, 石井克典, 本多典広, 酒井真理, 粟津邦男, レーザー凝固治療における生体組織の光学定数計測, 第29回日本レーザー医学会総会, 2008

N. Honda, K. Ishii, A. Kimura, M. Sakai, K. Awazu, Determination of optical property changes by laser treatments using Inverse Adding-Doubling method, Photonics WEST BIOS 2009, 2009

藤本尚弘, 酒井真理, 石井克典, 村田勲, 粟津邦男, 李千萬, 金田安史, 浅野智之, 中村浩之, 加速器及び HVJ-E を用いたホウ素中性子捕捉療法の基礎的検討, 日本原子力学会2009年秋の大会, 2009

藤本尚弘, 酒井真理, 石井克典, E. El-Zaria Mohamed, 潘鉉承, 中村浩之, 金田安史, 粟津邦男, 非ウイルスベクターHVJ-E を用いた高効率 PPIX-PDT の培養がん細胞での検討, 第31回日本レーザー医学会総会, 2010

藤本尚弘, 酒井真理, 石井克典, M.E. El-Zaria, 潘鉉承, 中村浩之, 金田安史, 粟津邦男, 非ウイルスベクターを用いたがんに対する光線力学療法, 電気学会光量子デバイス研究会（バイオメディカル・フォトニクス応用）S, 2010

藤本尚弘，酒井真理，石井克典，金田安史，M.E. El-Zaria，H.S. Ban，中村浩之，粟津邦男，非ウイルスベクターHVJ-E を用いた光線力学療法の基礎検討，レーザー学会学術講演会第 30 回年次大会，2010